2013-02-15

Micro-environmental factors directing differentiation of murine embryonic stem cells down osteogenic and chondrogenic lineages

Hazenbiller, Olesja

UNIVERSITY OF CALGARY

Micro-environmental factors directing differentiation of murine embryonic stem cells down osteogenic and chondrogenic lineages

by

Olesja Hazenbiller

A THESIS

SUBMITTED TO THE FACULTY OF GRADUATE STUDIES

IN PARTIAL FULFILMENT OF THE REQUIREMENTS FOR THE

DEGREE OF MASTER OF SCIENCE

DEPARTMENT OF BIOMEDICAL ENGINEERING

CALGARY, ALBERTA

February, 2013

Abstract

The field of bone tissue engineering (BTE) aims to develop graft substitutes for diseased or difficult to heal fractures. We used a BTE construct made of collagen type I and murine embryonic stem cells (mESCs) which has been shown to trigger mESCs differentiation into osteoblasts, and successfully contribute to fracture repair *in vivo* within a mouse model system.

Bone healing is a complex process involving the interplay of biochemical and biomechanical cues. Therefore, this project aimed to systematically emulate the roles of chemical and mechanical cues present during fracture repair on the differentiation of mESCs *in vitro* in order to optimize treatment strategies for BTE.

Further characterization of this cell/gel construct revealed that mESCs differentiate into a heterogeneous cell population of chondrocytes and osteoblasts, replicating the process of endochondral ossification that normally occurs during fracture repair. To study the effect of biomechanical cues, a loading system was specifically designed and characterized to apply confined compressive load to a soft, viscoelastic cell/gel construct. Mechanical stimuli enhanced chondrogenic differentiation but had no effect on osteogenic differentiation. Moreover, the role of integrins in directing mESCs differentiation and transducing mechanical signals was evaluated. Finally, the synergistic effect between extracellular matrix mediated differentiation, mechanical stimulation and BMP-2 delivery to the system using nano-particles was studied.

Acknowledgements

This work could not have been accomplished without the help and expertise of many people. My thanks go to my Supervisors Dr. Neil Duncan and Dr. Roman Krawetz for their confidence in my skills and their easy going manner.

Also, my thanks go to my supervisor committee, Dr. John Matyas, Dr. Michael Kallos and Dr. Wendy Hutchins for taking the time to read and examine my thesis. I will be always thankful to Dr. Derrick Rancourt for his optimistic and positive attitude. I would like extend my thanks to Dr. Uludag for hosting me in his lab, Gualing Wang for teaching me nanoparticle technology and Stephanie Fisher for fabricating nanoparticles before me and making my life much easier.

I would like to extend my thanks to Dragana Ponjevic, May Chung and Poh So Lee for all that you taught me and your assistance in my experiments.

My special thanks go to Artem Gubanov for his help with Matlab and for the critical discussions on the loading device which deepened my engineering and scientific understanding. Big thanks to Terri Semler for critical reviewing my work, Katie Sheehan for teaching me on the Zetasizer and Jaymi Taiani for inspiring conversations.

I am grateful to Marty DeFrancisco from Marco Rubber Company for helping to select the right material for the loading rings, Karen Balazy from Mott Corporation for her assistance on the porous platens, Len Lamberg from Champion Tape for suggesting a perfect adhesive, and Peter Byrne for making the loading chambers.

My final thanks go to all my friends around the world especially Katharina Wiecek for being there whenever I needed you.

I would never be able to fully express my gratitude to my parents and my family, who are always there for me. Diana, Daniel and David this Thesis is for you.

This project was supported by the Nanotechnology and Information and Communication Technologies Recruitment Scholarship funded by Alberta Innovates Technology Futures, by the Skeletal Regenerative Medicine Team funded by Canadian Institutes of Health Research, and by the BME Outstanding Performance Award funded by the Biomedical Engineering Graduate Program at the University of Calgary.

Table of Contents

List of Tables

List of Figures and Illustrations

List of Symbols, Abbreviations and Nomenclature

Symbol	Definition
ALP	Alkaline phosphatase
Anti-anti	Antibiotic-Antimycotic
ASCs	Adult stem cells
BMPs	Bone morphogenetic proteins
BMSC	Bone marrow stromal cells
BSA	Bovine serum albumin
BSP	Bone sialprotein
BTE	Bone tissue engineering
Col I	Collagen type I
Dextran-FITC	Dextran-Fluorescein isothiocyanate
EBs	Embryoid bodies
ECM	Extracellular matrix
ELISA	Enzyme-linked immunosorbent assay
ESCs	Embryonic stem cells
FGF	Fibroblast growth factor
GFs	Growth factors
H&E	Hematoxylin and eosin
ID	Inner diameter
IGF-1	Insulin-like growth factor 1
LIF	Leukemia inhibitory factor
mESCs	Murine embryonic stem cells

Micro CT	Micro chromotography
Min	Minutes
MSC	Mesenchymal stem cells
N	Newton
OB	Objective
OC	Octeocalcin
OD	Outer diameter
ON	Osteonectin
OPN	Osteopontin
OSX	Osterix
PDGF	Platelet-derived growth factor
PEG	Polyethylene glycol
PLL	Poly-L-Lysine
RAD	cyclo (Arg-Ala-Asp-d-Phe-Cys)
RANKL	Receptor activator of nuclear factor kappa-B ligand
RGD	cyclo (Arg-Gly-Asp-d-Phe-Cys)
rpm	rotation per minute
Runx-2/cbfa1	Runt-related transcription factor 2/ core-binding factor subunit alpha-1
SCID	Severe combined immunodeficiency
SCs	Stem cells
SD	Standard deviation

SE	Standard error
TE	Tissue engineering
TF	Transcription factors
TGFβ	Transforming growth factor beta
TK	Thickness
TNBS	2,4,6-Trinitrobenzenesulfonic acid solution
VEGF	Vascular endothelial growth factor
βGP	Beta glycerol phosphate

CHAPTER 1: INTRODUCTION

Bone is a highly dynamic tissue that has the ability to heal itself when injured, however, fracture repair is often slow and incomplete. The bone healing process can be delayed due to an inability to recruit mesenchymal stem cells (MSCs) to the site of injury or can be the consequence of musculoskeletal diseases such as osteoporosis, osteoarthritis, and large bone defects (*1-3*). These conditions can occur from fracture, surgery, or cancer, which can all lead to a weakened bone structure that is more vulnerable to fracture (*2, 4*).

Current treatment strategies for bone fractures include autologous graft transplantation or the use of artificial and synthetic graft materials. Autologous transplantation is used with noteworthy success however, its restricted availability, risk of infection, skin incision, and postoperative pain has encouraged scientists to find alternative treatment strategies (*5-7*). While the use of materials such as ceramics and metals are applicable for larger defects, major drawbacks exist due to their inability to degrade, resulting in the implant residing in the body in the long-term. Furthermore, the introduction of a foreign material (implant) into the body poses the risks of infection, structural failure and implant rejection (*8*).

Despite these drawbacks, these techniques are widely used to the present day and have produced excellent results in many situations. The amount of graft transplantations (250,000) undertaken annually in the United States from which 20% result in complications, and 15% are difficult to heal, leads to 87,500 people who require

alternative treatment strategies annually (27, 30). The rapid advance in tissue engineering (TE) has opened new opportunities in regenerative medicine with the ultimate goal to completely restore the organ to a pre-injured state (*9*). In particular, TE offers a promising treatment for replacing diseased tissue with a combination of cells, substrates and/or growth factors (GFs) that are used to promote regeneration.

The field of TE is relatively new, and irrespective of the tissue, a promising progression has been made in the last two decades (*10*). New biomaterials with conductive and inductive properties have been developed possessing different structural, chemical and physical properties (*11*). The discovery of embryonic stem cells (ESCs) and the deeper understanding in the field of gene therapy and nanotechnology have enabled the delivery of inductive substances incorporated into biomaterials (*12-14*). Moreover, bioreactors have been developed to scale up the production from the bench to bed side (*15-17*). Currently, different constellations of materials, cells and growth factors are under investigation for their use in bone TE.

In this study, we use a TE construct made of collagen type I and murine embryonic stem cells (mESCs) (*18*) that has been shown to promote bone regeneration in a mouse fracture model *in vivo (19)*. Bone healing is a complex process involving the interplay of biochemical and biomechanical cues leading to activation of signals to stop bleeding and form a clot, providing space for new tissue formation, activation of cell differentiation to form a bridge, stabilize the bone and finally to deposit new bone formation and regeneration. On the cellular level, cells can respond to changes in their intracellular or extracellular environment that can contribute to cell proliferation,

differentiation or apoptosis. The stimuli inducing such changes can be biological, chemical or mechanical by nature, each resulting in a specific cell response. Thus, this project aims to better understand how different micro-environmental factors influence mESCs fate decision, in particular their differentiation within this collagen scaffold. Over the last decade studies have evaluated the importance of soluble factors such as Bone morphogenetic protein 2 (BMP-2), which is now one of the widely studied, and used GF with the capacity to induce new bone formation (*6, 12*). However, it is also evident that other cues such as cell-matrix interaction and external mechanical loads can trigger stem cells (SCs) differentiation.

This project seeks to independently evaluate the role of collagen as a supportive matrix toward inducing mESCs differentiation, then combines compressive stress as an additional differentiation stimulus and finally the interplay between matrix, stresses and a well-defined GF are investigated. Each of these stimuli are known to be significant in bone physiology *in vivo,* however, their synergistic effect on mESCs differentiation is not fully understood in order to optimize their application.

The overall hypothesis of this thesis is that bone morphogenic protein 2 in combination with cell adhesion molecules such as integrins αvβ3 and/or α1β1 will act synergistically under compressive load to accelerate mESCs differentiation into osteoblasts.

To test this hypothesis this thesis is structured into five specific objectives:

Objective 1: to design and characterize a custom built loading device capable of subjecting a viscoelastic scaffold to a confined compressive load.

Objective 2: to determine the effect of collagen mediated differentiation of mESCs.

Objective 3: to determine the effect of confined compressive load on mESCs differentiation.

Objective 4: to determine the role of integrins in mediating mESCs differentiation and in transducing a compressive load into a biosynthetic response.

Objective 5: to examine the synergistic effect between extracellular matrix (ECM) mediated differentiation, mechanical stimulation, and BMP-2.

A schematic overview of the techniques and approaches used to achieve each objective is summarized in a flow chart shown in Figure 1.1. The objectives of this project originated from previous work done by Krawetz et al. (*18*) and Taiani et al. (*19*). They have shown that a collagen type I scaffold seeded with mESCs promote ESCs to differentiate into osteoblasts and transplantation of this scaffold into a mouse burr-hole fracture can promote bone regeneration. A conclusion from these projects was that cell-matrix interaction and/or mechanical stimuli contribute to mESCs differentiation and the positive healing outcome. In order to further characterize this cell/gel system, and better understand how mechanical stimuli influence mESCs differentiation, we designed a loading system capable of subjecting this cell/gel construct to confined compressive load. The differentiation capacity of mESCs was evaluated on the gene and protein level as well as visualization with von Kossa staining. Furthermore, the expression of integrins, which are responsible for cell-matrix interaction and their role in directing mESCs differentiation into osteoblasts, was tested on the gene expression level. Finally, the synergistic effect of ECM-mediated differentiation, mechanical stimulation, and

BMP-2 was evaluated on the gene expression level. In order to stabilize and prolong GFs activity, BMP-2 was incorporated into biocompatible and biodegradable nanoparticles.

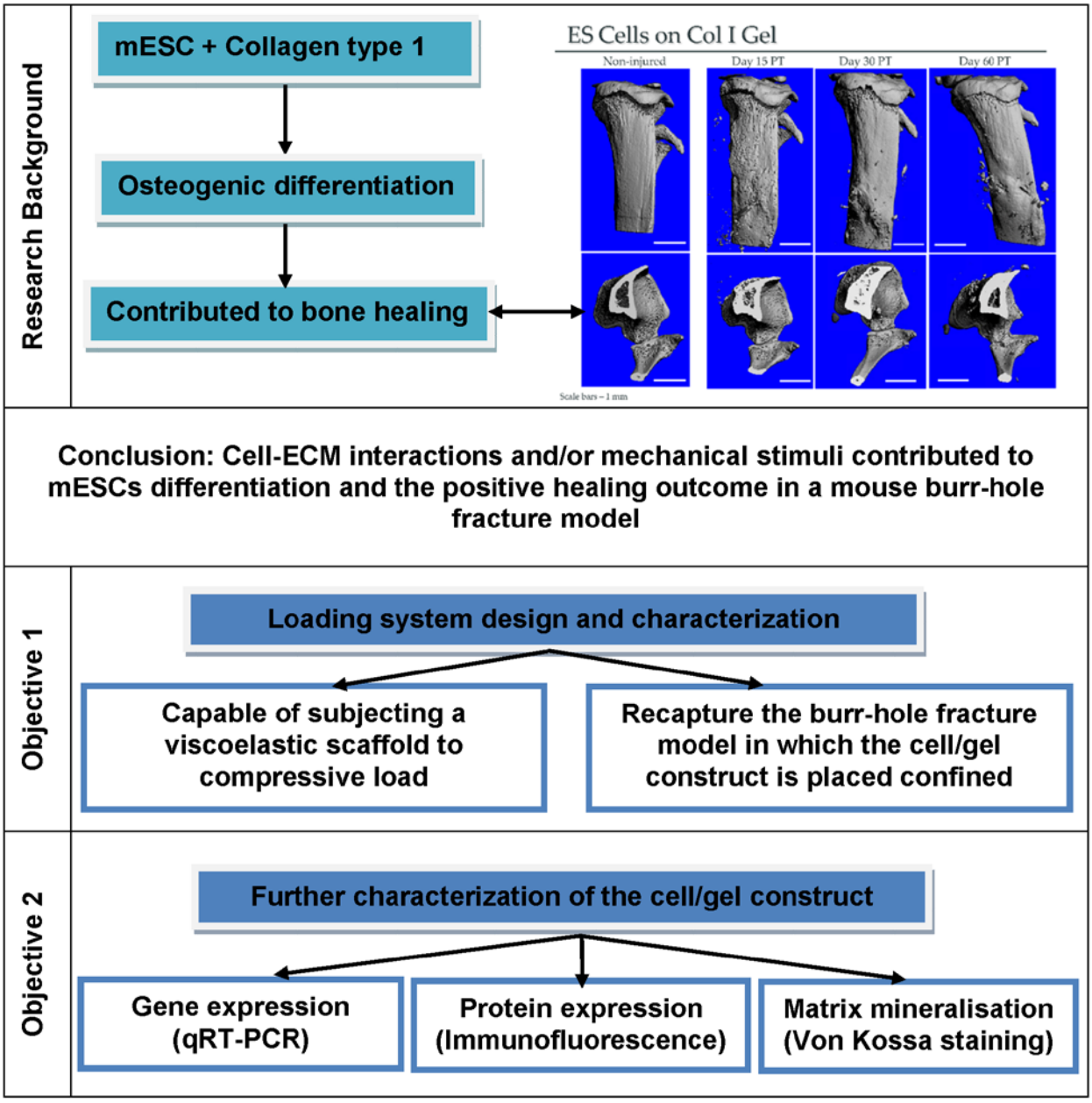

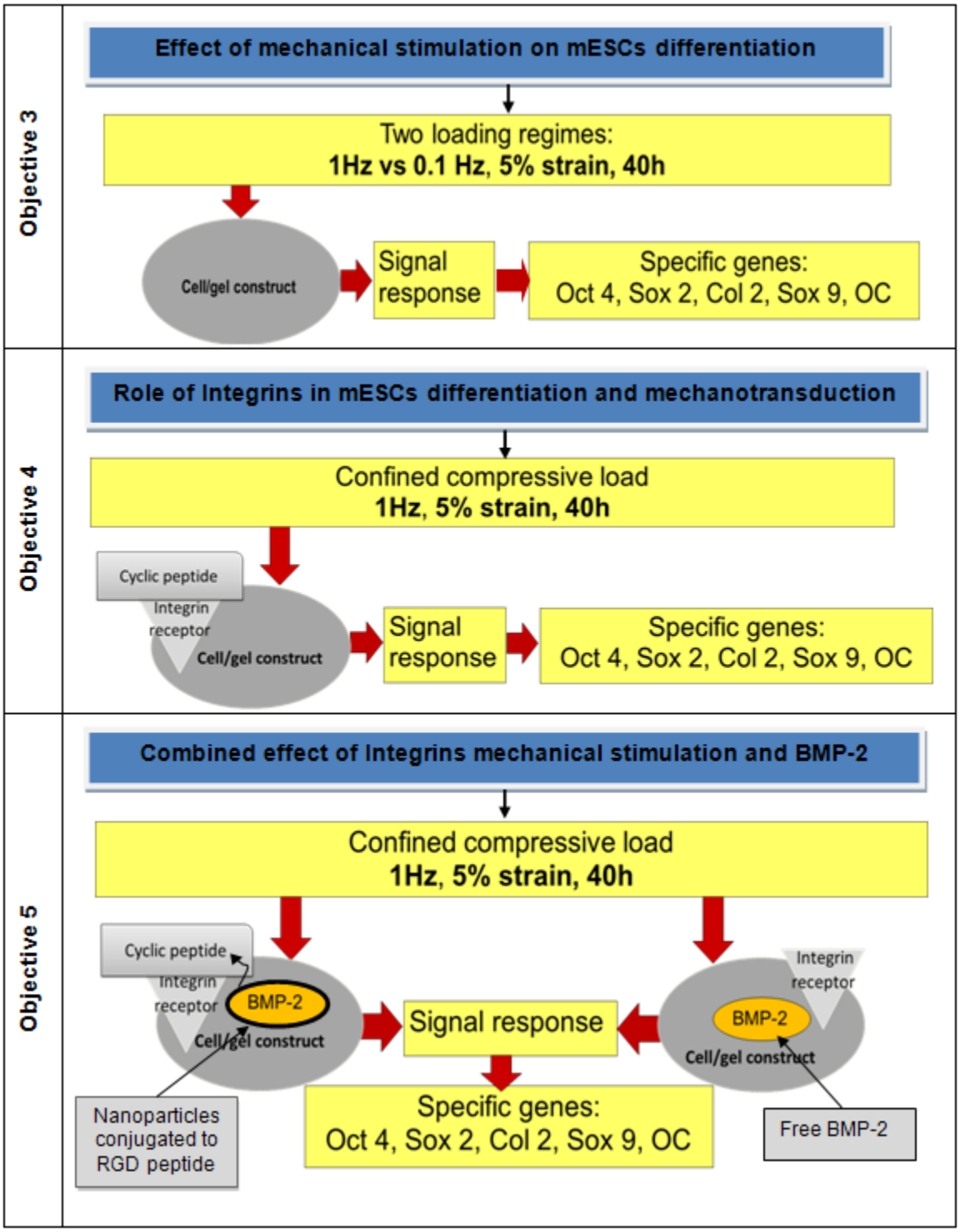

Figure 1.1: Overview of techniques and approaches used within each objective.

Micro CT image was kindly provided by Jaymi Taiani, PhD.

The remaining thesis is organized into seven chapters. The second chapter provides a summary of current literature relevant for this project. Chapter 3 focuses on the design and characterization of the loading system, including an example of system characterization as needed for objective 1. Chapter 4 outlines material and methods which were used throughout the experiments. The further characterization of the cell/gel construct (objective 2) and the effect of mechanical stimulation on mESCs differentiation (objective 3) are described in chapter 5 and chapter 6, respectively.

In chapter 7 the role of integrins in mediating differentiation (objective 4) and the combined effect of ECM, GF and mechanical stimuli (objective 5). Finally, chapter 8 provides a summary of relevant finding, conclusions and suggestions for future research.

CHAPTER 2: LITERATURE REVIEW

This chapter is subdivided into three parts. The first part provides an overview of the structure and function of bone tissue. The next section gives an overview of the requirements for using different scaffolds, cell types and the administration of GFs. Finally, the last part focuses on differentiation of mESCs induced by different cues.

2.1 Bone

The adult human skeleton consists of 206 bones, which differ in shape. Depending on their location and function, bones can be long, short, flat, or irregular. The skeletal system provides the body its structure, protects internal organs, enables mobility, stores minerals, and produces blood cells within the marrow (*20, 21*). To manage the complexity of these functions, bone tissue is organised in a hierarchical structure (*22*).

At the macroscopic level, bone is composed of cortical and cancellous tissues which differ mainly in their porosity and microstructure. Cortical bone forms a dense, solid frame that surrounds trabecular tissue (cancellous tissue) with a porosity around 5%-10% (*20, 23*). At the next level, cortical bone is composed of osteons which have a harvesian canal system containing blood vessels and nerve canals. The harvesian system is surrounded by concentric lamellae which are formed of collagen fibres. In comparison to cortical bone, cancellous bone forms a porous, sponge like meshwork with a porosity ranging from 50-90% (*23*). Cancellous bone does not have osteons on the micro structural level, but rather is formed of trabeculae and its lamellae are arranged longitudinally along the trabeculae. At the nanoscale, organic and inorganic

materials provide flexibility and strength. The organic matrix, responsible for flexibility, is formed from collagen molecules and other non-collagenous proteins such as bone sialprotein, osteonectin, and glycoprotein. The non-collagenous proteins are required for a healthy bone structure. For example, the presence of bone sialprotein and alkaline phosphotase is necessary for matrix mineralization and osteonectin regulates osteoblasts proliferation and growth (*20*). The inorganic component provides stiffness and strength and is primarily composed of hydroxyapatite crystals ($Ca_{10}(PO_4)_6(OH)_2$ (*24, 25*).

There are at least five cell types involved in the formation, maintenance and repair of bone:

- Osteoblasts: bone forming cells which produce proteins and proteoglycans,
- Osteoclasts: bone resorption cells through the release of acids and proteolytic enzymes,
- Osteocytes: bone maintaining cells originating from osteoblasts and constitute 90% of all bone cells and are believed to play a role in bone mechanotransduction,
- Bone lining cells: inactive osteoblasts that can be activated on demand,
- Osteoprogenitor cells: derived from mesenchymal stem cells (MSCs) found in the bone marrow, these cells differentiate into osteoblasts.

Osteoblasts, bone lining cells and osteoprogenitor cells reside within the periosteum. The periosteum covers bone tissue, separating it from its surroundings and is important

for bone growth and repair. The periosteum has an outer, fibrous layer and an inner, cellular layer. The endosteum is another cellular layer that lines the marrow cavity and covers the trabeculae. It consists of osteoprogenitor cells, osteoblasts and the majority are osteoclasts. Osteocytes are involved in the maintaince of bone tissue and thus are distributed across the bone extracellular matrix (*20, 24, 25*).

2.1.1 Formation and Remodelling

Bone formation occurs by replacement of a pre-existing tissue; this can occur during embryonic development or after bone fracture. When replacing hyaline cartilage, bone forms through a process known as endochondral ossification. Replacement of mesenchyme tissue is known as intramembranous ossification. In the process of endochondral ossification, chondrocytes produce cartilaginous tissue, which is followed by initiation of vascularisation, and finally cartilage is replaced with trabeculae bone. Over a period of several months bone remodelling continues and trabecular tissue is replaced with compact tissue (*24*). This process of bone formation and remodelling is determined by the interaction of osteoblasts and osteoclasts; osteoclasts remove old bone and provide space for new bone deposited by osteoblasts.

The bone remodeling process can be subdivided into four stages: 1) activation, 2) bone resorption, 3) reversal and 4) bone formation (*20*). During the activation stage, osteoclast progenitor cells are recruited to the site where new bone formation is needed. These progenitor cells fuse to multinucleated osteoclasts and begin the bone resorption process. This process starts when osteoclasts secrete acidic factors such as metalloproteinase's and acid phosphotase to digest bone tissue and upon completion

osteoclasts undergo apoptosis. The reversal stage is also known as the transition phase. During this stage, osteoprogenitor cells are recruited to the site where bone resorption took place to form new bone. During this process, osteoblasts release new collagenous matrix following by matrix mineralization. The released matrix surrounds osteoblasts and they become osteocytes, the bone maintaining cells. Approximately 50% of osteoblasts become osteocytes and the remaining cells undergo apoptosis. The process of remodelling is tightly regulated by the activation of RANKL and osteoprogenirin that are important in regulating the rate of bone resorption and formation (*20, 26*). The remodelling process is especially important in maintaining bone mechanical strength and can be activated in response to conditions such as loading (weight bearing activity), hormones (estrogens), and mineral balance (fluoride, calcium level).

2.1.2 Bone Diseases and Current Treatment Strategies

Bone diseases and failure can be a result of hormonal (osteoporosis), genetic (osteogenesis imperfecta), or idiopathic (Paget's disease of bone) reasons, due to a lack of weight bearing activities or as a natural part of the aging process. Regardless of causation, all of the above lead to a weaker and thinner bone structure and as a consequence increased fracture vulnerability to bone fracture (*4*). Different fracture types exist that can be classified as open or closed fracture and as union and non-union (*27*). Open fractures affect the surrounding tissue and project through it. They are more dangerous in comparison to closed fractures due to the risk of infections. Closed fractures are internal and occur without penetrating the skin. In a union fracture,

the broken ends are still connected and in a non union fracture the two ends are separated or disconnected from each other. In union fractures, bone has the ability to regenerate itself, whereas the non union fractures and defects due to cancer resections and trauma are the difficult to heal fracture types (*27, 28*). During the natural healing process, a cascade of events occurs that stops the bleeding through the adhesion of platelets to the injury site and the formation of a fibrous clot. In the reparative phase callus formation occurs. The inactive progenitor cells found in the periosteum and endosteum are activated and form a callus by differentiating into chondrocytes and osteoblasts. A callus is a configuration of connective tissue and cartilage tissue and is necessary to stabilize bone. It is also provides the first connection between the broken bone parts. Then, the callus hardens and remodelling occurs to replace trabecular bone with compact bone. The smooth process of injury healing depends on physical and biological factors such as proper fracture stabilization and the presence of GFs, hormones, adequate nutrient transport to the injury site, and mechanical stimulation (*29, 30*). In non unions, delayed fracture repair, or in elderly populations the natural healing process is interrupted and the stimulation of bone regeneration is required. From all fractures occurring, approximately 15% are difficult to heal (*27*).

The current standard treatment strategies for difficult bone fractures include autologous bone graft transplantation, the use of artificial and synthetic graft materials with or delivery of biological agents (*27, 30*). The advantage of autologous transplantation is the reduced possibility of immune rejection but possesses the disadvantage that only a limited amount can be taken from a patient without causing morbidity. So far,

autologous transplants are most commonly isolated from the pelvis and although autologous treatment is used with noteworthy success it has been shown that the harvesting procedure leads to complications in about 20% of the patients (*30*). Artificial and synthetic materials can provide stability to diseased bone but can lead to infection and implant failure. The use of biological agents such as BMP-2 and vascular endothelial growth factor (VEGF), platelet-derived growth factor (PDGF) have shown to promote bone healing. The biggest problem associated with biological agents is the lack of understanding about the mode, the time and the dose of delivery(*30*).

Annually, 250,000 graft transplantations are undertaken in the United States (*27*), and this number is increasing with the rise in the population ageing which subsequently leads to the need of more graft materials and alternative treatment strategies. One research area falls within the realm of TE that aims to develop new graft materials, in combination with cells and biological agents and thus is the focus of the next section (*31, 32*).

2.2 Tissue Engineering

TE aims to develop functional tissue substitutes which can restore and replace diseased tissues or stimulate new tissue formation. To achieve this goal, TE follows a multidisciplinary approach by integrating engineering and biological sciences. For musculoskeletal applications, TE combines osteoinductive cells and/or bioactive molecules and osteoconductive scaffolds to replicate an *in vivo* environment. To develop successful TE treatments will require an understanding of the behaviour and response of the potential tissue substitute to extrinsic and intrinsic signals that occur *in*

vivo (*23*). The general considerations for cells, scaffolds and GFs are briefly summarized in this section.

2.2.1 Cells

The choice of cell source and cell type is a critical component for the development a successful TE construct. The best choice appears to be the use of cells from an autologous source, meaning that the donor is also the recipient of the cells (*4, 33*). Autologous sourcing has the advantage of non-immunogenicity (*31*). However, limitations arise from the fact that the patient cells may not be useful due to pathological conditions and, in practice, relatively low numbers of fully matured cells can be isolated and expanded. The limitation of low cell number can be overcome with the use of a xenogeneic source where cells are isolated from other species and transplanted into the injury site. This would enable a greater number of potential cells to be transplanted, however, this may lead to problems of immunogenicity (*23, 34*).

Independent of cell source, mature cells or SCs can be used. The use of mature cells (i.e. osteoblasts) for bone TE may not be optimal due to possible pathological conditions. Thus, much research is directed to the use of SCs. SCs have the ability to self renew and to differentiate into a variety of cell types. Adult stem cells (ASCs) can be isolated from various adult tissues such as bone marrow, cartilage, periosteum, fat aspirants and placenta. These cell types have the ability to differentiate only within their lineage i.e. MSCs can give rise to osteoblasts , chondocytes, adipocytes and others among their lineage (*33*).

Another cell source is ESCs. ESCs are derived from the inner cell mass of a blastocyst. At this stage, the cells are pluripotent and can differentiate into all three germ layers: the ectoderm, the mesoderm and the endoderm (*35*). The benefits of unlimited cell number, high self-renewal potential and the ability to obtain tissue-specific cells make ESCs a unique cell source. Despite ESCs properties, many issues arises with this cell type. The use of human ESCs has generated many ethical issues. ESCs potential to form all cell types of the body is also a hurdle because ESCs possess the capacity to spontaneously differentiate into many cell types, in addition to the cell type of interest (*33*) and if ESCs are not completely differentiated this can result in teratoma formation (*36*). Therefore, it is still necessary to improve techniques to selectively distinguish specific and fully differentiated cell types from others.

2.2.2 Scaffolds

Scaffolds manufactured from various biomaterials, provide the architectural basis (template) to the human tissue undergoing treatment. This means that ideally their characteristics should match those of the living tissue. A gold standard scaffold should 1) be biocompatible (i.e. the implanted scaffold adapts and interacts with the living tissue without causing an immune response); 2) be biodegradable (i.e. the implanted scaffold is completely replaced by the ECM, meaning that the TE scaffold degrades while new tissue formation occurs); 3) possess suitable porosity to allow cell migration and interaction (porosity is also important for vascularisation, diffusion of nutrients and waste removal), and 4) possess mechanical properties that match those of living tissue. Salgado et al. (*23*) summarized the variety of materials used for BTE, along with the

advantages and disadvantages of each. Metals and ceramics have the disadvantage of being non-biodegradable. However, ceramics have been successfully used due to their osteoconductive and osteoinductive properties. The main disadvantage with the use of ceramics is that the degradation rate is unpredictable and therefore this type of material is not useful for large bone defects. The authors propose polymers from natural (collagen, fibrin, chitosan, starch etc.) and synthetic (poly(a-hydroxyacids), poly(e-caprolactone), poly(propylenefumarates), poly(carbonates) origins as an optimal biomaterial for bone TE. These materials have low immunogenic potential, allow cell attachment and host tissue interaction, are bioactive and easy to obtain.

2.2.3 Growth Factors

The combination of cells with matrices may not be ideal and the incorporation of additional biologics may be required to develop a functional TE construct. GFs are signalling molecules that are secreted by cells to initiate various cellular responses such as cell proliferation, migration, differentiation, apoptosis, and/or survival. *In vivo*, GFs act in a paracrine signaling mechanism and thus affect the neighboring cells. Due to their action on just neighbours GFs have a very short half life (which may be just minutes). Moreover, GFs are very temperature, pH, and pressure labile. Due to these characteristics, local administration of soluble GFs into the blood stream has had little success as GFs do not reach target cells. Furthermore, the direct administration requires a high concentration dose which can have a negative effect on tissue regeneration. The encapsulation of GFs in scaffolds by either chemical immobilization or physical encapsulation enables the possibility to stabilize GFs and control their

release rate by changing the porosity of the deliverable material (*12*). The use of nanoparticles (NPs) for physical encapsulation is of advantage because they can pass natural barriers occurring in the body and penetrate deeper in the tissue. Moreover, the use of nano size particles improves GFs diffusion, activity and release rate in comparison to other techniques (*37*). Furthermore, the replacement of harsh solvents with safer solvents and chemicals make the use of NPs attractive for TE therapies.

To stimulate bone regeneration, different GFs have been studied (i.e. fibroblast growth factor (FGF), PDGF, insulin-like growth factor 1 (IGF-1), osteogenic protein-1, parathyroid hormone, etc.) from which the different types of BMPs and transforming growth factor beta 1 (TGFβ-1) consider special attention (*27*). There are 7 types of BMPs with osteoinductive properties from which BMP-2 and BMP-7 have already undergone a clinical trial with a positive outcome when incorporated into collagen sponge and collagen matrix (*12*). This clinical trial showed an 80% success rate, however, the obtained results were not consistent and the dramatic increase in cost makes this type of therapy currently commercially unavailable.

2.3 Embryonic Stem Cell Differentiation

Increasing attention has been directed towards the use of ESCs for regenerative medicine due to their capabilities to differentiate into 210 different cell types of the body including osteoblasts and chondrocytes. Initial results of their use were encouraging but it quickly became clear that ESCs have tumorgenic potential if not completely differentiated (*38*). In static culture, mESCs proliferate while maintaining their ability to

differentiate in the presence of leukemia inhibitory factor (LIF) or on feeder layers (*39*). After removal of LIF, mESCs differentiate spontaneously and randomly into all three germ layers. Similarly, during teratoma formation cells from all three germ layers can be observed (*40*). Therefore, it is of crucial interest to find signals to initiate specific lineage commitment. The following section focuses on mESCs differentiation toward osteogenic and chondrogenic cell lines as a result of chemical, ECM mediated and mechanical cues, and later describes the importance of the synergistic interplay of these factors.

2.3.1 Media-Induced Differentiation

A common method to induce osteogenic and chondrogenic differentiation is the formation of embryoid bodies (EBs). EBs form a spherical shape in suspension culture forming the mesoderm which contains progenitor cells for skeletal tissue formation. Specific differentiation is induced through supplementation of osteogenic or chondrogenic factors (*35*). Osteogenic differentiation of mESCs grown in static culture has been successfully induced in the presence of β-glycerolphosphate (βGP), vitamin D3, dexamethasone, retinoic acid and ascorbic acid (*41-43*). The induction of mESCs differentiation into any cell type is associated with the up regulation of gene expression characteristics for an osteogenic phenotype. Some of the major genes and proteins important for maturation of mESCs towards osteoblasts are summarized in Table 2.1.

Table 2.1: Genes and proteins involved in osteogenesis (*41, 44*).

Gene/Protein	**Function**
Alkaline Phosphatase (ALP)	-Expressed at an early stage of differentiation -Glycoprotein -Induces mineralization
Collagen I (Col I)	-Early stage protein -Most abundant protein in bone tissue -Structural function
Osteonectin (ON)	-Most abundant non-collagenous protein in bone tissue -Binds calcium and hydroxyapatite during mineralization -Modulator of cell matrix interaction -Expressed in numerous cells
Osteopontin (OPN)	-Early stage ECM protein -Bind calcium and hydroxyapatite during mineralization -Expressed by a variety of cells in the body
Bone sialprotein (BSP)	-Late stage ECM protein -Nucleator for mineralization
Cbfa1/Runx-2	-Transcription factor

	-Activates gene expression of Col I, OPN, BSP and OC or their promoters
Osteocalcin (OC)	-Final stage bone matrix protein -The only true osteoblast-specific marker -Recruitment of osteoclasts
Osterix (OSX)	-Transcription factor
BMP-2	-Involved in tissue repair and remodelling -Potent inducer of osteogenesis

The expression of these markers is temporally regulated and specific for three distinct, phases of osteogenesis. The first stage involves cell proliferation, ECM secretion encompasses the second stage and matrix mineralization characterizes the late stage of osteogenesis. The regulation of these processes requires temporal and consecutive activation and the interplay of genes and proteins (*41, 45*)

In addition to osteoblasts, chondrocytes which make cartilage represent another important cell source for bone formation, considering that during endochondral bone development cartilage is formed as an intermediate step (*35*). Similar to osteogenic differentiation, chondrocyte differentiation requires the supplementation of exogenous factors such as ascorbic acid, dexamethasone, vitamin D3, thyroid hormone and other factors (*46, 47*). Interestingly, similar factors described for osteogenic differentiation are utilized for chondrogenic induction. This is most likely because osteogenesis and

chondrogenesis are closely related in skeletal development although the latter is regulated by the expression of different genes and proteins which are summarized in Table 2.2

Table 2.2: Genes and proteins involved in chondrocytes differentiation (*48*).

Gene/Protein	**Function**
Sox 9	-Transcription factor -Acts downstream of chondrogenic differentiation
Aggregan (Agg)	-Proteoglycan -Expressed by a variety of cells in the body -Links ECM and helps to resist compression
Collagen 2 (Col 2)	-Major natural collagenous protein in cartilage

The differentiation potential of different cell types into osteogenic and chondrogenic lineages are evaluated on the above described transcription factors (TF) and matrix proteins (*44, 48, 49*).

2.3.2 Extracellular Matrix-Mediated Differentiation

The human body is organised in a hierarchical order where cells represent the basic unit of the body forming the tissues and organs. One of many cell functions is the synthesis, secretion and modification of the ECM. Together, the ECM and cellular components form the complex and dynamic tissues of the body (*31*). The interaction between cells and the ECM occurs via specific cell surface receptors called integrins.

Integrins are transmembrane receptor proteins which bind with their alpha/βeta domains to fragments of ECM on one side and to the intracellular cytoskeleton network, formed through actin filaments on the other side.

The interaction of cells with the ECM plays an important role in determining cell functions such as cell migration, proliferation and differentiation (*31, 50, 51*). Moreover, to initiate these functions, activation of signalling pathways can be regulated bi directionally, from outside to the inside and vice versa (*52*). Outside-in signalling occurs by binding of a ligand (typically an amino acid sequence of ECM to the integrin ECM domain leading to integrin protein conformation changes and activation of focal adhesion complexes. The focal adhesion complex is directly linked to the actin cytoskeleton, and the actin cytoskeleton to the cell nucleus, this can induce a signal response. Inside-out signalling requires first the activation of integrins from the inside of the cell which show low affinity to their ligand and upon activation shift to high affinity (*51, 52*). To date, 18 alpha and 8 βeta integrin subunits have been identified which form 24 integrin constellations as shown in Figure 2.1.

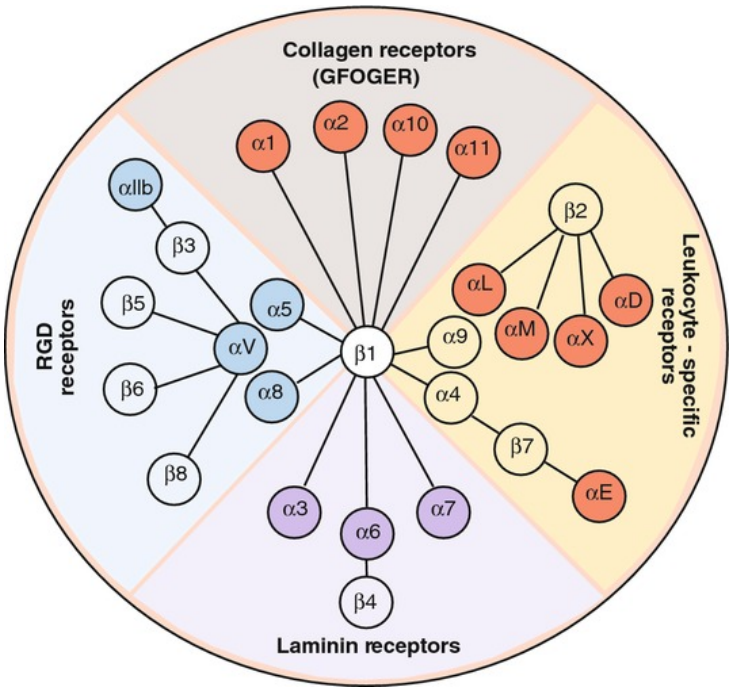

Figure 2.1: Different alpha and βeta integrin subunits form up to 24 integrins which recognize specific sequences in the ECM. With permission (*51*).

Integrins can be subdivided into four ligand binding groups based on integrin recognizing sequences in the matrix. The cell recognizing sequences in different types of collagens are GFOGER or DGEA, and RGD in fibronectin, vitronectin, and fibrinogen, respectively (*53*). The interaction of cells with the surrounding matrix is crucial for cellular processes and functions which can be regulated differently depending on the ECM characteristics such as matrix type, geometry or stiffness (*54*).

The discovery that matrix stiffness can influence SCs commitment revolutionized the field of TE (*55-57*). Matrix stiffness can influence the degree of integrins binding which can lead to diverse signal transduction pathways. This mechanism is attributed to the ability of cells to generate intrinsic tensional forces by contracting or pulling on the

matrix (*54*). Based on this, it is believed that mechanical properties coincident to a specific tissue will guide SCs differentiation into their particular cell type. The tissue specific elastic properties of several tissues are summarized in Table 2.3.

Table 2.3: Tissue specific ECM and its elastic properties ranging from soft to rigid as measured by atomic force microscopy (*54*).

Tissue	**Elasticity, E (kPa)**	**Characteristics**
ESC	~ 0.2-0.3	Compliant or soft
Endoderm	~ 0.1-0.3	Soft
Mesoderm	~ 0.5-1	Soft
Nerve	~ 0.5-1	Compliant
Skeletal muscle	~ 8-17	Semi-compliant
Demineralised bone	> 30	Rigid or stiff

A variety of studies reported that matrix compliance can influence cell differentiation into a specific lineage. For example, Huebsch et al. (*55*) showed that murine MSC differentiate into an osteogenic lineage when encapsulated into alginate polymers with a matrix moduli of 11 to 35 kPa whereas a matrix moduli of 5 kPa can direct adipogenic differentiation.

2.3.2.1 Collagen-Based Scaffolds

Collagen proteins can be found in a variety of different tissues including skin, tendons, bone and cartilage. Twenty nine distinct tissue-specific collagen molecules have been identified to date. Among these collagens, collagen type I is the most commonly used natural polymer in BTE applications (*58*).

Collagen scaffolds resemble the natural environment for cells by supporting their growth, attachment, migration and differentiation (*18, 58-60*). Furthermore, their use is promising because of their biocompatible and biodegradable properties and porous structure which allows nutrient and gas exchange (*61*). In general, α1β1 and α2β1 integrins are specific in recognizing collagen matrix sequences and might control cell functions such as cell differentiation. However, the precise mechanism of integrin-mediated cell differentiation is not completely understood. It seems that the β1 subunit is predominant in controlling cell attachment (*62, 63*) but has no regulatory effect on mESCs differentiation (*62*). However, blocking the α2 subunit inhibits matrix contraction in mature osteoblasts and leads to a down regulation of osteogenic gene expression (*64*), and reduced matrix synthesis in MSCs (*65*). Several studies have confirmed the positive effect of 3-D collagen matrix-induced differentiation of cell types taken from different origins and stage of differentiation into osteogenic lineage. However, it has also been found that collagen induces heterogeneous cell differentiation into cell populations of osteogenic, chondrogenic, adipogenic and myogenic lineage, and additional factors are required for the final lineage commitment (*66*). A summary of previous studies, focusing on the role of collagen-mediated cell differentiation and in particular on collagen dependent integrins is provided in Table 2.4.

Table 2.4: Collagen scaffolds seeded with different cell types to initiate osteoblast differentiation.

Reference	**Matrix**	**Cell Type** **Cell Density**	**Aim**	**Significant Findings**
Krawetz, 2012 (*18*)	Col I 3mg/ml bovine from skin	mESCs $1x10^6$ cells/ml	Differentiation into osteogenic and chondrogenic lineage	Collagen gel polymerized with βGP or chondrotin induces osteogenic and chondrogenic differentiation, respectively.
Evans, 2010 (*62*)	ECM secreted by osteoblast or col I surface 2.2. mg/ml	mESCs 30,000 cells/cm^2	Effect of bone-specific ECM and Col I on mESC differentiation and role of integrins	Col I induce mESCs differentiation into osteoblast. Soluble RGD decreases cell attachment to Col I and inhibits differentiation. β1 is critical for cell attachment but has no effect on mESCs differentiation.
Warstat, 2010 (*63*)	Col I or Laminin	human bone marrow cells (hMSCs)	Degree of hMSCs attachment to Col I w/ or w/o Tgfβ1	β1 necessary for cell attachment to Col I α2β1regulates hBMSCs attachment to Col I, regulated by Tgfβ1.
Parreno, 2008 (*64*)	Col I 3 mg/ml bovine from skin	osteoblast like human MG-63 $5x10^5$/ml	The interaction of osteoblast like human MG-63 cell with type I collagen matrix	Collagen gel enhance osteoblastic phenotype by increasing osteocalcin level. α2 integrin important for collagen contraction and initiating intrinsic signals.
Mizuno, 2000 (*65*)	Col I 0.35 % calf from skin	rat bone marrow stoma cells (rMSCs)	Differentiation into osteogenic lineage	Collagen gel induces osteogenic differentiation. Mineralized nodules detected on day 12 Blocking α2 integrin downregulated ALP and Col1 synthesis.
Lund, 2009 (*66*)	Col I 2mg/ml calf from skin	hMSCs $1x10^6$ cells/ml	Role of Col I in osteogenic differentiation and ERK pathway	3-D collagen gel enhances and accelerates hMSCs osteogenic differentiation and induces chondrogenic gene expression, resulting in a heterogenous cell population. Blocking ERK enhances differentiation.
Fernandes, 2009 (*67*)	Culture in presence of BAPN which inhibits collagen crosslinking	mouse osteoblast precursor cells (MC3T3) and hMSCs	Effect of collagen crosslinking on MC3T3-E1 cells and hMSCs	BAPN inhibits osteogenic differentiation and matrix mineralization in MC3T3 but had no effect on hMSCs differentiation, indicating different regulatory mechanism.

2.3.2.2 β-Glycerol Phosphate Polymerization Agent

Collagen for biomaterial applications is usually isolated from tissues using proteolytic enzymes such as pepsin. Pepsin removes the telo-peptide regions, located at the N-and C-terminus of collagen molecules and lead to the formation of soluble collagen aggregates which can be preserved in soluble form in acidic buffer solutions at low temperatures (4ºC). Collagen has an equivalent structural composition of acidic and basic side-groups; the electrical charge thus being neutralized at physiological pH values. This feature is important in collagen fibril formation due to the interaction of the acidic and basic side chains that form a salt. Consequently, during exposure to physiological pH and room temperature values, soluble collagen spontaneously polymerizes and rebuilds its native fibril structure, in a process also known as fibrillogenesis (*68*).

Recently, beta glycerol phosphate (βGP) has been proposed and identified as a possible crosslinking agent that can be supplemented to acid soluble polymers. The weak basic properties of βGP neutralize the pH when mixed with an acid soluble polymer and subsequently lead to protein self assemble. In addition to pH, temperature appears to be another important gelation parameter (*69*). It has also been reported that the addition of βGP can increase the strength of a scaffold mixture between βGP, collagen and chitosan via ionic interaction. It appears that under acid condition an ionic interaction occurs between the ($-NH^{3+}$) of the collagen chain and the polyanionic group ($-OPO(O^{-})_2$) of βGP (*70*). During pH neutralization, new hydrogen bonds are formed leading to collagen fibril crosslinking and thus increased material strength.

Additionally, βGP is supplemented in cell culture media to induce osteogenic differentiation in static culture (*41*) and is a stimulator of mineralization in the presence of an intact ECM by providing a phosphate group to form calcium phosphate salt (*71*). Not surprisingly, collagen scaffolds polymerized with βGP have been shown to induce osteogenic differentiation (*18*).

2.3.3 Mechanical-Mediated Differentiation

Mechanical stresses associated with compression, tension, and fluid flow, are important during embryo development and in maintaining the functionality of living tissue throughout life. For example, in the developmental stage of the skeleton, cartilage is encapsulated by the perichondrial membrane, the relaxation of which leads to changes in tissue growth. Tension also plays an important role in the skeletal system, where tendon and muscle contraction result in bone movement (*72*). Bending loads on bone lead to stretching of the osteocytes biaxially within the canaliculae, resulting in the cyclic movement of extracellular fluids. The emerging pressure gradient conducts fluid flow from the compression site to the tension site, thus leading to shear stress (*73*).

The ability of cells to adapt and change their functions according to mechanical stimuli is known as mechanotransduction. Mechanotransduction is the process by which mechanical signals are transduced into biological responses. Stresses such as tension, compression, pressure and shear force may be sensed via the cell interior through cell surface receptors such as integrins, G-protein, Stretch activated ion channels, receptor

tyrosine kinases, and mitogen activated protein kinases, and can ultimately lead to changes in cell functions (*74*) as shown in Figure 2.2.

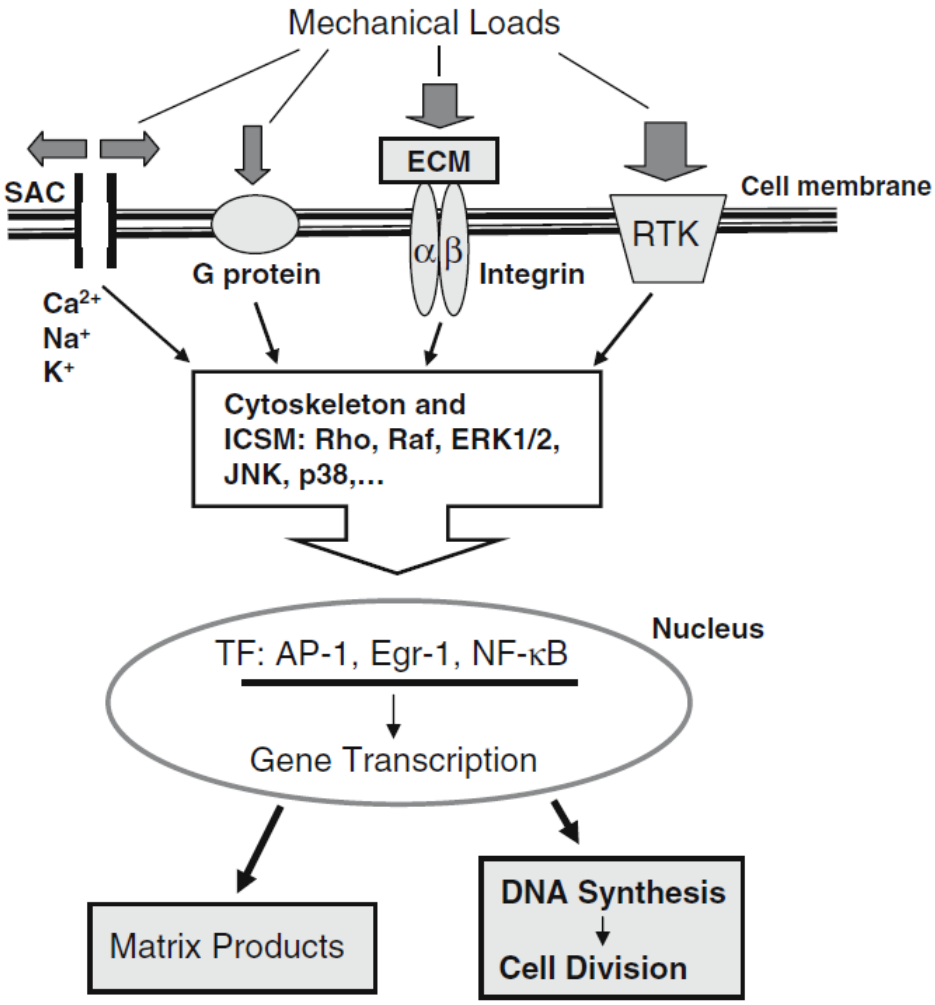

Figure 2.2: Mechanotransduction occurs via mechanosensitive cell surface receptors such as integrins, G-proteins, stretch-activated ion channels, and receptor tyrosine kinases (RTK) activating intracellular signalling which can cause a cellular response on the transcriptional level leading to changes in cell function i.e. matrix production. Figure adapted from Wang et al. (*75*) with kind permission from Springer Science and Business Media.

The mechanism of mechanotransduction is not fully clear, it is known that the reaction of cells depends on the constitution of the applied load. Therefore, variations of the load duration, magnitude and frequency consequently lead to different cell biosynthetic responses. In general, bone and cartilage related studies have examined cellular responses in a strain range of 1%-20% and a frequency between 0.1-1 Hz (*76*). Overall, it appears that lower strain and frequency regulate MSCs differentiation towards osteoblasts whereas higher strain and frequency trigger chondrogenic differentiation (*77*). This is not surprising considering that strains in human tibia are around 0.2% and cartilage can undergo compression to 10% (*78, 79*). In addition to the loading regime, the type of load applied is important in directing specific differentiation.

Among other loading types, tensile loading has been extensively studied on osteoblast functions and SCs commitment towards bone (*80*) and compressive loading has been more the focus of cartilage formation (*81*). Both types of applied loads can differentially regulate cell functions by changing their gene expression and cell morphology. For instance, compressive stress has been shown to change cells to aligned parallel to the direction of load (*81*) while tensile stress showed morphological variation depending on the location within the scaffold. Different cell morphologies could mean different cell types and thus lineage commitment towards a heterogeneous cell population (*76*).

The above described studies applied cyclic loading where the force (stress) is changing over time periodically. In contrast to cyclic loading, the force is kept constant over time in static loading. Static compression has been shown to inhibit matrix production or had no effect on gene expression (*82*), while others have reported that gene expression

changes directly proportional to the magnitude of static strain (*83*). Selected publications on the effect of mechanical stimuli on osteogenic and chondrogenic differentiation are summarized in Table 2.5.

An interesting study has been performed by Maul et al. (*84*) by systematically evaluating the influence of changing all the parameters of a loading regime (duration, magnitude and frequency) including the type of force (stretch, pressure and shear stress) on MSCs differentiation. Although the primary focus was on MSCs endothelial differentiation, this group evaluated other genes specific for muscles, skin, fat, bone, and cartilage in response to loading type and duration. Cyclic tensile stretch for 72 hours and laminar shear stress for 24 hours initiated the highest expression of bone related markers. Gene expression specific for MSCs chondrogenic differentiation was predominant after 24 hours cyclic pressure, whereas cyclic tensile stretch for 72 hours and laminar shear stress for 24 hours had a moderate to diminishing effect respectively on chondrogenic gene expression. This study and others show that cells can adapt and differentiate towards a specific cell line depending on the particular loading regime and loading type. However, the fundamental mechanism to mechanically induce differentiation has not been found, mainly because these studies are difficult to compare and the underlying processes complex with built-in redundancies. The use of different cells, with a distinct cell origin (i.e. human vs. mouse), culture conditions (i.e. complex vs. defined media), and stage in the differentiation process (i.e. ESCs vs. MSCs) can all contribute to varying responses. Therefore, it appears that for the development of successful TE engineering constructs, the cell response to mechanical stimuli requires individual

consideration and an understanding of the underlying mechanism of how integrins and other mechanosensors transduce the mechanical signals to a particular response.

Table 2.5: Effect of mechanical forces on cell differentiation into osteogenic and chondrogenic lineage.

Reference	**Matrix**	**Cell Type Cell Density**	**Loading Regime**	**Loading System**	**Aim**	**Significant Findings**
Ignatius, 2005 (*80*)	Col I 3 mg/ml rat tail	human fetal osteoblast (hFOB) $1.5x10^5$/3ml	cyclic stretch 1%, 1Hz 30min/day for 3 weeks	Custom made	Effect of strain on osteoblastic genes over longer period of time	Cells proliferated, synthesized new ECM and expressed osteogenic genes on Col I In stretched samples, proliferation and gene expression upregulated
Terrachiano 2007 (*81*)	PEGDA hydrogel	MSCs from goat (gMSCs) and MSCs from hESCs (hMSCs)	Unconfined, cyclic compression 10%, 1Hz 1h/day for 3 and 6 days,	Custom built	Comparison between adult and embryonic derived MSCs w/ and w/o TGFβ1	Compressive force upregulate chondrogenic gene expression in gMSCs but down regulated in hMSCs. hMSCs need GFs supplementation additional to mechanical stimuli to initiate chondrogenesis.
Hunter, 2002 (*82*)	Col I 2 mg/ml Rat tail	bovine articular chondrocytes $1x10^6$/0.5ml	Static unconfined 0, 25 & 50% Cyclic unconfined compression 25%, 1Hz	Custom made	Changes in gene expression of chondrocytes to static and cyclic following static loading	Static compression inhibited matrix synthesis. Oscillatory cyclic compression had no effect on gene expression after static loading.
Takahashi, 1998 (*83*)	Col I 1.5 mg/ml calf skin	mouse embryonic limb bud MSCs $2.5x10^6$/ml	Static compression 1, 1.5 & 2kPa	Weights on top of gel	Effect of static compressive load on chondrogenesis	Compressive force promotes chondrogenic differentiation. Col 2 expression level directly corresponded to level of strain.
Au-Yeung, 2010 (*85*)	Col I 2mg/ml Rat tail	hMSCs $1x10^6$/ml	10-15%, 1Hz 1h/day for 7 days	Custom made	Compressive loading on hMSCs ECM production	Unconfined compressive loading had no effect on GAG production and chondrogenic gene expression of Col 2 and Sox 9.
Sumanasinghe, 2008 (*86*)	Col I 3 mg/ml	hMSCs $3x10^4$ & $6x10^4$ per 0.2ml	Tensile strain 10 or 12%, 1Hz 4 h/day for 7 /14 days	Flexcell FX-4000 strain	Cell density and media on contraction of hMSCs derived osteoblasts	Tensile strain increased cell contraction. Collagen gel with differential medium showed higher contraction in comparison to complete medium.

2.3.4 Combining Micro Environmental Cues to Guide Differentiation

As described, understanding the micro environmental factors which guide cell fate is important when trying to engineer functional replacements for living tissue. Factors associated with ECM, presence of GFs, external stimuli or presence of other cell types (*87*) are all interconnected and act in a temporal, spatial and sequential order in directing cell functions. In the past two decades much has been learned about how soluble, adhesive, and mechanical signals individually influence cell differentiation, however, our understanding on how these factors work together within the complex micro environment surrounding the cells *in vivo* is limited (*88, 89*).

The connection of the ECM and the cell interior occurs via integrins. This interaction leads to bidirectional interplay between the cell interior and cell exterior leading to the activation of the TF machinery and consequently to functions such as ECM remodelling and cell differentiation. Hsiong et al. (*90*) examined the integrin matrix interaction of SCs versus differentiated osteoblasts. SCs showed a high expression of αv and β1 subunits and only negligible expression of α5 and α2. When SCs initiated differentiation, the expression of αv subunits increased resulting in an up regulation of BMP-2 expression. BMP-2 morphogen is one of the best studied regulatory factors and has been shown to induce SCs differentiation and bone formation (*91, 92*). Furthermore, to induce human and mouse osteoblast differentiation, it has been shown that the interplay of αvβ, α1β1 and α2β1 integrins with BMP-2 was necessary (*93, 94*).

In addition to being involved in ECM-mediated signal transduction, evidence has emerged that Integrins, especially RGD-dependent integrins are involved in

mechanoregulation (*95*). For example, blocking RGD-dependent integrins and subjecting chondrocyte/agarose constructs to compressive load resulted in impairment of gene expression in contrast to loaded constructs that have free integrin receptors. Interestingly, this effect seemed to be frequency dependent. Cells changed their gene expression in an integrin-dependent manner at 1 Hz, however, a lower frequency of 0.33 Hz seemed to act via different mechanosensitive cell surface receptors. Moreover, it is well known that integrins and GFs can interact and modulate each other's response, and indeed, when MSCs are subjected to mechanical load then BMP-2 expression is highly up regulated (*91*). Overall, the understanding of GFs, ECM and external loading interaction could potentially help to understand the complex microenvironment which cells experience *in vivo* and contribute to more robust therapies.

Table 2.6: Summary of the interplay between ECM, GFs and/or mechanical stimulation.

Reference	**ECM mediated**	**Cell type**	**Growth factor mediated (concentration)**	**Mechanical mediated**	**Synergy**	**Significant findings**
Warstat, 2010 (*63*)	Col I	hMSCs	TGF-β1	N/A	GFs and ECM	α2β1 regulates hBMSCs attachment to Col I which is regulated by TGF-β1.
Fernandes, 2009 (*67*)	BAPN	MCT3-E1	BMP-2 (100ng/ml)	N/A	GFs and ECM	Functional ECM is necessary for ALP and calcium accumulation in response to BMP-2.
Chung, 2012 (*76*)	monolayer on Col I	MCT3-E1 murine pre osteoblast	TGF-β1 (2ng/ml) BMP-2 (50ng/ml) simultaneously	1, 3, 5,10% strain, 0.2Hz for 24 h	GFs and tensile stress (TS) on osteogenesis	Synergistic effect of TS and GFs on cell proliferation and on the expression OPN (1%), BSP (3, 5,10%), OCN (5%), Col I (5,10%) was loading mode dependent.
Kock, 2009 (*95*)	Agarose +RGD blocking peptide	Chondrocytes	N/A	15% strain, 0.33Hz and 1Hz for 12 h	Compressive load and RGD dependent integrins	In loaded constructs RGD integrins act as mechanotransducer but frequency dependent.
Lai, 2005 (*93*)	αvβ integrin	human osteoblasts	BMP-2 (100ng/ml)	N/A	Integrins and GFs	BMP-2 increased expression of αvβ and αβ1 and these Integrins overlap with BMP-2 receptors All αv integrins necessary for BMP-2 function

CHAPTER 3: LOADING SYSTEM DESIGN AND CALIBRATION

Cell types of load bearing tissues such as osteoblasts in bone, chondrocytes in cartilage or fibroblasts in tendons have been shown to alter their biosynthetic behaviour in response to mechanical environment. Consequently, when directing SCs differentiation into osteoblasts or chondrocytes, it is critical to understand how these cells response to a loading regime of interest. A variety of loading systems mostly applying compression, tension or shear stress have been developed to subject cells cultured in monolayer or seeded on biomaterials (*96, 97*). Collagen is one of the most commonly used biomaterials for bone tissue engineering because organic matrix of bone consists mainly of collagen type I. When a collagen scaffold is prepared by a fibrillogenesis or self-assembly process, the initial collagen network has a high liquid content (~97%) and low protein content (~3%), resulting in a 3-D matrix that is very soft with biphasic or viscoelastic properties.

The properties of a self assembled collagen scaffold can depend on cell interaction with the matrix because different cells can interact with the material by pulling on the matrix via integrins which leads to matrix contraction and thus changes in stiffness. ESCs on the other hand are mostly round shaped cells and although they interact with the surrounding matrix, they have a less well developed cytoskeleton (lower level of actin filaments in comparison to developed cell types) and thus exert little tensile forces on the matrix (*98*).

As the overall aim of this project is to investigate the effect of mechanical stimuli on mESCs seeded in collagen gel, the main challenge was to apply mechanical stimuli to a soft, viscoelastic scaffold. Only a few commercial loading systems are available and most of the loading systems are custom made for specific needs (*96, 99-101*). Therefore, the first objective of this project was to design and characterize a custom-built loading device capable of subjecting a soft viscoelastic scaffold to a confined compressive load. In the current project, the Flexcell™ system was chosen as a base and its primary loading chamber was modified.

3.1 Overview of the Flexcell Loading System

The Flexcell FX-4000™ system is designed to apply tension or unconfined compression to cells and TE constructs under a variety of mechanical conditions. It mainly consists of a control computer, Flexlink pressure control unit and up to four culture plates which are fixed within a clamping device during loading. A schematic diagram of the system is shown in Figure 3.1.

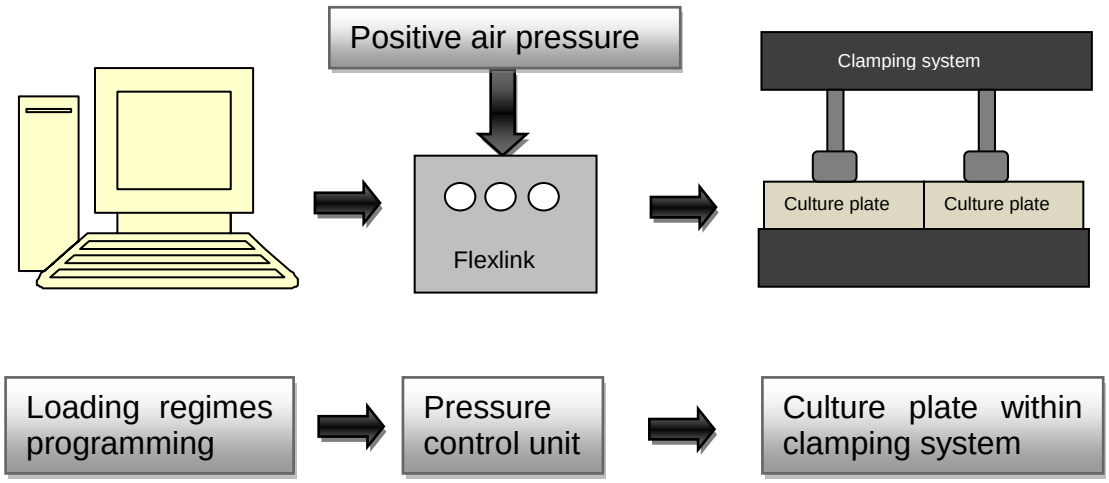

Figure 3.1: Schematic of the Flexcell system components: 1) control computer; 2) Flexlink pressure control unit; 3) culture plate within clamping system.

The Flexlink unit is programmed using the Flexcell software. Various regimes, such as static, sinusoidal, heart wave, triangular, square or a custom waveform with a frequency ranging from 0.1 Hz to 3 Hz can be specified. The Flexlink is the key component of the system which converts a specified air pressure into a compression regime. An additional pressure regulator (not shown in Figure 3.1) is provided in order to control the initial building source pressure which should not exceed 140 kPa. During loading, the BioPress™ compression culture plates are fixed in the clamping system and placed inside an incubator to provide physiological conditions. The clamping system has space for up to four 6 well culture plates and thus up to 24 samples can be loaded simultaneously.

3.2 Modification of the BioPress™ Compression Loading Cell

The BioPress™ compression culture plate consists of six wells. Each well contains a round platen which is fixed to a flexible membrane. On top of the platen is an attached foam ring which keeps the removable sample holder centric. The assembly of the Flexcell compression culture plate and an enlarged version of its corresponding well are shown in Figure 3.2.

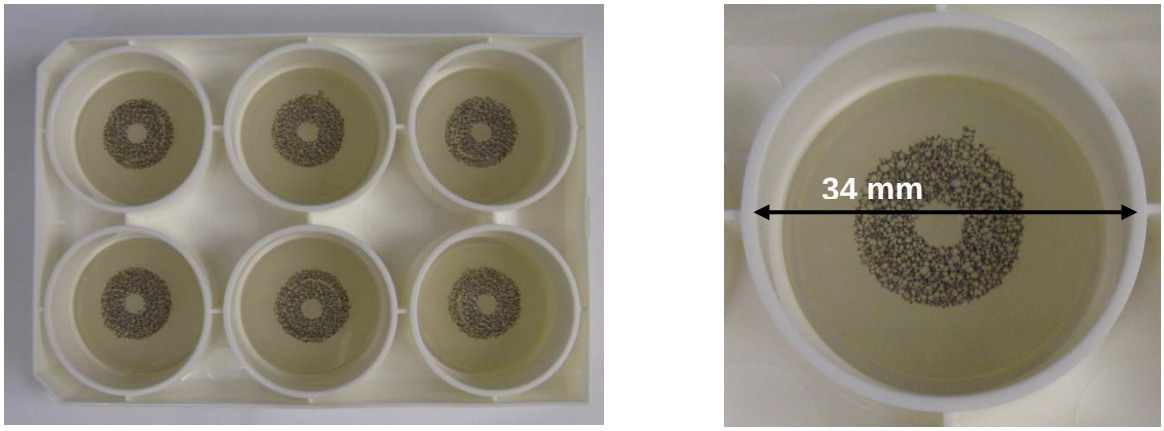

Figure 3.2: On the left side the BioPress™ compression culture plate is shown. The culture plate contains of 6 wells. For better illustration, the right picture shows a single well (34 mm) containing a foam ring with a sample holder.

As described, the collagen gels are soft (<0.1 MPa) and viscoelastic, therefore, the use of the Flexcell BioPress™ compression culture plates presented several limitations. It is assumed that when collagen gels are placed within the foam ring, compressive loads would cause the expulsion of liquid, which would not completely return to the collagen gels and they would dry-out during any lengthy investigation. The major limitation is related to the porous nature of the foam ring to which collagen fibrils could penetrate. Specifically, the gel could migrate through the pores of the foam and thus lose its form and function. This behaviour cannot be controlled and would lead to significant loading variations from sample to sample. Overall, the Flexcell BioPress™ compression culture plates are suitable to compress TE constructs which can maintain their own shape. Furthermore, when studying cell responses to mechanical stimuli the loading system should mimic as close as possible the *in vivo* environment.

Due to similarity of confined compressive loads to physiological condition in bone and the burr-hole fracture model (see Figure 1.1), the BioPress™ compression culture wells were modified. The modifications were achieved through replacement of the original platen by a custom designed one. A detailed technical drawing of this new culture platen is provided in Appendix A. The assembly of the modified Flexcell compression culture plate system and an enlarged version of one culture platen are shown in Figure 3.3.

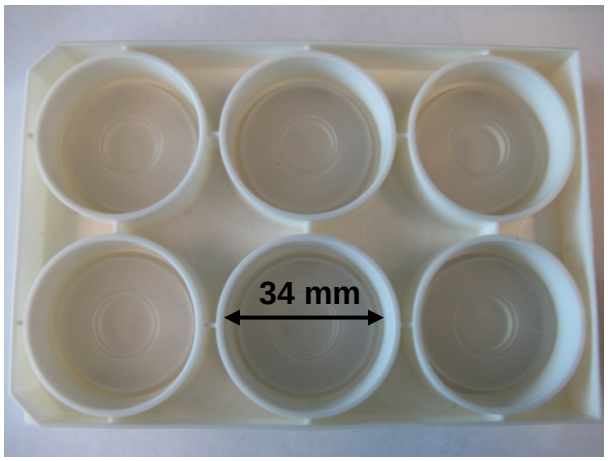

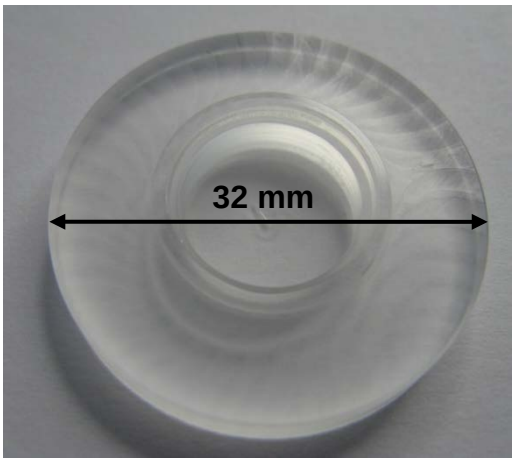

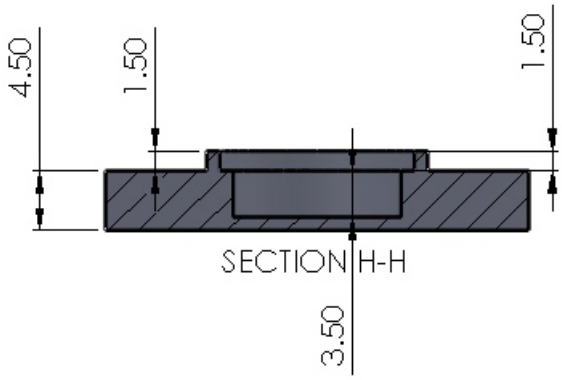

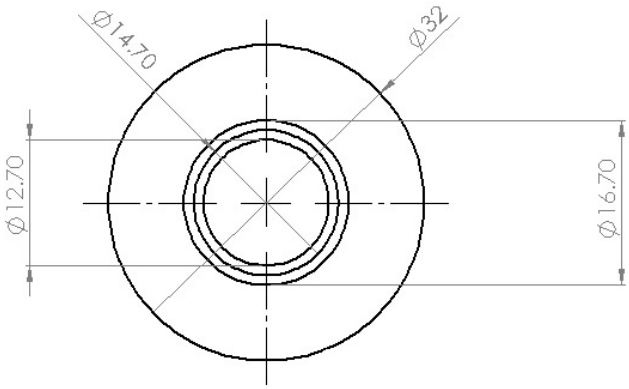

Figure 3.3: On the top left: BioPress™ compression culture platen with modified loading cell plates. On the top right: enlarged depiction of modified plate. On the bottom left: cross section of the chamber. On the bottom right: top view of the chamber.

The developed culture platen has the same outer dimension as the BioPress™ one of 32 mm and a height of 6 mm. To maintain confinement of the sample, the design incorporates an inner chamber with a diameter of 12.7 mm and a height of 3.50 mm. The chamber has an extension on the top in the form of a rounded edge which provides room for media and prevents its overflow. The diameter of this extension is 16.7 mm with a height of 1.50 mm. Furthermore, the original loading cell has a foam ring which allowed the sample expansion and media exchange. The modified system has a solid well and therefore a porous platen on top is required. This platen has to be solid to apply uniform compression loads but porous to enable oxygen and media exchange. For this purpose a platen (316L stainless steel, Mott Corporation) with dimensions of 12.7 mm in diameter and 3.175 mm height was chosen. The media grade of the platen is 10 which mean that 90% of solid particles of diameter greater 10 micrometer cannot pass through. Thus, a media grade of 10 allows media and oxygen penetration, but also ensures the gel surface remains intact.

In the next step we focused on fixation of the new developed culture platen to the membrane which transfers the applied air pressure to a compressive load. The original loading cell platen is glued to a membrane by an adhesive; the type and properties of this adhesive are proprietary to Flexcell company and unknown. Thus we required an adhesive that could stick to both the plexiglass plate and to the Bioflex membrane

(Silicone rubber, Durometer, Shore "A"), and at the same time satisfy the following specifications: 1) double coated; 2) high bond; 3) function at room temperature up to 40ºC; and 4) less than 0.5 mm thick and not a spongy material. All of the above requirements were fulfilled by an acrylic/silicone adhesive (#D5910, Champion Tape). The acrylic adhesive adheres to the plexiglass plate, and the silicone adhesive adheres to the silicone membrane. The specification data sheet can be found in Appendix B.

In summary, a system design was required that takes into account the gels soft, viscoelastic properties (confined compression), oxygen and nutrients penetration (porous platen) and allows us to apply both static and cyclic compression simultaneously (Flexcell system allows wide range of input parameters). To establish the feasibility of the modified system a pilot run was performed. Gels were subjected to confined compressive load at 1 Hz and 70 kPa for 4 hours. As shown on one gel morphology in Figure 3.4 after loading, a thin layer of collagen gel remained; the gels did not dry out but also did not maintain its viscoelastic properties. This was assumed to be due to lack of time to allow liquid to be drawn back into the gel and thus provide time for collagen gel recovery.

Figure 3.4: Collagen gel after dynamic loading in the modified system at 1 Hz and 70 kPa for 4 hour.

Based on these observations, additional modifications were required that would allow liquid to be drawn back into collagen gels. The performed modifications are shown in Figure 5. To accomplish this, a silicon ring (specifications provided in Appendix C) with a square cross section (1 mm TK X 10.7 mm ID X 12.7 mm OD) was placed inside the inner cell. The main function of the silicon square ring is to support the weight of the platen during the rest period while media is drawn back into the collagen fibrils and thus allow recovery from the applied load.

Finally, it must be ensured that there is a consistent loading procedure for initialization and pre-loading across samples. In the case of Flexcell compression, assembly of the corresponding lid has an adjustable centre which can be screwed up and down in order to just touch the top of the sample. The amount of rotation can be calculated using an equation provided by Flexcell. This equation considers sample height and compression plate parameters to uniformly initialize all samples. However, in our case, the height of

the gels is not fully consistent during their formation. Therefore, a silicon ring with a round cross section (2 mm TK X 6 mm ID X 10 mm OD) was placed on the top of the platen to control the moment when the moveable centre of the lid just touches the ring and thus applies an initial tare load to the samples. Individual components of the modified system are shown schematically in Figure 3.5.

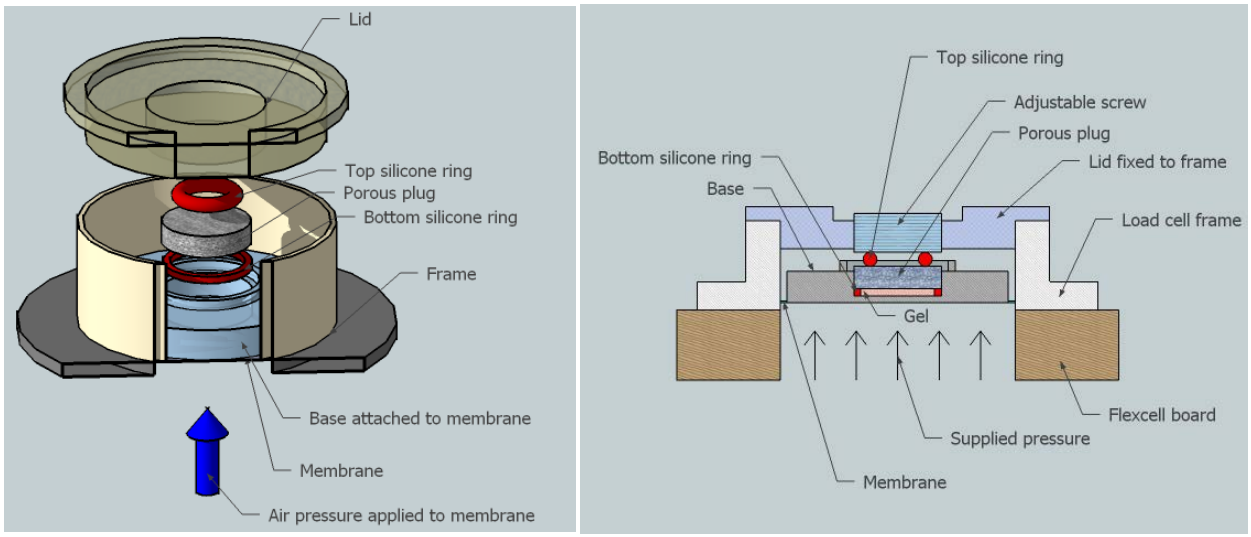

Figure 3.5: Left: schematic 3-D assembly of the load chamber components. BioPress™ compression culture plate with modified loading cell plates and additional components consisting of modified cell plate, a silicon ring with square cross section, porous platen, ring with round cross section and lid to seal the components. Right: Cross-section of the load chamber and the individual components.

The operation of the system is as follows: a collagen gel, cut from a 12 well plate is placed into the cell base within the silicon square cross section ring, and the ring holds the gel in a confined configuration. On the top of the gel the porous platen is placed. A silicon ring with round cross-section is placed on the platen. The lid seals the system and compression occurs by applying positive pressure that deforms a flexible

membrane and thus compresses the collagen gel. A real photo of the modified chamber and the individual components is shown in Figure 3.6.

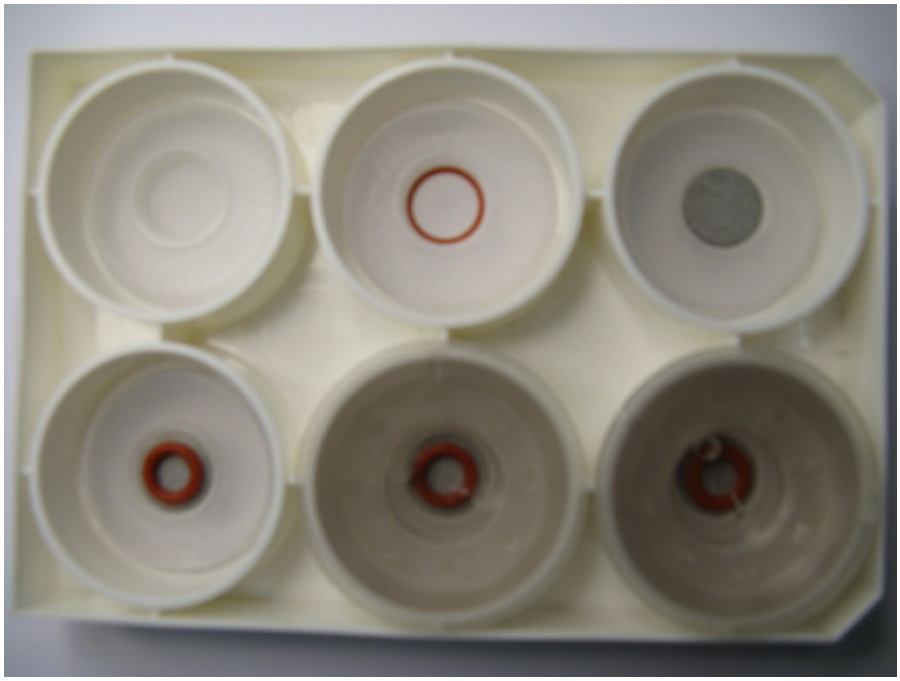

Figure 3.6: Six well compression culture plate with modified loading cell plates and additional components consisting of modified cell plate, a silicon ring with square section, porous platen, ring with round cross section and lid to seal the components.

To establish the feasibility of the rings a pilot run was performed. Again, gels were subjected to compressive load at 1 Hz and 70 kPa for 4 h following 16 h rest. In comparison to previous experiments, with the presented modifications, a collagen gel was shown to maintain its shape and hydration within the chamber. In other words, during the rest phase of the load cycle, the inner ring supported the weight of the platen and enabled liquid to be imbibed by the gels. A comparison between loaded and unloaded gels is shown in Figure 3.7.

Figure 3.7: Left: collagen gel before loading demonstrating its very soft structure. Right: collagen gel after loading demonstrating its integrity was retained.

As modification of the Flexcell system involved the replacement of the base plate, extra calibrations were required. The calibration steps are described in the next sections.

3.3 Calibration of Modified Load Cell within the Flexcell System

The modified Flexcell system required calibration to establish the relation between applied air pressure and compressive strain. As mentioned above, the Flexlink supplies and distributes the air pressure to the system according to a specific regime. The regime is determined by the minimum and maximum values of the loading waveform. In our case, the waveform is sinusoidal, the minimum value is zero and the maximum value should correspond to the desired level of the total force F_T applied to system. Originally, the input parameters of the Flexcell system are in force pounds (lbf) for compression rather than pressure distributed to culture plate (see Figure 3.5). As a result of the load cell modifications, the input parameter in lbf units would no longer

match the actual applied force to the chamber. Therefore, we considered this input parameter as unitless and established its new relationship to actual pressure and force acting on the modified load chamber. A simple test program was run during which the maximum input parameter was gradually increased and the corresponding pressure was registered. The results are shown in Figure 3.8, where experimental data is approximated using linear trend line.

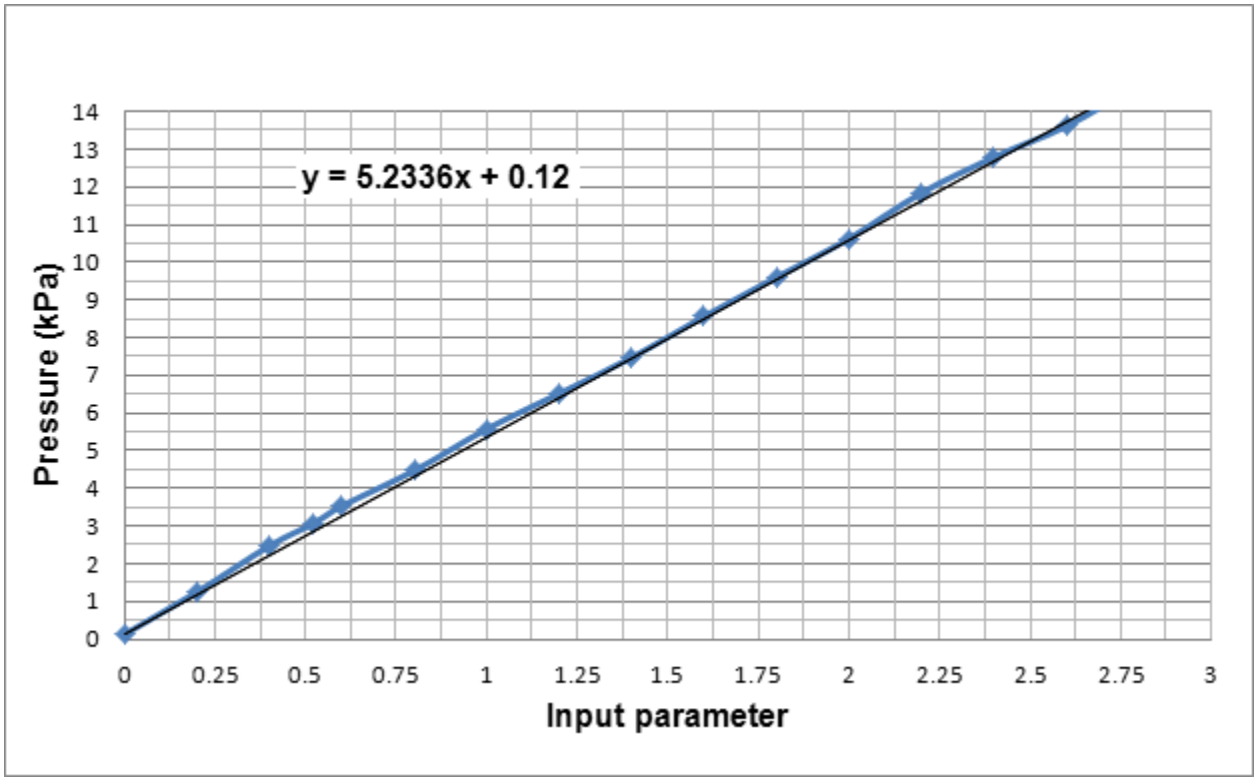

Figure 3.8: Calibration diagram represents the values of maximum unitless input parameters of the Flexcell system on the x-axis and corresponding distributed air pressure to load chamber on the y-axis.

As a result, the following formula reflects the relationship between input parameter and actual air pressure in the system:

$$P\ (kPa) = 5.2336 * Input\ Parameter\ (considered\ unitless) + 0.12 \qquad \text{(Equation 3.1)}$$

The second step was to correlate the pressure in the system to the force acting on the base plate. When a pressure *(P)* is applied to the cell base membrane with the area *A*, the resulting force *F* in Newtons (N) can be found as:

$$F\ (N) = P(Pa) *\ A\ (m^2) \qquad \text{(Equation 3.2)}$$

The area of any cylindrical shape can be found according to the general formula:

$$A\ (m^2)\ = \frac{\pi *\ d^2\ (m^2)}{4} \qquad \text{(Equation 3.3)}$$

The diameter d, of the attached base plate is 34 mm, thus, the calculated area is 0.00090792 m^2. Using this information, the actual force in Newtons can be calculated from the above pressure readings:

$$F\ (N) = 0.90792 * P(kPa) \qquad \text{(Equation 3.4)}$$

Finally, the force acting on the load chamber can be calculated in terms of input parameter as:

$$F\ (N) = 4.7517 *\ Input\ Parameter\ +\ 0.11 \qquad \text{(Equation 3.5)}$$

Therefore, for any input parameter we can calculate the corresponding applied force.

Also, if we need to find the input parameter for some desired force, the above formula can be re-written in the following form:

$$Input\ Parameter = 0.2105 *\ F\ (N)\ -\ 0.02 \qquad \text{(Equation 3.6)}$$

In conclusion, the calibration for the modified load chamber within the Flexcell system was completed, and a functional dependence of force versus input parameter was established using linear regression.

3.4 Modified Load Cell Characterization

This section describes the mechanical behavior of the modified load chamber. First, an analytical analysis of the applied loads is presented; then, the corresponding system of equations are derived and reduced to two equations which are required to determine the displacement and force acting on the gel in the load chamber.

Second, the required experimental tests for calibration were performed and analyzed. Also, a simplified method of calculation, based on analytical and practical findings was proposed and utilized for the case of the gels at time zero. Experimental tests were conducted using a sinusoidal loading waveform from 0.1 N to 2.85 N and two different frequencies: 1 Hz and 0.1 Hz. One sample of the same type of gel was used for each experiment.

3.4.1 Theoretical Analysis of the Load Cell Unit

The modified load chamber has more components involved in the overall function. Thus, the standard method provided by the Flexcell Company for displacement and force estimation on the sample, i.e. gel, cannot be applied. As a result, a full mechanical characterization of the load chamber was required in order to determine the actual force acting on the gel and its corresponding displacement. Subsequently, the force-displacement diagram can be converted to a stress-strain one.

For this purpose, the modified load chamber (see schematic representation in Figure 3.5 above) can be considered as a system of springs of equivalent elastic properties as presented in Figure 3.9 below. For better presentation, the bottom square cross-section

silicon ring is shown as two springs, nevertheless, it is actually represented as a single one.

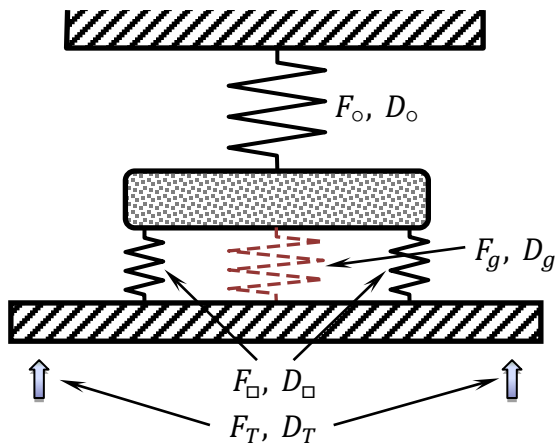

Figure 3.9: Schematic representation of the loading cell.

Corresponding forces and displacements are denoted by subscripts as following:

$F_\circ$: force acting on the top round cross-section ring in the loading chamber,

$D_\circ$: displacement corresponding to force $F_\circ$,

$F_\square$: force acting on the bottom square cross-section ring in the loading chamber,

$D_\square$: displacement corresponding to force $F_\square$,

F_g: force acting on the gel into the bottom square cross-section ring,

D_g: displacement corresponding to force F_g,

F_T: total force applied to the system corresponding to maximum input parameter in Flexcell (see Chapter 3.3),

D_T: total displacement corresponding to F_T.

The bottom elastic membrane is not included in the analysis as it is an order of magnitude less stiff than the system and the expected total displacement of the

membrane during loading is estimated at less than 0.25 mm. The gravity force of the top ring and porous platen does not exceed 0.05 N and was also neglected. The porous platen was considered rigid. We considered the system as quasi static due to the relatively low frequencies of motion (1 Hz and 0.1 Hz). Additionally, we neglected the frictional forces on the sides because in practice, all load chamber parts are “lubricated” with media during function.

The above system of springs is described by the following system of equations:

$$\begin{cases} F_{\circ} = F_T \\ F_{\circ} = f_{\circ}(D_{\circ}) \\ F_T = f_T(D_T) \\ D_T = D_{\circ} + D_{\square} \\ D_g = D_{\square} \\ F_T = F_{\square} + F_g \\ F_{\square} = f_{\square}(D_{\square}) \end{cases} \qquad \text{(Equation 3.7)}$$

where $f_{\circ}$, $f_{\square}$, f_T are functions of displacement related to displacements $D_{\circ}$, $D_{\square}$, D_T and describe the force-displacement relationship of the top ring, bottom ring, and the whole system, respectively.

The specific value for total force F_T was set by programming the Flexcell control unit, and thus, it was a known input parameter (see (Equation 3.6). The top ring and gel with bottom ring work in-series, therefore $F_{\circ}$ is equal to F_T: $F_{\circ} = F_T$. To determine the corresponding displacement $D_{\circ}$ related to the force $F_{\circ}$, the function $f_{\circ}$ (to be more precise the inverse function $f_{\circ}^{-1}$), i.e. force-displacement diagram, is required. The latter was obtained by conducting independent tests for the top ring on a Bose Electroforce material testing machine. Similarly, the total displacement D_T was defined from the

force-displacement diagram of the whole system including the gel. On the other hand, it is also the sum of $D_\circ$ and $D_\square$: $D_T = D_\circ + D_\square$. Thereby, one can determine $D_\square$ as $(D_T - D_\circ)$ which is identical to the desired displacement of the gel D_g: $D_g = D_\square$, since the gel must follow the contraction of the bottom ring due to the rigid platen above and rigid chamber below.

The final part was to determine the force acting on gel F_g by taking into account that the gel and bottom ring act in-parallel and experience jointly the same force as the top one $F_\circ$ (which is equal to F_T, as mentioned above), i.e. $F_T = F_\square + F_g$. Therefore, $F_g = F_T - F_\square$, while $F_\square$ was determined by a test for the bottom ring within the chamber but without the gel.

In summary, the system has seven unknown variables $F_\circ$, $D_\circ$, $F_\square$, $D_\square$, F_g, D_g, D_T, one input variable F_T, and three functions of force-displacement relationship $f_\circ$, $f_\square$, f_T which had to be established by performing independent tests using the Bose Electroforce machine. Then, the system can be reduced to following two governing equations:

$$\begin{cases} D_g = f_T^{-1}(F_T) - f_\circ^{-1}(F_T) \\ F_g = F_T - f_\square(D_g) \end{cases} \qquad \text{(Equation 3.8)}$$

where $f_\circ^{-1}(F_T)$ and $f_T^{-1}(F_T)$ are inverse functions to corresponding functions $f_\circ$ and f_T, respectively.

3.4.2 Force-Displacement Estimation of Collagen Gel

This section describes the procedure of estimating the force-displacement response of the collagen gel at a time-point, using a day one gel as an example. As mentioned

above, three functions of force-displacement relationships must be determined by conducting loading tests: 1) $f_{\circ}$ for the individual top ring, 2) $f_{\square}$ for the bottom ring within the system but without the presence of the gel and top ring, and 3) f_T for the whole system with the inclusion of a specific gel type.

The first two functions have no relationship to gel type and it was sufficient to establish them once. However, the last function f_T is dependent on the gel type and, thus, the loading test on the whole system should be repeated for each gel type in order to extract mechanical properties of that particular type of gel.

Any possible dynamic effect on the load calibration was also considered. In order to verify that dynamic effects are negligible and elastic spring theory (working in series and parallel) was applicable, first two experiments as described above and the third one for the entire system but without presence of the gel were performed. Using this approach the response from the sum of individual parts and the entire system response for chosen frequencies was compared. If they matched, than the approach of spring theory was appropriate for the load chamber characterization.

First, an experimental test was performed for the top ring which has a round cross-section and was constrained between the plexiglass lid and porous platen. The subsystem of the lid, top ring, and porous platen were placed into the Bose machine. In addition to that, all these parts were immersed in media in order to reproduce the friction conditions close to those we have with the presence of gel. The conducted test applied loading perpendicularly to the ring plane while force and displacement values were

collected for further analysis. More details on current set up and control of the Bose machine can be found in Appendix D.

The Flexcell system can generate various loading waveforms (with different frequencies) such as triangle, sine, and heart rhythm. It is expected that the loading profile has no effect on the force-displacement diagram for the top ring; however, it could influence the bottom ring in the system as there is a flow of media thought the porous platen which might produce a hydrodynamic drag force. And in the case of having the gel in the system, the resistance force could be higher due to viscoelastic properties of the gel. On account of this, loading tests should reproduce the actual loading waveform and frequency. Therefore, this approach required performing loading tests for all elements using a specific load waveform; in our case sine loading.

Since it was suggested to use sine-shape load waveform with a frequency of 1 Hz and 0.1 Hz with an amplitude range of 0.1 N to 2.85 N with the Flexcell system, all the tests on the Bose Electroforce machine were performed using these specifications. Ideally, we need only one half-cycle of loading, but multiple cycles were run to investigate the system (and all its elements) consistency of the loading behaviour.

The typical loading diagram (force-time) for 1 Hz is shown in Figure 3.10. It illustrates the first 5 cycles of the top ring loading (plastic lid, top silicon ring, and porous platen moisten with media). The absolute values of force and displacement are taken for analysis while the actual force and displacement are negative which correspond to compressive loading.

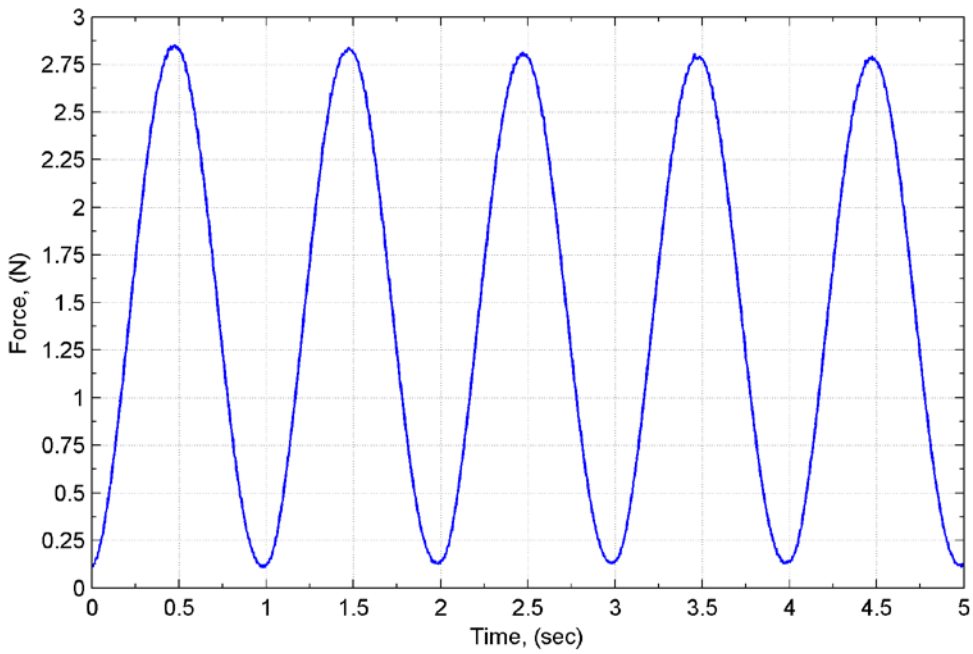

Figure 3.10: Force-time diagram for the top ring, 1 Hz.

The force-displacement diagram for the top ring (100 cycles) is provided in Figure 3.11 below.

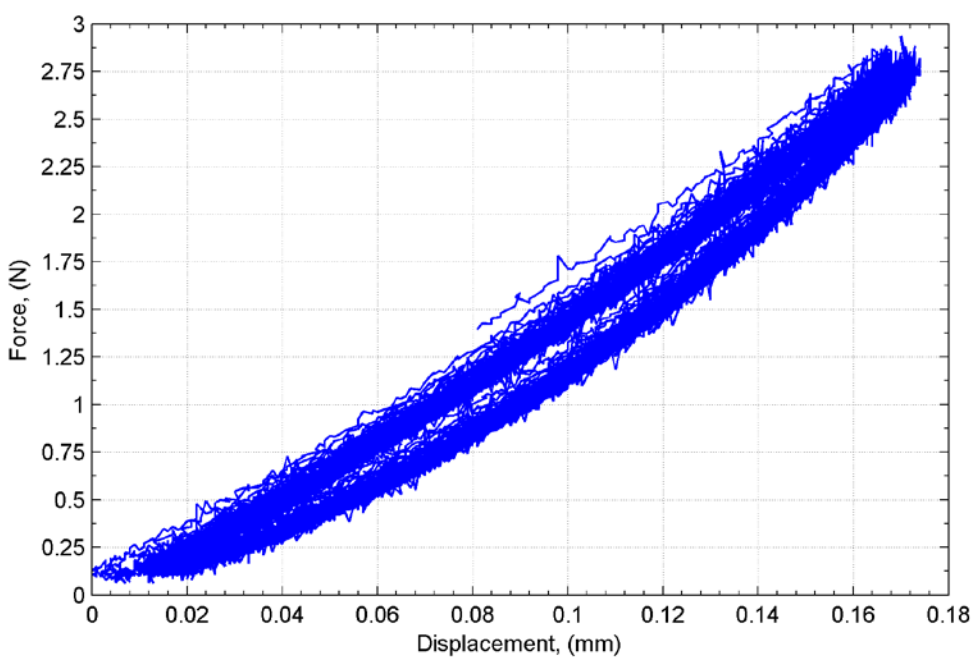

Figure 3.11: Force-displacement diagram for the top ring, 1 Hz.

Some drift in the displacement was occurred during the initial loading cycles. Therefore, out of the conducted 100 cycles, the cycles from 70 to 90 were selected and the data was averaged as shown in Figure 3.12. The selected 20 cycles are shown in gray color and corresponding averaged curves are displayed in green and red for loading and unloading parts of load cycle, respectively. The data was quite consistent and averaging removed some noise in the data.

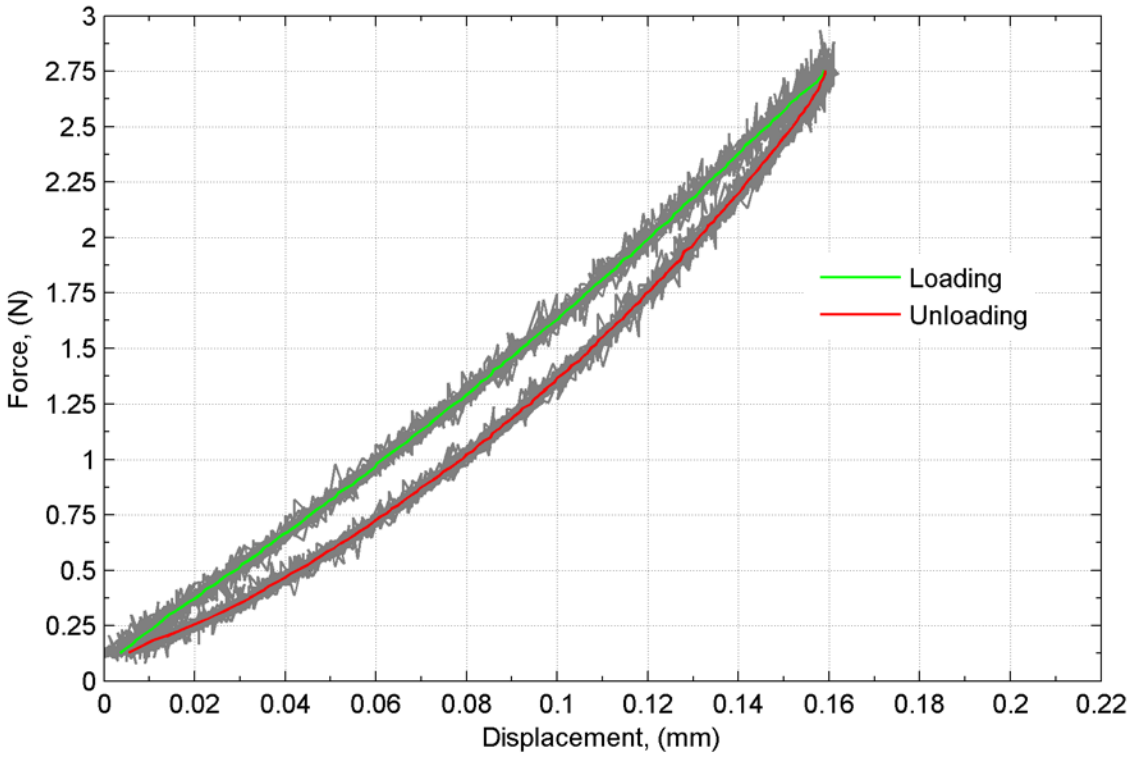

Figure 3.12: Force-displacement diagram for selected cycles (grey) and averaged load-unload curves (green and red) for top ring.

One can see that the top silicon ring exhibits some hysteresis and the gap reflects the amount of energy dissipated during the cycle.

Similarly, the bottom ring within the system (base plate, ring, and moistened porous platen) and the whole system (lid, top ring, porous platen, bottom ring, and base plate) were also tested and analysed. The summary is given in Figure 3.13. In order to evaluate data consistency and verify our assumptions, the displacement of the top ring was subtracted from the displacement of the system (for the same force level) and plotted in the black dashed line. Almost complete overlap of the experimental and calculated load-displacement curves for the bottom part confirms consistency of the data and supports our assumptions.

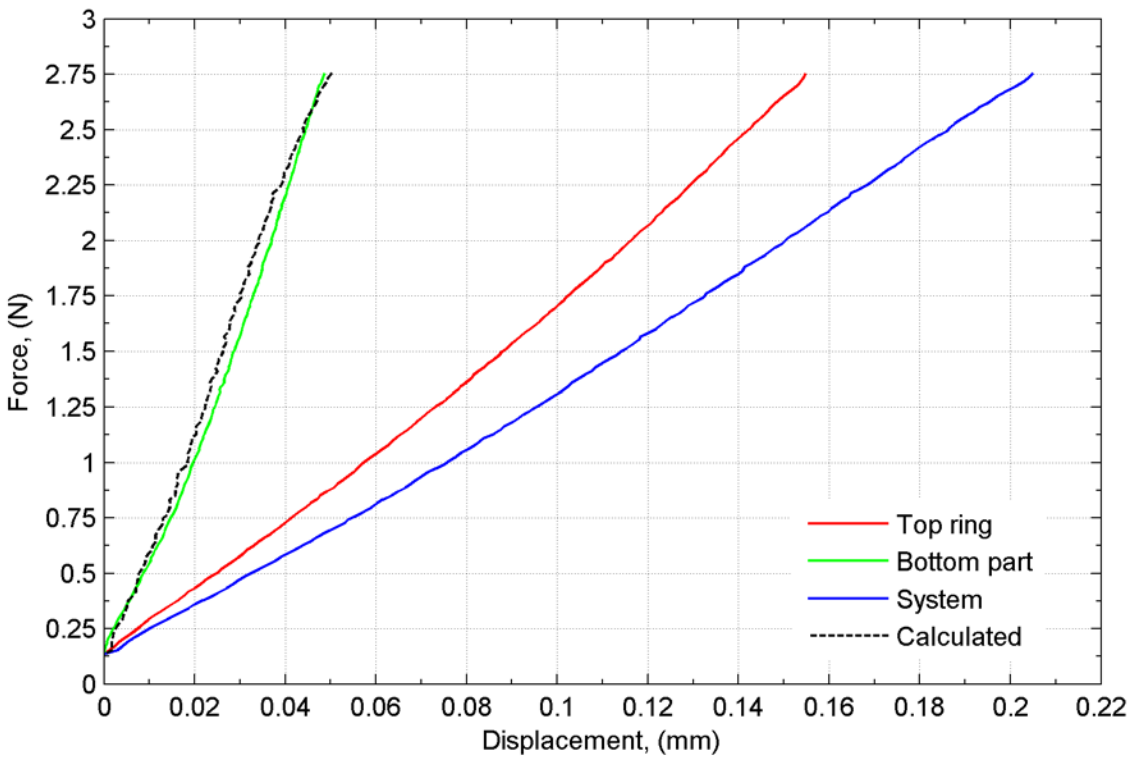

Figure 3.13: A summary of top ring, bottom part, whole system and calculated force-displacement for bottom part, 1 Hz.

Similarly, for 0.1 Hz frequency the load-displacement data was analyzed and as shown in Figure 3.14, it also demonstrated a good agreement between the system and the corresponding elements. This allowed us to simplify the method by physically eliminating the top ring from the tests. Specifically, as the bottom part response was coinciding with the calculated one, it was sufficient to perform only two tests to estimate the force displacement of the collagen gel: 1) bottom part of the system without gel, and 2) bottom part with gel.

The first experiment can be done once for each of the frequencies and the second one should be repeated every time a new type of gel of different material is used. The second experiment directly provided the gel displacement (as it works in parallel with the bottom ring) and the force was found by comparing these two tests.

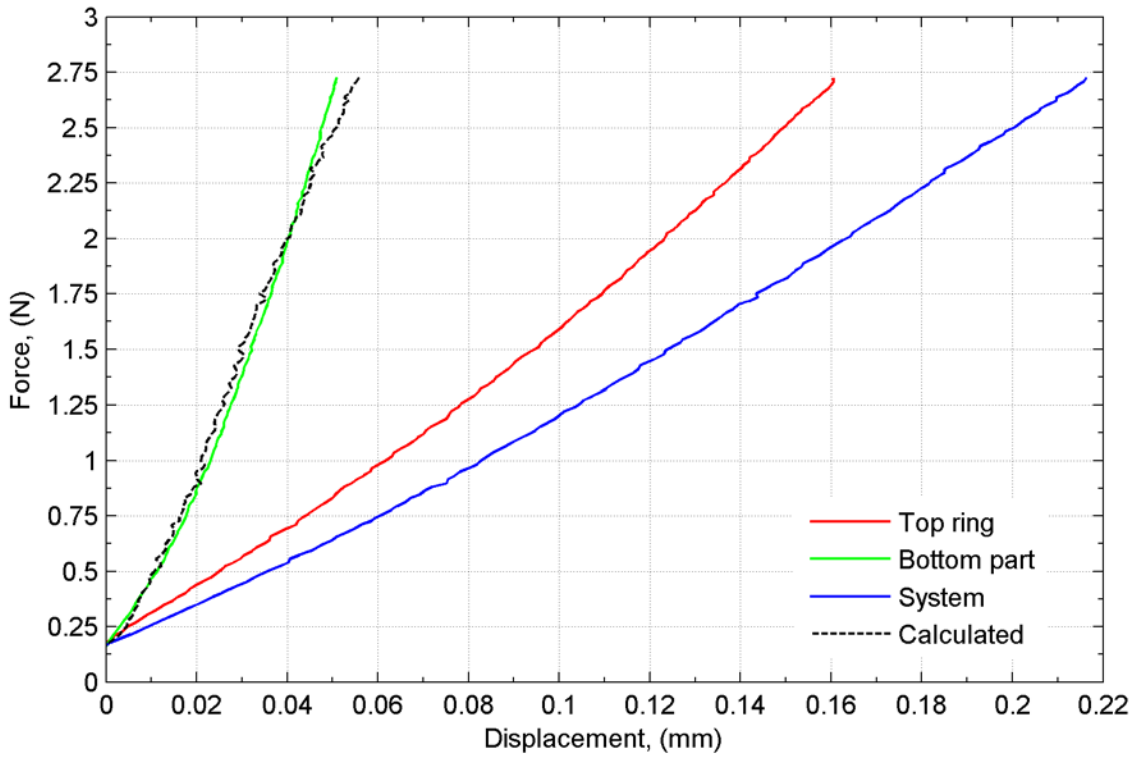

Figure 3.14: A summary of top ring, bottom part, whole system and calculated force-displacement for bottom part, 0.1 Hz.

Also, it was interesting to compare the force-displacement curves between 1 Hz and 0.1 Hz as shown in Figure 3.15.

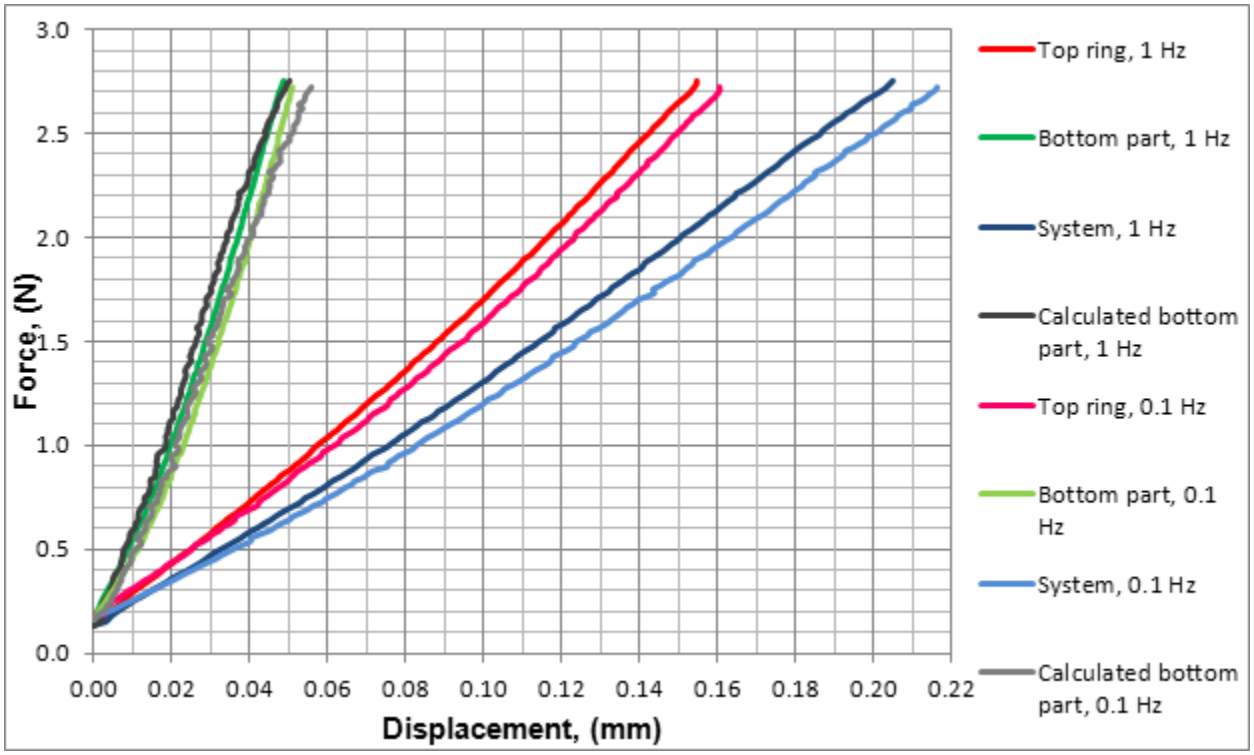

Figure 3.15: Comparison of top ring, bottom part, whole system and calculated force-displacement for bottom part without the gel for 1 Hz and 0.1 Hz.

After determining the performance of the modified system, the gel contribution was then evaluated. As suggested, the gel was tested within the bottom part without presence of the top ring at 1 Hz. Two hundred load cycles were performed as gel adaptation can take a longer time. The raw force-displacement data is shown in Figure 3.16. Initial cycles (especially the very first one) show higher displacement amplitude, i.e. the initial gel thickness was higher than the thickness of the bottom ring but become more stable

in time. The assumption was that porous platen initially compressed the gel to the bottom ring height and then the gel and bottom ring strains fully coincide.

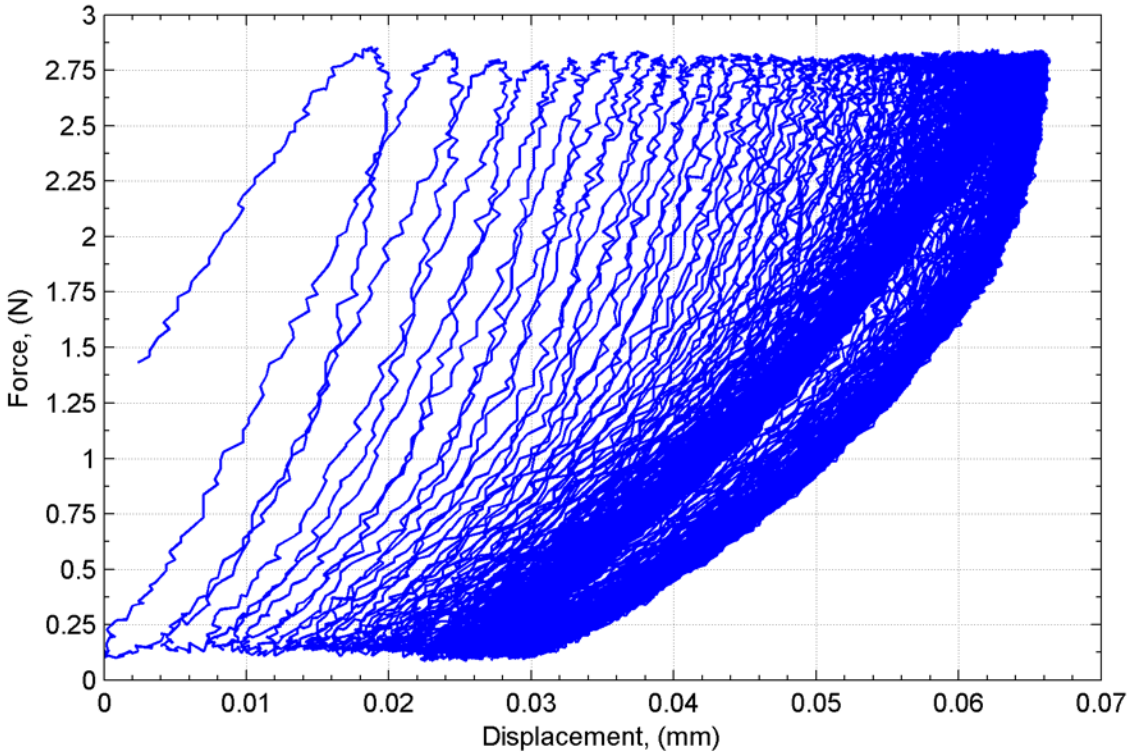

Figure 3.16: Force-displacement diagram for collagen gel within the bottom part of the system, 1 Hz.

As before, the data from a range of 70% to 90% of applied cycles (140 to 180 cycles) was chosen and averaged to reduce the noise. The averaged data is presented in Figure 3.17.

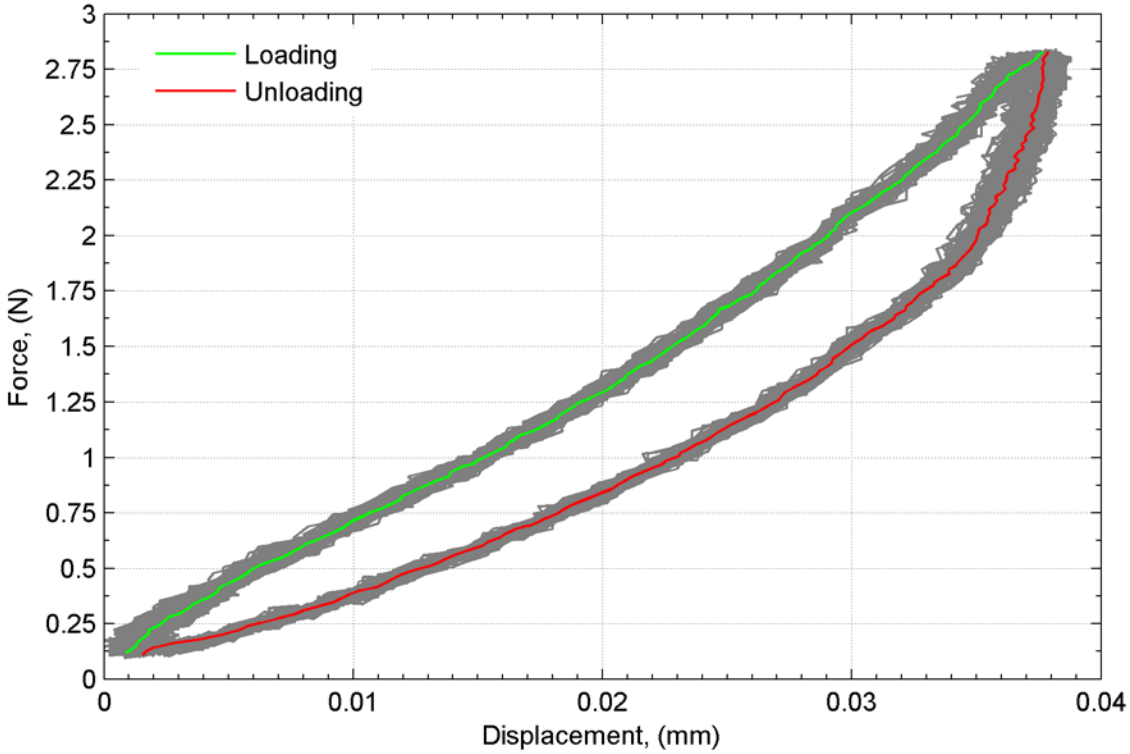

Figure 3.17: Force-displacement diagram for gel showing average data of chosen 40 cycles, 1 Hz.

Finally, the force of the bottom part without the gel was subtracted from the above loading curve for the same values of displacement. The results are shown in Figure 3.18.

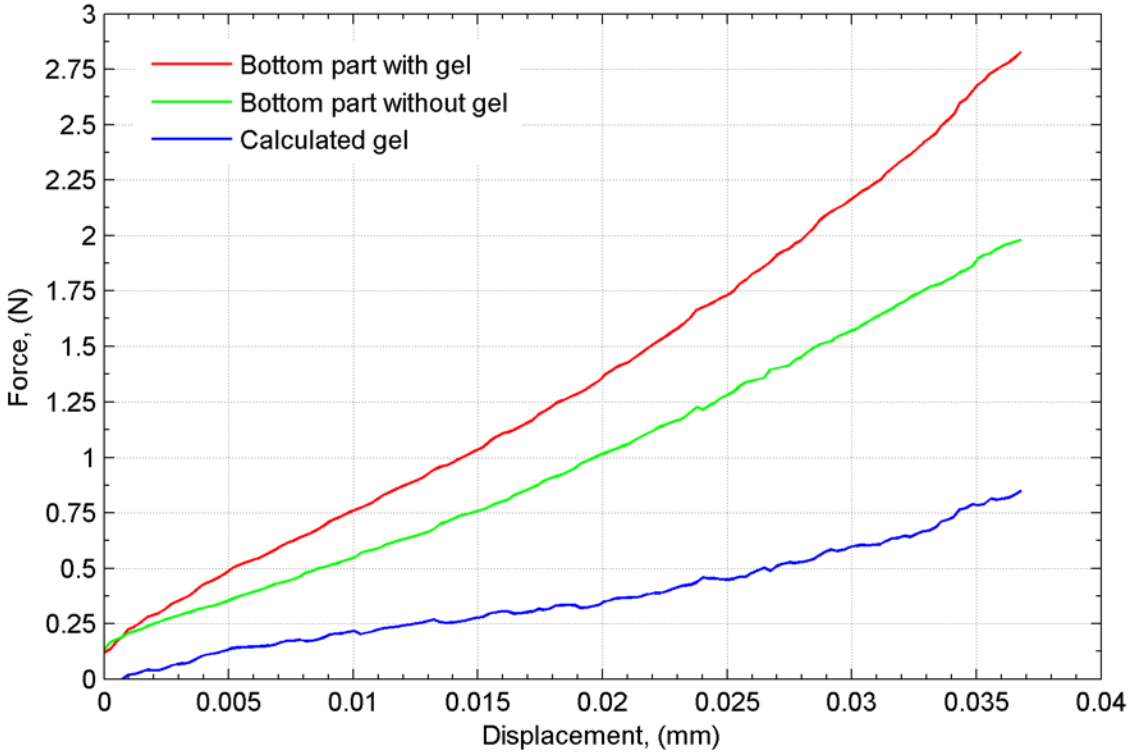

Figure 3.18: Force-displacement diagram for the bottom ring (green), the bottom part with the gel (red), and a gel itself (blue, calculated as a force difference between previous two curves for the same values of displacements), 1 Hz.

As one can see, the maximum force was about 0.9 N and the corresponding strain was 0.037 (3.7%).

Similarly, the force-displacement diagram was determined for 0.1 Hz and is presented in Figure 3.19. In this case the maximum force was around 1 N and strain was about 0.039 (3.9%).

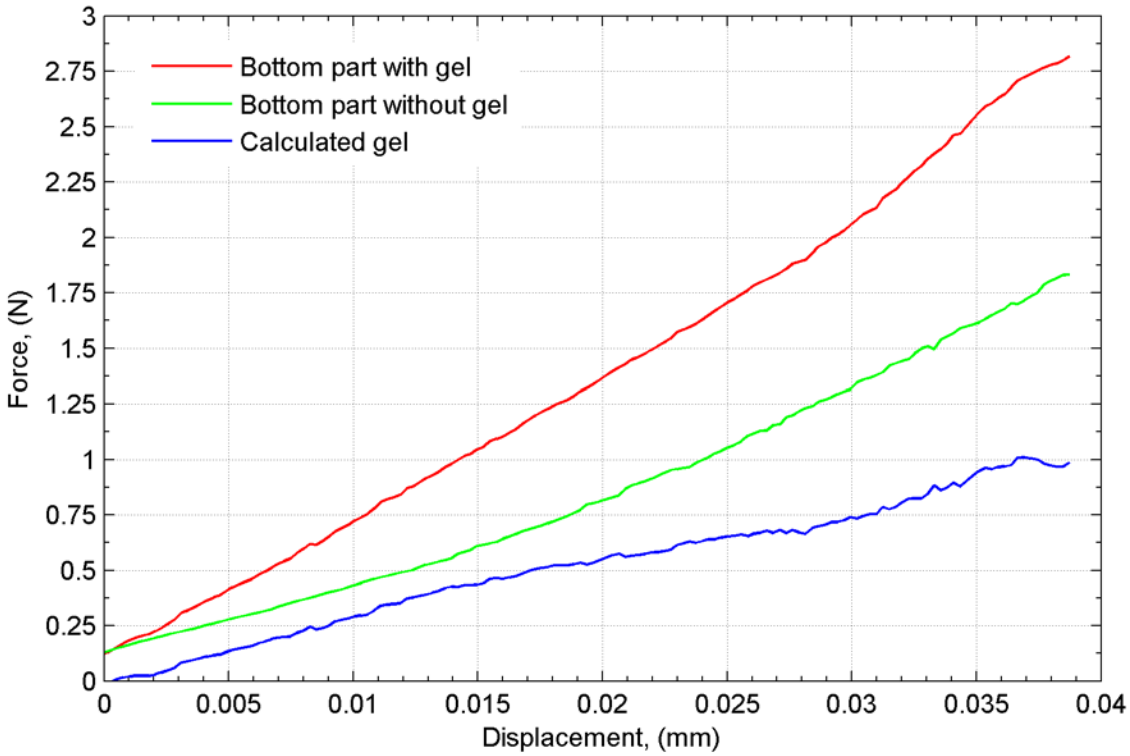

Figure 3.19: Force-displacement diagram for the bottom ring (green), the bottom part with the gel (red), and a gel itself (blue, calculated as a force differences between previous two curves for the same values of displacements), 0.1 Hz.

The initial inner diameter of the bottom ring is 10.7 mm and the engineering stress can be calculated as force divided by corresponding area. The stress-strain diagram can be approximated linearly and the estimated Young's modulus was about 205 kPa at 1 Hz and 308 kPa at 0.1 Hz for a gel one day post-polymerization as shown in Figure 3.20 and Figure 3.21, respectively.

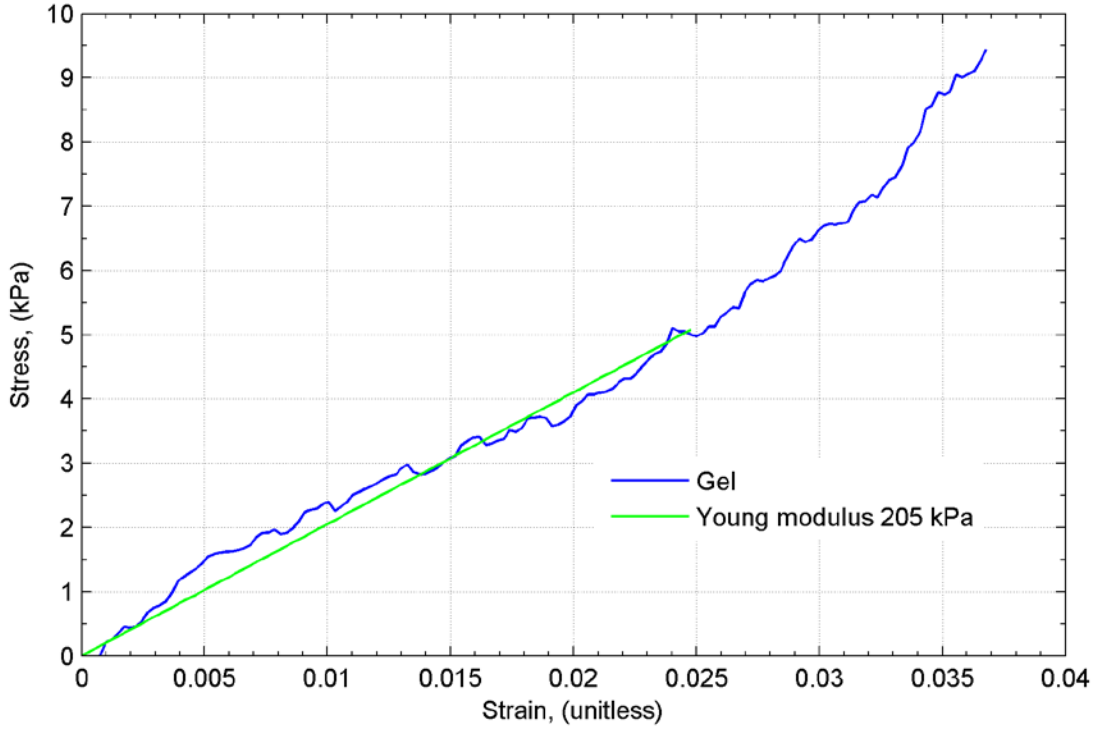

Figure 3.20: Young's modulus estimation for collagen gel at day 1, 1 Hz.

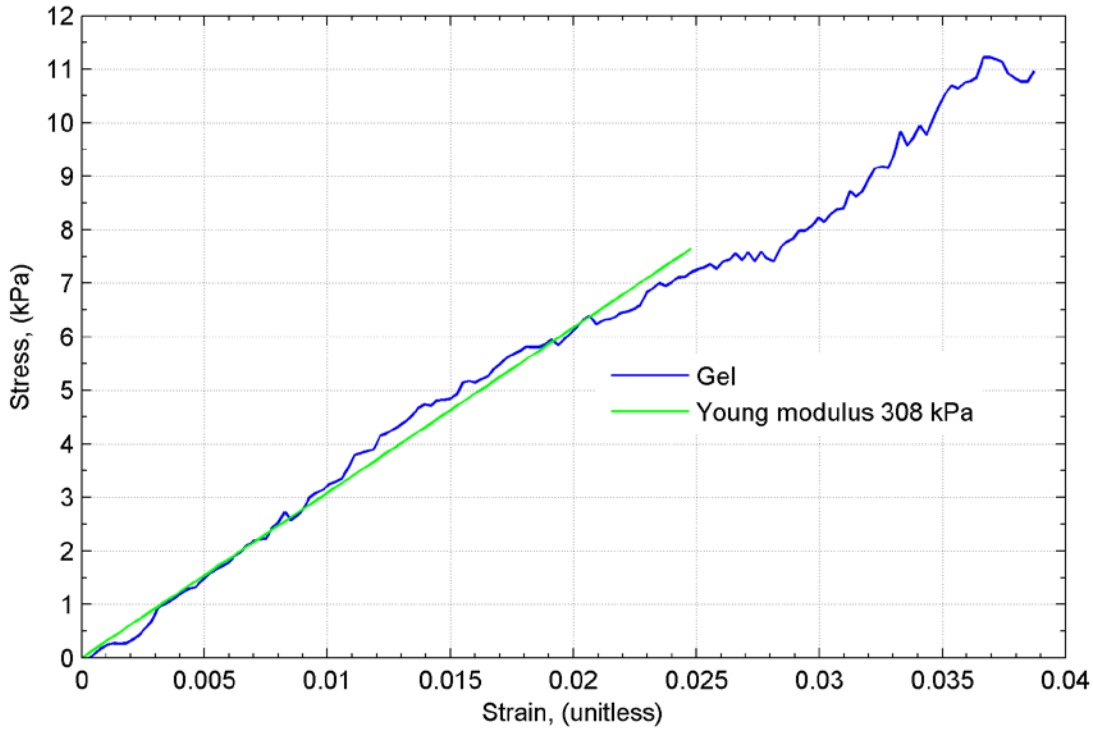

Figure 3.21: Young's modulus estimation for collagen gel at day 1, 0.1 Hz.

3.5 Discussion and Conclusion

Cells are exposed to different, specific mechanical environments *in vivo* and therefore, most of the loading systems found in the literature are custom designed to a particular experiment. Only a few commercially available systems exist for which the Flexcell system is one of the most recognized. This chapter presented the modification and calibration of a modified Flexcell load chamber for subjecting a soft, viscoelastic scaffold to confined compressive load. The presented system is unique as it was specifically designed for a biphasic material. However, it could be adapted for use with other 3-D scaffold systems.

The system was analyzed theoretically based on spring theory and experimentally characterized by testing the individual components and assembled system using a Bose Electroforce machine. It was shown that the system responded consistently and that evaluating the scaffold contribution can be reduced to the bottom part of the system which makes the application to various scaffolds easier. The application of this method was illustrated in details using collagen gels one day post polymerization. As a result, two stress-strain curves for 1 Hz and 0.1 Hz were obtained and a Young's modulus for each was estimated.

One of the limitations of the system is that it is impossible to specify directly the force and/or displacement applied to a sample because the Flexcell functions with a pressure applied to the entire load chamber. Thus, the pre-testing of the sample must be performed on a material test machine to estimate the relationship between total force, sample force, and sample displacement. Then, the force required for specific strain can

be assessed by running several experiments with different level of force and registering the output displacement. In order words, this pre-testing involved a trial and error method and required several attempts while every subsequent test is corrected by result of the previous one. Therefore, the method needs immediate response analysis for the each test. However, the sample force-displacement estimation is based on a complex post processing of experimental data. To overcome this difficulty, it was decided to apply the same force to the entire load chamber for all types of gel. This means, that the maximum input parameter was estimated once and set to a constant for all further experiments. As a result, the gel strain should vary slightly from the desired input value.

Another limitation of the system is the possibility of contamination. The materials used for its design, the rings and porous platen cannot be autoclaved and thus the system was disinfected with ETOH. However, it was successfully used with synovial fluid cells seeded on agarose gel for two days and collagen gel over the course of 40 hours and no contamination was observed. Also, the system is not limited to the above materials and could be used with other TE constructs in the future.

Overall, this chapter provided a methodology for the mechanical characterization of the system and demonstrated its feasibility while the determining the results for the gels at different time points that are presented and discussed later in Chapter 6.

CHAPTER 4: MATERIALS AND METHODS

This chapter describes standard procedures used throughout the experiments. The following Table 4.1 summarizes the methods to test each objective and used in specific Chapters.

Table 4.1: Summary of methods.

Methods	Objectives (OB)				
	OB 1	OB 2	OB 3	OB 4	OB 5
	Chapter 3	Chapter 5	Chapter 6	Chapter 7	
Cell Culture	X	X	X	X	X
mESC Differentiation	X	X	X	X	X
RGD incorporation				X	X
Gene Expression		X	X	X	X
Cell Viability		X	X	X	X
Immunofluorescence		X			
Von Kossa Stain		X			
Mechanical stimuli	X		X	X	X
Nanoparticles					X

4.1 Cell Culture

Murine ESCs (D3 line), provided by the Dr. Rancourts laboratory, Department of Oncology, Medical Genetics and Biochemistry & Molecular Biology, University of Calgary, were cultured on gelatin (Gelatin Solution, Type B from bovine skin, 2%, cell culture tested) coated flasks (Nunc) for one passage, after which they were expanded in a stirred bioreactor at 100 rotations per minute (rpm) as described previously (*102*). Culture medium consisted of high glucose Dulbecco's Modified Eagle Medium (DMEM) supplemented with 1% non-essential amino acid (NEAA), 10,000 U/mL of penicillin and 10,000 µg/mL streptomycin, 15% fetal bovine serum (FBS), and 0.1 mM ß-

mercaptoethanol (obtained all from Invitrogen). In order to maintain mESCs pluripotency, culture medium was supplemented with 1000 U/mL leukemia inhibitory factor (LIF) (Chemicon International). Cells were maintained in a humidified incubator with 5% CO_2 at 37°C and routinely passaged (passages 10 to 16) upon reaching confluence every third to fourth day and.

4.2 mESCs Differentiation in Collagen Matrix

Cell differentiation and matrix seeding was performed according to the protocol described by Krawetz et al. (*18*). Briefly, differentiation medium was prepared using DMEM high glucose medium (Invitrogen) powder according to the manufacturer's instructions with a final volume of 200 mL to obtain a 5 times concentrated DMEM. Medium was supplemented with 10 mM β-glycerol phosphate (βGP) (Sigma) and filter sterilized using a 0.2 micro filter (Corning). Then, medium was supplemented with NEAA, penicillin-streptomycin solution, FBS and β-mercaptoethanol equal to the standard mESC culture procedure. To prepare the final cell/gel construct, mESC were collected from the bioreactor, trypsinized (Trypsin from Invitrogen) and counted using a haemocytometer applying trypan blue (0.4%, Sigma) exclusion. For one cell/gel construct, $1x10^6$ cells were resuspended in 200 µL differentiation medium and mixed with 800 µL collagen type I solution (3 mg/mL, bovine, AdvancedBioMatrix), pipetted into a 12 well plate and allowed to polymerize in a humidified incubator with 5% CO_2 at 37°C.

4.3 RGD Incorporation

RGD (cyclo (Arg-Gly-Asp-d-Phe-Cys)) and RAD (cyclo (Arg-Ala-Asp-d-Phe-Cys)) were purchased from peptides international and dissolved in 3% citric acid to obtain a final concentration of 0.5 mM RGD and 0.5 mM RAD. For 2-D studies, 12 well plates were coated with gelatin, allowed to dry for 10 min and rinsed 3x with phosphate buffered saline (PBS). Murine ESCs were seeded at a cell density of 30,000 cells/well supplemented with 500 µL DMEM in the presence of LIF and were allowed to attach for 24 h. On the next day a media change was performed and 0.5 mM RGD or 0.5 mM RAD were added to the wells. Every day, pictures were taken for morphological analysis. Three groups were examined; mESCs with no treatment and mESCs cultured with either RAD or RGD in the presence of LIF.

Viability assay was conducted on the same groups using trypan blue exclusion and cells counted using BioRad TC-10 cell counter.

For 3-D studies, 0.5 mM RGD was added to 200 µL differentiation medium prior mixing with 800 µL collagen type I solution. Cell/gel solution in the presence of RGD was pipette into 12 well plates and allowed to polymerize as described above.

4.4 Gene Expression

4.4.1 RNA Extraction

For the extraction of RNA from mESCs/Col I constructs, three different methods were compared: Trizol (Invitrogen), Trizol with addition of glycogen (Invitrogen) and RNAeasy Mini Kit (Qiagen). Trizol with addition of glycogen resulted in the best RNA yield thus was used for subsequent extractions. The RNA extraction procedure using Trizol and

glycogen (Ambion) was performed according to the manufacturer's instructions with small modifications. Gels were harvested at time points of interest in 1.5 mL eppendorf tubes and centrifuged at 12,000 rpm for 3 minute (min) at 4ºC to separate the solid phase from the liquid. This step is important in maintaining the functionality of the lysate. Gels were supplemented with 800 µL Trizol and homogenized using 18 gauge needle and syringe, followed by a 20 and 23 gauge needle until collagen matrix disruption was achieved. After homogenization, 0.25 µg/µL glycogen (Ambion) was added to Trizol and stored at room temperature (RT) for 5 min to complete dissociation. Samples were vortexed for 10 seconds (sec) and transferred to a new 1.5 mL eppendorf tube. For the phase separation, 160 µL chloroform (200 µL chloroform per 1 mL Trizol) was added, pipetted up and down for 30 sec and centrifuged at 12,000g at 4ºC for 5 min. Then, the upper phase (containing RNA and DNA) was carefully transferred into a new eppendorf tube and supplemented with 0.4 mL isopropanol (Sigma) (0.5 mL isopropanol per 1 mL Trizol) to precipitate RNA. Finally, the RNA solution was mixed and stored at -20ºC for at least 1hour (h) or overnight. Afterwards, the solution was centrifuged at a maximal speed of 14,000 rpm at RT for 15 min, the supernatant discarded and 0.2 mL of 70% ETOH was added. RNA with ETOH was mixed by inverting the tube and by briefly vortexing then spinning it down at maximal speed for 10 min at RT. Again, the supernatant was discarded (as much as possible without touching the pellet) and RNA was allowed to air dry on ice for 7 min. Finally, 30 µL ultra pure water was added to the RNA sample, pipetted up and down and stored at -70ºC for further use or directly quantified as described below.

4.4.2 RNA Quantification

RNA was quantified using a NanoVue spectrometer. For the spectrometric analysis, the spectrometer was blanked using the same solution which was used to dissolve RNA. Then, 2µL of total RNA was pipetted in the centre and values for RNA yield observed.

The RNA yield obtained using NanoVue spectrometer was used for the following complementary DNA analysis.

4.4.3 Complementary DNA Synthesis

Complementary DNA (cDNA) was prepared using High Capacity cDNA Reverse Transcription Kit (Applied Biosystems) by mixing 10 µL cDNA master mix with 10 µL of the RNA sample. Components supplied with the kit were allowed to thaw on ice, after which a 2x master mix reaction was prepared according to Table 4.2 below. The specified amount is specific for a 20 µL final cDNA reaction which can be proportionally increased with increasing final volume.

Table 4.2: cDNA master mix for one sample reaction by 20 µL final volume.

Reaction components	**Volume (µL)**	**Final Concentration**
10x RT Buffer	2	1x
25X dNTP Mix	0.8	0.08 mM
10x RT Random Primers	2	1x
MultiScribe Reverse Transcriptase	1	50 U
Nuclease free H_20	4.2	-
Total Volume:	**10**	**-**

For a 20 µL reaction, 2 µg of total RNA was diluted with ultra pure water (Invitrogen) to a final volume of 10 µL. Master mix and RNA samples were mixed in a PCR tube (Sigma) and placed into a thermo cycle (C1000™ Thermal Cycler, BioRad). Reverse transcription was performed using the following cycle conditions: cycle 1: 25ºC for 10 min, cycle 2: 37ºC for 120 min, cycle 3: 85ºC for 5 min and cycle 4: 4ºC on hold. Generated cDNA was stored at -20ºC until use for real time polymerase chain reaction.

4.4.4 Quantitative Real Time Polymerase Chain Reaction

Quantitative real time polymerase chain reaction (qrt-PCR) was performed using TaqMan® Universal PCR Master Mix with no AmpErase (Applied Biosystems) according to the manufacturer's instructions. One qrt-PCR reaction was made of the components listed in Table 4.3.

Table 4.3: Reaction components for qrt-PCR.

Reaction components	**Volume (µL)**	**Final Concentration**
TagMan Universal PCR Master Mix 2x	10	1x
Primer	1	1x
Nuclease free H_20	6	-
cDNA	3	2 µg
Total Volume:	**20**	**-**

All samples were run in triplicate for each gene using a 96 well plate (Applied Biosystems). Seven samples and four genes (four different reaction mixes), including an

endogenous control, were tested simultaneously. The tested genes are listed in Table 4.4.

Table 4.4: Genes and their encoding proteins used for qrt-PCR.

Genes	Translated Protein	Reference
BGLAP	Osteocalcin	Mm.389459
SRY-box containing gene 9	Transcription factor SOX-9	Mm.286407
Col2a1	Collagen alpha-1(II) chain isoform 2 precursor	Mm.2423
SRY-box containing gene 2	Transcription factor SOX-2	Mm.65396
POU domain, class 5, transcription factor 1 (Oct-4)	Octamer-binding transcription factor 4	Mm.17031
Eukaryotic 18S rRNA	Not available	HSRRN18S

The last row of 96 well plate served as a negative control in which master mix was added with only ultra pure water. The 96 well plate was then covered and sealed with plastic tape (Applied Biosystems), briefly vortexed and spun down at 1000 rpm for 30 sec to place all liquid to the bottom. qrt-PCR was performed using Applied Biosystems 7900HT Fast Real-Time PCR System.

4.5 Cell Viability

Cell viability of mESCs maintained in collagen gels was assessed using a LIVE/DEAD viability and cytotoxicity kit from Invitrogen. Gels were washed 3x with 1xPBS and

incubated with 2 μM Calcein acetoxymethyl ester (Calcein AM) and 4 μM ethidium homodimer-1 solution dissolved in 1xPBS in a humidified incubator for 45 min at 5% CO_2 at 37°C. After the incubation time, constructs were rinsed 3x with PBS and placed on glass slides or in small petri dishes and whole gels were imaged using a Zeiss LSM 510 confocal microscope using 10 x/0.3 Plan-Neofluar objective and 488 nm Argon laser (30% intensity). Z-stack pictures (10.4 μm slices with a total depth of approximately 156 μm) were obtained for projection purposes at two different locations (middle and right or left side) of each construct in duplicates.

Percentage of cell viability was calculated according to the general formula:

$$\%\ viability = \frac{live\ cells}{live\ cells + dead\ cells} * 100\% \qquad \text{(Equation 4.1)}$$

In z-stack pictures the live cells fluoresced green and dead cells fluoresced red. Thus, the term “live cells” is associated with number of green pixels while “dead cells” is associated with red particles on pictures. Therefore, the green and red image channels were analysed separately in Matlab using Image Processing Toolbox. Pixels with intensity level less than 30% were considered as a noise and removed from picture. The next step was to define enclosed objects which are separate groups of pixels connected together. The number of pixels in each object was defined and all objects of size less than eight pixels were considered as noise and removed while objects of size of eight pixels and greater were considered as a cell or group of cells. The total number of pixels of remained objects represented the number of cells. Finally, the viability was calculated as a ratio of green pixels to sum of green and red pixels.

4.6 Immunofluorescence

For fixation, 500 µL of 4% paraformaldehyde (PFA) (Invitrogen) in 1xPBS was added to the gels and stored at 4ºC overnight. Afterwards, gels were rinsed 3x with PBS for 5 min each. Then, gels were permeabilized with 500 uL of 1% saponin (Invitrogen) in PBS and stored at 4ºC overnight. Prior to blocking, saponin was discarded, gels rinsed with PBS and supplemented with 500 uL of 3% BSA (Invitrogen). Samples were blocked overnight at 4ºC or for 2 h at 37ºC. Primary antibodies (Santa Cruz) were added to the gels (diluted 1:50) in 3% BSA and gels were incubated overnight at 4ºC. Antibodies were then activated for 1 h at 37ºC, and blocked again with 500 uL of 3% BSA for 2 hs at 37ºC. Secondary antibodies, anti-goat, anti-mouse or anti-rabbit and phalloidin counter stain (Molecular Probes) were diluted 1:50 in 3% BSA and incubated overnight at 4ºC. Samples were washed 3x with PBS and images obtained with a Zeiss LSM 510 or LSM 720 Zeiss confocal microscope. The primary antibodies are listed in Table 4.4.

Table 4.5: Primary antibodies.

Primary Antibodies
Anti-Osterix (OSX)
Anti-Bone sialprotein (BSP)
Anti-Sox9
Anti-Aggrecan (Agg)
Anti-Col 2
Anti-Oct 4

To estimate the amount of positive stained cells, two pictures from two samples were analysed and averaged using Matlab. A cell was considered as positive stained if both the green and red color channels were greater than 15% of intensity (mixture of the channels appears as yellow colour on the picture) and its size was equal to or exceeded eight pixels. Therefore, the number of positive stained cells was considered as a percentage of yellow colour presented on picture. Thus, the ratio of yellow pixels and total number of picture pixels were calculated and expressed as a percentage.

4.7 Von Kossa Stain

Cell mineralization was examined by von Kossa stain on gel slides using a protocol described previously (*104*). For this protocol, the following solutions were required: 1) 1% Aqueous Silver Nitrate; 2) 5% Sodium Thiosulfate; and 3) 0.1% Nuclear Fast Red (dissolved in distilled water) (all obtained from Invitrogen). Sections were incubated with 1% silver nitrate solution under UV light for 30 min and rinsed with distilled water. They were then incubated with 5% sodium thiosulfate for 5 min to remove un-reacted silver and rinsed again with dH_2O. Sections were then counterstained with nuclear fast red for 5 min. After this step, the gel sections required an additional rinse with dH_2O and dehydration in 100%, 95% and 70% ETOH. Finally, sections were protected with a cover slip and imaged using an Olympus BX61 microscope at 10x magnification. For the positive control and negative control a mouse embryo and a calcified mouse tibia were used respectively.

4.8 Mechanical Stimuli to Cell/Gel construct

The modified compression culture plate was disinfected by spraying excessive amounts of 70% ETOH and afterwards placed into a biosafety hood to allow ETOH evaporation. The plate (unmodified plate can be obtained from Flexcell) was then rinsed 3x with sterile PBS following a rinse with DMEM medium. Also, both types of rings (Marco Rubber) and porous platens (Mott Corporation) were kept in a sterile environment filled with 100% ETOH within a beaker. In a biosafety hood, ETOH was discarded and the components rinsed 3x with sterile PBS, following a rinse with DMEM medium. The lids were autoclaved for 30 min. The procedure steps of assembling the loading plate are shown in Figure 4.1.

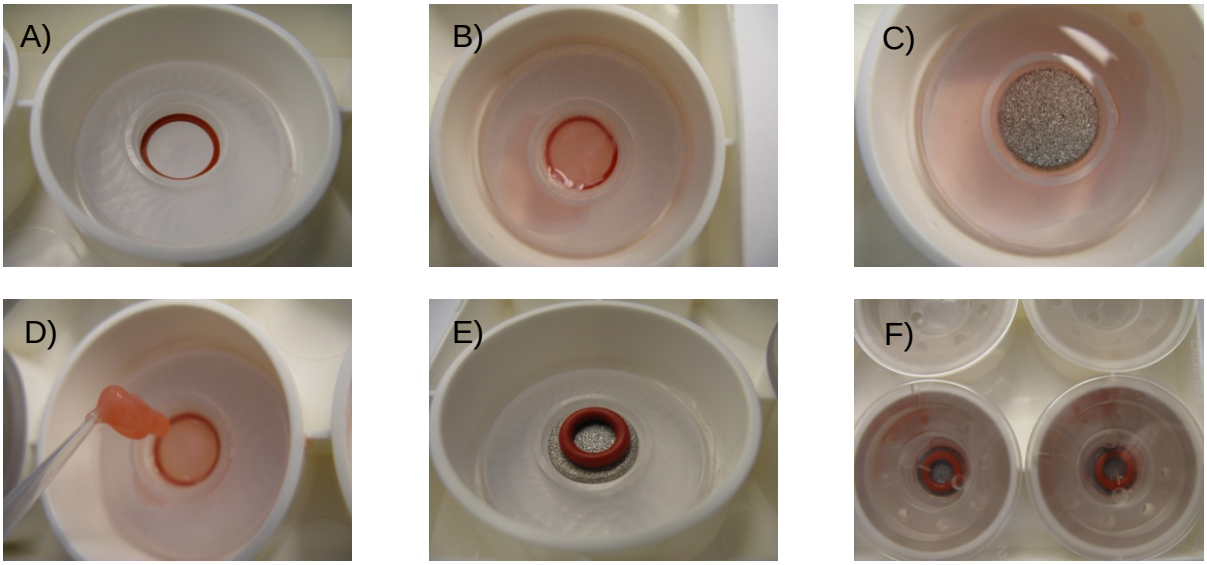

Figure 4.1: Stages of compression plate preparation for loading procedure. A) placement of bottom ring, B) adding first gel, C) placement of porous platen on top of the gel and applying pre-loading, D) placement of second gel, E) placement of porous platen on top of the gel and applying pre-loading, F) securing the system with a lid.

The system was assembled by placing the ring with a square cross section in the inner cell (A), then one cell/gel construct was placed inside that ring (B) and a porous platen placed on top of it (C). To remove excess liquid, collagen gels were pre-loaded using a 50 mL tube which was filled with 50 mL water. This is equivalent to a pre-load force of about 0.5 N (procedure not shown in Figure 1). The platen was carefully removed with tweezers and a second gel was placed inside that ring (D). The pre-loading procedure was repeated for 5 min. Again, the platen was removed and it was ensured that the collagen gel was well fitted inside the ring. The gel was centered in the ring using a pipette tip if necessarily. Then, the platen was carefully placed on top of the collagen gel and the ring with round cross section was positioned on top of the platen (E). Finally, the Flexcell lid, which has an adjustable centre, was secured on top of the load cell (F). The adjustable centre was screwed down till it just touched the ring. The plate was placed in an incubator with 5% CO_2 at 37°C and fixed within the Flexcell clamping system. The loading regime was programmed as described in Chapter 3.

4.9 Nanoparticles

4.9.1 Buffer preparation

Phosphate buffer was prepared by mixing monobasic sodium phosphate (NaH_2PO_4) (Sigma) with dibasic sodium phosphate (Na_2HPO_4) (Sigma) in a ratio of 19.7% volume per volume (v/v) to 80.3% (v/v), respectively. To receive a stock solution of 0.1 M, sodium phosphate monobasic was prepared by dissolving 11.998 g in 1 L double-distilled water (ddH_2O), pH 4.3 and dibasic sodium phosphate by dissolving 14.196 g in

1 L ddH_2O, pH 9.3. Both solutions were filter sterilized and diluted to a 10 mM working solution.

0.5 M carbonate buffer was prepared by dissolving 42 g of sodium bicarbonate ($NaHCO_3$) (Sigma) in 1 L ddH_2O. Then, 200 mL of 0.5 M stock solution was mixed with 800 mL ddH_20 to receive 0.1 M working solution. Finally, pH was adjusted to 8.5 and the solution was sterile filtered.

0.1 M borate buffer was prepared by dissolving 6.183 g boric acid (H_3BO_3) (Sigma) in 1 L ddH_2O, adjusted to pH 9.4 and sterile filtered before use.

A summary of the stock and working solutions with the corresponding pH of individual buffers is summarized in Table 4.5.

Table 4.6: Summary of buffers used throughout the preparation procedure of NP.

Buffers	**M.W. g/mol**	**Stock concentration (pH)**	**Final concentration (pH)**
Carbone buffer	84.01	0.5 M	0.1 M (8.5)
Sodium phosphate monobasic	119.98	0.1 M (4.3)	10 mM (7.4)
Sodium phosphate dibasic	141.96	0.1 M (9.3)	10 mM (7.4)
Borate buffer	61.83	N/A	0.1 M (9.4)

4.9.2 Polymer Coating

Bovine serum albumin NPs (preparation described below) were stabilized with polyethylene glycol (PEG) (JenKem Technology) and poly-L-Lysine (PLL) (Sigma) coating. For polymer conjugation, 4 mg of PLL and 11 mg PEG were dissolved in 1 mL of 10 mM phosphate buffer to obtain a concentration of 0.166 mM and 3.2 mM, respectively. Each solution was vortexed and prior to combining PLL and PEG, a 40 µL aliquot of PLL was stored in a 1.5 mL tube and at 4ºC for subsequent 2,4,6-trinitrobenzene sulfonic acid (TNBS) assays (Sigma). PLL and PEG were combined in 1:1 ration in a 2.0 or 15 mL tube to receive final coating concentration of 0.083 mM and 1.6 mM, respectively. To allow reaction between PLL and PEG, the polymer mixture was placed on shaker (Reciprokal shaker, Lab-Line) for 1 h. The solution was then transferred to 12-14 kDa dialysis (Spectrum Labs) tubing and dialysed against 0.1 M carbonate buffer under constant stirring for 12 h (up to 24 h possible). Next, carbonate buffer was exchanged with ddH_2O and dialyzed for an additional 2 h. The last step was performed 3x in total, each time exchanging clean ddH_2O. Finally, PLL-grafting-PEG (PLL-g-PEG) solution was transferred to 2.0 mL tube and stored at 4ºC. Solution was used within 24 h or frozen at -80ºC for future use.

4.9.3 Polymer Coating Conjugation Efficiency using TNBS Assay

TNBS assay was performed as described previously with small modifications (*105, 106*) and was used to determine the amine concentration in PLL and PLL-g-PEG solution. The assessment of unknown amine concentration in these samples is estimated based on a standard curve generated with known L-Lysine (Sigma) concentrations ranging

from 0 – 1 mM. A stock solution of 1 mM was prepared by dissolving 1.82 mg L-Lysine in 10 mL of 10 mM phosphate buffer and further diluted as outlined in Table 4.6 to receive 1 mM, 0.5 mM, 0.25 mM, 0.125 mM, 0.06 mM, 0.03 mM and 0 mM L-Lysine concentrations.

Table 4.7: Standard curve with known L-Lysine concentrations.

Final concentration (mM)	**Amount of L-Lysine stock solution (µL)**	**Amount of 10mM phosphate buffer (µL)**	**Final concentration (mg/mL)**
1	20	0	0.182
0.5	10	10	0.091
0.25	5	15	0.0455
0.125	2.5	17.5	0.0228
0.0625	1.25	18.75	0.0114
0.03125	0.625	19.375	0.0057
0	0	20	0.0028

TNBS was prepared by mixing 20 µL TNBS stock solution with 22 mL of 0.1 M borate buffer which provides enough reaction solution for two independent experiments. PLL stock solution containing 0.166 mM was diluted 1:1 in 10 mM phosphate buffer to obtain 0.083 mM accounting for the dilution in PLL during PLL and PEG conjugation. Then, PLL and PLL-g-PEG were diluted 20 times in 10 mM phosphate buffer to have 0-1 mM

amines per sample. Finally, test or standard curve samples, phosphate buffer and TNBS were mixed together in 1.5 mL tubes, as specified in Table 4.7.

Table 4.8: TNBS assay

Sample	Volume (µL)
Test Sample (PLL and PLL-PEG) or standard curve samples	20
10 mM Phosphate buffer	130
TNBS in 0.1 M borate buffer	850
Total	**1000**

The mixture was briefly vortexed and incubated for 1 h at 37ºC. Afterwards, 200 µL of each sample, in duplicates, were pipetted into a 96 well plate and protein absorbance measured at 405 nm using Microplate Reader (VICTOR X, PerkinElmer).

Based on the absorbance readings of PLL and PLL-g-PEG and the generated standard curve, the amount of PLL conjugated to PEG was determined according to following equation (*107*):

$$\%\text{conjugated} = \frac{[\mathrm{NH_2}_{\mathrm{PLL}}] - [\mathrm{NH_2}_{\mathrm{PLL-g-PEG}}]}{[\mathrm{NH_2}_{\mathrm{PLL}}]} * 100\ \% \qquad \text{(Equation 4.2)}$$

where $\mathrm{NH_2}_{\mathrm{PLL}}$ is the initial amine concentration and $\mathrm{NH_2}_{\mathrm{PLL-g-PEG}}$ is the final amine concentration of reacted PLL with PEG.

4.9.4 Synthesis of Bovine Serum Albumin Nanoparticles

Bovine serum albumin (BSA) nanoparticles (NPs) were prepared by a simple coacervation procedure as described by Wang et al. (*108*). Briefly, 250 µL of 10 mg/mL BSA (Sigma) solution was mixed with an equal volume of 10 mM phosphate buffer and incubated under constant stirring at 600 rpm for 5 min at RT. In order to determine PLL-g-PEG NPs encapsulation efficiency, Dextran was used as a model drug instead of BMP-2. In this experiment, 25 µL of different Dextran-FITC (Sigma) concentrations containing 0 mg/mL, 1.25 mg/mL, 2.5 mg/mL and 5 mg/mL were added to BSA solution and incubated for 30 min under constant stirring at RT. The remaining Dextran-FITC stock solution was stored at 4ºC to determine the encapsulation efficiency of NPs. After the incubation time, 2000 µL of 100% ETOH was added drop wise to the solution under stirring and stirring maintained for an additional 1 h at 600 rpm. Afterwards, 500 µL of PLL-g-PEG was combined with 500 µL NPs solution in a 1.5 mL tube and allowed to react for 1 h on an orbital shaker. The remaining NPs solution (uncoated NPs) was stored at 4ºC for encapsulation efficiency evaluation. BSA-Dextran-FITC-PLL-PEG mixture was then transferred into dialysis tubing (12-14 Da) and dialyzed against 1xPBS for 12 h. Finally, NPs were removed from dialysis tubing and transferred into a1.5 mL eppendorf tube and stored at 4ºC until use. NPs were utilized for experiments within 24 h. For BMP-2 (BMP-2 purchased from Dr. Sebald, Germany) encapsulation, 25 µL of 1.25 mg/mL BMP-2 was added to the BSA solution and performed as described for Dextran.

4.9.5 Encapsulation Efficiency

BSA NPs with 0%, 1.25%, 2.5% and 5% (w/w) Dextran-FITC were prepared as described above. The encapsulation efficiency was determined for coated and uncoated NPs based on a standard curve prepared with known Dextran-FITC concentrations. Stock solution of 0%, 1.25%, 2.5% and 5% (w/w) Dextran-FITC used for NPs preparation was diluted 1:200 in 10 mM phosphate buffer to take into account the dilution during the NP coacervation procedure. Uncoated NPs were diluted 1:2 with 10 mM phosphate buffer to take into account additional dilution of NPs during polymer coating. Then, 200 µL of phosphate buffer (blank), standard curve, uncoated NPs (control) and coated NPs (unknown samples) with 0%, 1.25%, 2.5% and 5% Dextran-FITC concentrations were pipetted in duplicate into a 96 well plate. The fluorescence of FITC was measured at excitation 485 nm and emission 535 nm using a microplate reader to determine Dextran-FITC fluorescence.

The encapsulation efficiency of BMP-2 was determined for BSA NPs coated with PLL-PEG, PLL-PEG-RGD and free BMP-2. BSA NPs with 1.25 mg/mL BMP-2 were prepared as described above, however, prior the final dialysis step, 20 µL of the tested NP samples or free BMP-2 in duplicates were transferred to 1.5 mL tube and stored at -80º C until quantified using enzyme-linked immunosorbent assay (ELISA) (R&D System) as described below. Prior to performing ELISA, samples were thawed at RT and diluted with 80 µL PBS to have a total volume of 100 µL. The concentration of BMP-2 in all samples was determined based on a standard curve with known BMP-2

concentration. Finally, the encapsulation efficiency was calculated using following equation:

$$\%encapsulation\ efficiency = \frac{C_{encapsulated}}{C_{initial}} * 100\% \qquad \text{(Equation 4.3)}$$

where $C_{encapsulated}$ is the determined concentration of Dextran-FITC in NPs after dialysis and determined concentration of BMP-2-NPs with different coatings before dialysis. $C_{initial}$ is the initial concentration of Dextran-FITC (i.e. 0, 1.25, 2.5 and 5 mg/mL) or BMP-2 (1.25 mg/mL) added to the NPs.

4.9.6 Release Rate of Dextran-FITC and BMP-2

Nanoparticles with different dextran-FITC concentration were prepared as described above and the release experiment was performed after the final dialysis step. After preparation of the NPs, 100 µL samples were placed in 100 kDa dialysis tubing (Spectrum Labs) which was sealed on both ends with dialysis clamps. Then, the dialyses tubing was placed in a petri dish and immersed in 5 mL PBS and 1 mL Antibiotic-Antimycotic (anti-anti) (Invitrogen) and placed in an incubator with 5% CO_2 at 37°C. A sample of 100 µL was taken daily and the fluorescence of FITC was measured at excitation 485 nm and emission 535 nm using a microplate reader to determine Dextran-FITC release to the supernatant. Finally, the removed amount was replaced with PBS to maintain constant volume over time. The release experiment was performed over a time period of 6 days.

To determine BMP-2 release rate to the supernatant, NPs containing BMP-2 were prepared as described above and the release experiment was conducted before the

final dialysis. A similar procedure was performed as described for the release experiment with NPs containing Dextran-FITC. However, after collecting samples, samples were stored at -80ºC and BMP-2 was detected using ELISA.

4.9.7 BMP-2 Concentration using ELISA

ELISA was performed to quantify BMP-2 concentration in different experimental conditions. BMP-2 concentration was evaluated for the encapsulation efficiency within BSA-NPs with different coatings such as PLL-PEG and PLL-PEG-RGD and to determine BMP-2 release rate in a dish to estimate its release when incorporated into cell/gel construct.

ELISA was performed using a BMP-2 Immunoassay kit (R&D System) according to the manufacturer's instructions. The reagents supplied with the kit were allowed to equilibrate at RT for 15 min before use. Concentrated wash buffer was diluted 1:25 and calibrator diluent RD5P was diluted 1:10 with ddH_2O, respectively. Substrate solutions consisting of color reagent A and color reagent B were mixed together at 1:1 ratio. The BMP-2 standard was prepared by adding 1 mL of ddH_2O to BMP-2 powder which resulted in a concentration of 20 ng/mL. This stock solution was allowed to mix under gentle agitation for 15 min and a standard dilution was prepared in the range of 4 ng/mL to 0.0625 ng/mL. For the assay, 100 µL of RD1-19 diluent, followed by 50 µL of standard solution or samples were pipetted into a 96 well plate, covered with an adhesive strip and shaken for 2 h on an orbital shaker (Reciprokal shaker, Lab-Line). After the incubation time, the solution was aspirated and the wells rinsed 4x with 200 µL wash buffer. Then, 200 µL BMP-2 conjugate was added to each well, covered with an

adhesive strip and incubated for 2 h with shaking. After the incubation, the washing step was repeated as described. In the next step, 200 µL of substrate solution was added to each well and incubated for 30 min at RT. To stop the reaction, 50 µL of stop solution was pipetted into each well, gently mixed and the absorbance measured at 450 nm with a correction reading at 540 nm using microplate reader.

4.9.8 Nanoparticle Size and Zeta Potential

Particle size and zeta potential of BSA NPs were determined using Malvern Zetasizer Nanoseries ZS using DTS software. All experiments were performed at 25ºC and at a scattering angle of 173º. Prior to the actual measurement, the absorbance of NPs was determined using an UV-Vis spectrometer which was a necessary input parameter for the DTS software in order to determine particle size. For the size measurement, 100 µL of NPs stock solution was diluted 1:10 in PBS. Then, 1 mL of the solution was pipetted into a disposable cuvette and loaded into the Zetasizer. After measuring particle size, the solution was reused for zeta potential measurements with an additional 1:10 dilution. For the zeta potential measurement, a special surface zeta potential cell (Malvern) was used which was rinsed first with water and then filled with NPs solution. This cuvette was loaded into the Zetasizer and zeta potential measured. The Malvern Zetasizer performed 15 and 5 measurements to obtain the mean particle size and zeta potential for one sample.

4.10 Statistics

Quantitative rt-PCR was quantified using the established $2^{-\Delta\Delta CT}$ method (*103*). All gene expression data was normalized to 18S and then against a control sample. All statistics evaluations were made using one-way ANOVA using GraphPad Prism 4 software otherwise specified. Statistical significance level α was chosen as 0.05, and an experiment was considered as significant when the p-value was less or equal to α level. If samples were significant then a within groups Bonferroni's Multiple Comparison Test was performed. The log10 RQ values were ploted as mean + standard error (SE).

Descriptive statistic was conducted in duplicates for viability, immunofluorescence, polymer conjugation, polymer encapsulation and release rate and the results are expressed as mean ± standard deviation (SD). Statistical evaluation were made using one-way Anova when more than three groups were compared while two groups were compared using an unpaired t-test.

CHAPTER 5: COLLAGEN-MEDIATED MURINE EMBRYONIC STEM CELL DIFFERENTIATION

The application of ESCs in regenerative medicine is promising due to their unique ability of self-renewal and to differentiate into any cell type in the body (*109*). Before ESCs-related therapies can be utilized for clinical application, it is necessary to identify and optimize the cues that drive ESCs differentiation into a specific lineage. For example, bone and cartilage cells (osteoblasts, osteoclasts, chondrocytes) can be produced by exposing ESCs to soluble factors or by forming embryoid bodies (which mimic early development) (*41, 110*). With advances in TE and the understanding that cells behave differently in 3-D culture (*111*), the identification of biomaterials that support ESCs differentiation is critical to successful TE. Various synthetic (i.e. polymers, ceramics, metals) and naturally derived biomaterials (i.e. collagen, fibrinogen, hyaluronic acid) have been investigated for their use in BTE. The preference of collagen over other materials arises because collagen type I is a natural component of bone ECM and thus supports cell attachment, proliferation and differentiation.

In a recent study by Krawetz et al. (*18*), the differentiation ability of mESCs supported by collagen type I was investigated. They showed collagen gels polymerized with βGP support osteogenic differentiation while collagen gels polymerized with chondrotin sulfate and βGP induce chondrogenic differentiation. When this gel system was transplanted subcutaneously into a SCID mouse (severe combined immunodeficiency mouse), no tumors were observed six to eight months post-transplantation.

The cell-matrix interactions play a fundamental role in determining cellular fate, especially natural biomaterials such as collagen are utilized. Integrins recognize an amino acid repetition sequence in ligands such as collagen (*51*). To date, research has shown that collagen-dependent integrins (i.e. α subunits 1, 2, 10 and 11 bind to β1 subunit and form the collagen-recognizing receptors) bind to the GFOGER amino acid sequence of collagen upon which conformation changes occur leading to integrin activation. Another class of integrins is known as RGD integrin receptors (i.e. αv bind to β3, 5, 6 and 8 subunits while α5 subunit specifically bind to β3), these integrins recognize a RGD amino acid sequences presented in ECM of fibronection, vitronectin, osteopontin and bone sialprotein (*112*). The role of integrins in mediating differentiation fates still requires additional research due to the diversity of integrins expressed in different cell types and the distinct responses to interaction of different materials different integrin pairs can exhibit.

Due to these promising findings, this chapter focuses on further development and characterization of this gel scaffold system with the objective of closely examining and understanding the effect of the collagen-βGP ECM on ESCs differentiation.

First, the general handling and morphological appearance of the collagen gel was examined and mESCs viability was identified over an extended time in cell culture. Cell differentiation was examined at the gene and protein level, and cells were evaluated on their ability to mineralize the collagen matrix. Next, we examined the integrin gene expression when mESCs were seeded on collagen gels over time to evaluate their role in mediating differentiation. Specifically, we evaluated the role of α1, β1, αV and β 3

subunits. This specific set of integrins represent one class of collagen dependent Integrins (α1β1) and one class of RGD dependent Integrins (αVβ3).

5.1 Results

5.1.1 Macroscopic Analysis of Cell Seeded Collagen Matrix

The morphology of the collagen constructs was evaluated over time. ESCs were seeded at a cell density of 10^6 cells per 1 mL gel and the gel morphology was examined after 1 and 15 days post-seeding as shown in Figure 5.1.

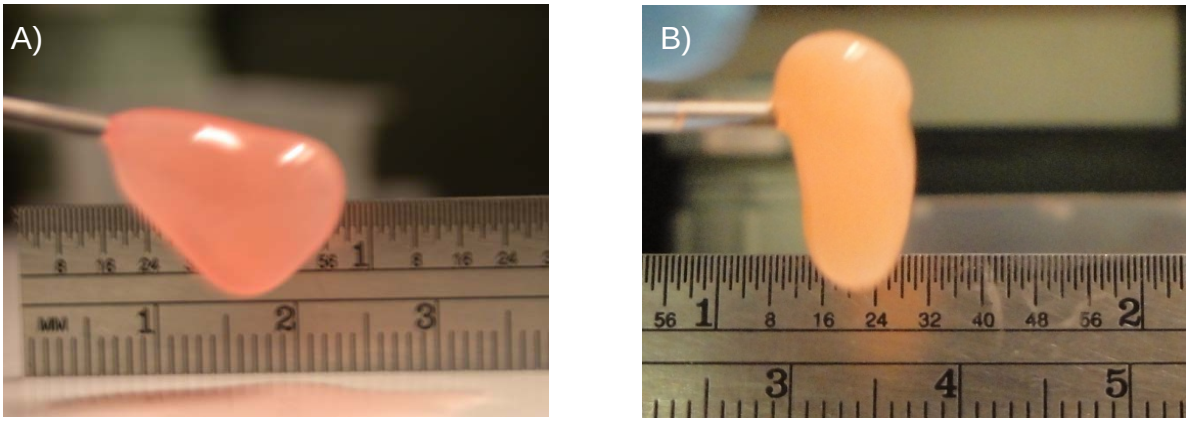

Figure 5.1: Macroscopic view of collagen gels seeded with mESCs (A) at day 1and (B) at day 15 post seeding. Gels were seeded with 10^6 mESCs per gel. At both time-points collagen gels exhibited soft properties and a colour change occurred by day 15.

The collagen gels exhibited biphasic properties with both liquid and solid phases. Gels were soft but did not pull apart due to their own weight when lifted and maintained their general shape when returned to a flat surface. After 15 days, a slightly colour shift from rose to orange was observed. Most likely the mESCs metabolic activity caused a pH shift in the media and a resultant change in colour, becoming slightly more acidic.

5.1.2 Cell Viability

An essential requirement for any cell based scaffold construct is the maintenance of cell viability. The viability of mESCs seeded in a collagen gel was determined after 1, 15 and 30 days of differentiation using Calcein AM and Ethidium homodimer-1 stain. Calcein AM will fluoresce green in the presence of intact esterase activity which exists only in viable cells. Ethidium homodimer-1 only passes through a damaged plasma membrane and will fluoresce red after binding to nucleic acids in a cell. This characteristic allows the distinction between live (green) and dead cells (red). The viability of mESCs seeded on collagen gels over time is shown in Figure 5.2.

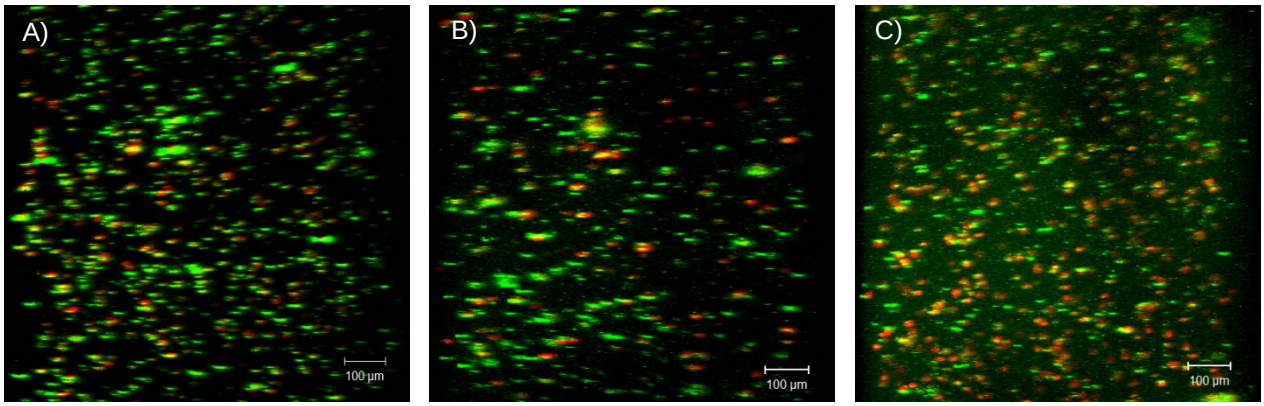

Figure 5.2: Three-dimensional projection images were created to determine mESCs viability when seeded at an initial seeding density of 10^6 cells per collagen gels over 30 days. A) On day 1 83% of cells survived; B) on day 15 cell viability increased to 85%; and C) on day 30 cell viability decreased to 43%. Green dots represent viable cells and red dots dead cells. Mean ±SD, n=2.

mESCs maintained their viability within the collagen scaffold over the investigated time period. On day 1, cells had a viability of 83%±7 which remained unchanged on day 15 to 85%±5.6. By day 30, cell viability decreased to 43%±2.6.

5.1.3 Cell Differentiation

The differentiation behaviour of the mESCs seeded in the collagen gels was assessed over time based on their gene expression level using quantitative real-time polymerase chain reaction (qrt-PCR), on their protein level using immunofluorescence, and on mineralization using von Kossa staining.

5.1.3.1 Gene Expression

The expression of genes specific for mESCs pluripotency, osteogenesis and chondrogenesis were examined on day 1, day 15 and day 30 using qrt-PCR. All genes, expressed at the specified time points, were normalized to the gene expression of 10^6 mESCs cultured in 2-D in the presence of LIF and to a housekeeping gene (18S). In general, when analysing the gene expression with the $2^{-\Delta\Delta Ct}$ method, the expression of the control sample (i.e. mESCs cultured in a dish) is set to 1 and the gene expression of the treatment groups is shown in respect to this control. In this study, the same method is applied, however the gene expression is shown as $\log_{10}$ RQ values, and because $\log_{10}$ of 1 is 0, the relative expression of the control samples is set to 0. The treatment groups are shown in respect to the calibrator and a RQ value of 1 means that the expression is 10 times higher in comparison to the control sample. Similarly, when the RQ value is shown as -1, the relative gene expression is 10 times lower in comparison to the control samples.

The gene expression of Oct 4 and Sox 2 is an indication for mESCs pluripotency while the down regulation indicates initiation of differentiation as shown in Figure 5.3.

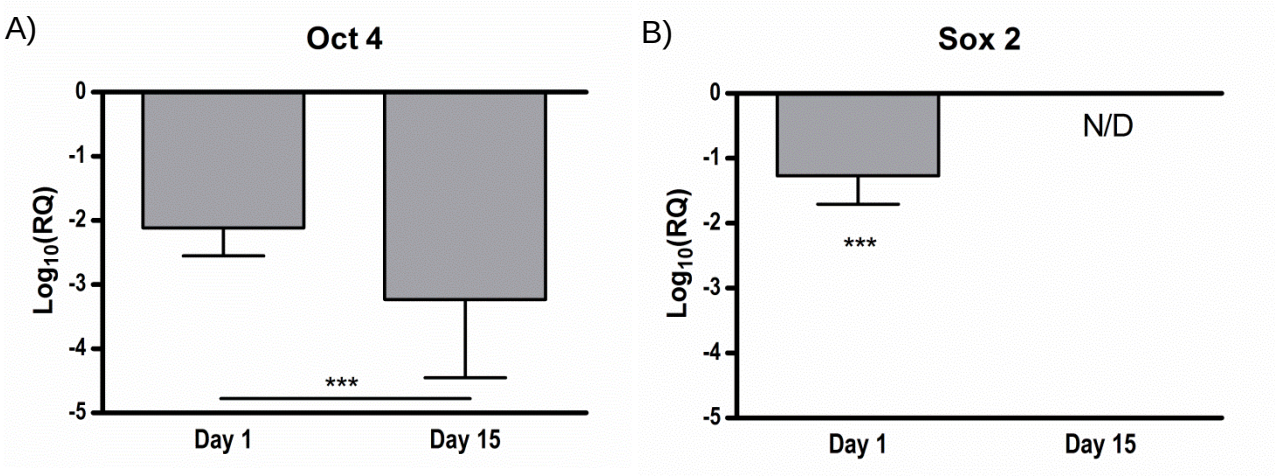

Figure 5.3: Pluripotent gene expression of mESCs seeded in collagen gels after 1 and 15 days post polymerization relative to mESCs cultured in 2-D. A) Oct 4 gene expression was significantly down regulated at day 1 and day 15, $p < 0.0003$. B) Sox 2 gene expression was significantly downregulated at day 1 and was not detectable at day 15, $p<0.0001$. Mean + standard error (SE), n = 3. Abbreviation: RQ=Relative Quantification; N/D= not detectable.

The gene expression of both pluripotent markers was down regulated in comparison to mESCs control groups over time indicating initiation of differentiation. The relative gene expression of Oct 4 was down regulated 20 fold at day 1 and 35 fold on day 15 and the relative gene expression of Sox 2 was down regulated 12 fold and not detectable at day 15, $p<0.0001$.

In the next step, the ability of mESCs to differentiate into osteogenic and chondrogenic lineages, supported by the collagen matrix, was evaluated over 30 days. The gene

expression patterns specific for both osteogenic and chondrogenic lineage was detected and normalized to mESCs cultured in the dish as shown in Figure 5.4.

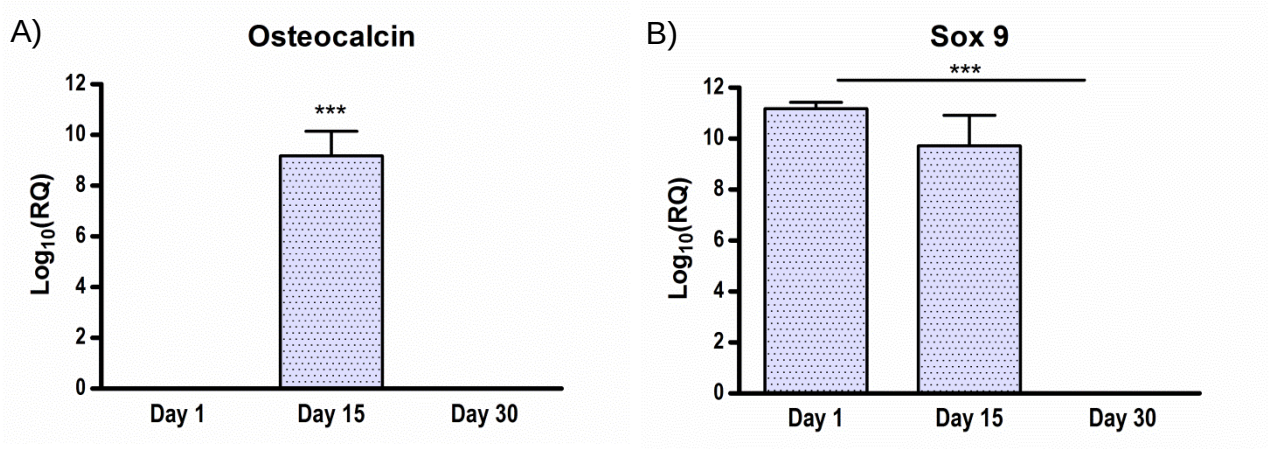

Figure 5.4: Gene expression of differentiation markers over 30 days of culture. The gene expression of mESC seeded in Col I is shown relative to mESCs cultured in the dish: A) Osteocalcin expression and B) Sox 9 expression. Mean + SE, n = 3. Abbreviation: RQ=Relative Quantification.

Based on the gene expression data obtained at day 15, it appeared that mESCs differentiate into heterogeneous cell population of osteoblasts and chondrocytes.

Osteocalcin, which is a marker for osteoblasts was 90 fold up regulated on day 15. However, no osteocalcin expression was detected in the mESCs control samples, in either the day 1 or day 30 samples, $p<0.0001$.

The gene expression of Sox 9, which is a TF for chondrocyte differentiation was 110 fold and 95 fold up regulated on day 1 and day 15, respectively but was undetectable in the mESCs control and day 30 samples, $p<0.0001$.

Due to the presence of a heterogeneous cell population, especially on day 15, immunofluorescence was performed to show both osteogenic and chondrogenic proteins.

5.1.3.2 Immunofluorescence

Immunofluorescence was performed on mESCs seeded on Col I gels on day 15 and day 30 of differentiation. Protein expression specific for pluripotency (Oct 4) as well as osteogenic (OSX, BSP), chondrogenic (Sox 9, Col 2, Agg) differentiation was evaluated and is shown in Figure 5.5 for day 15 and in Figure 5.6 for day 30, respectively.

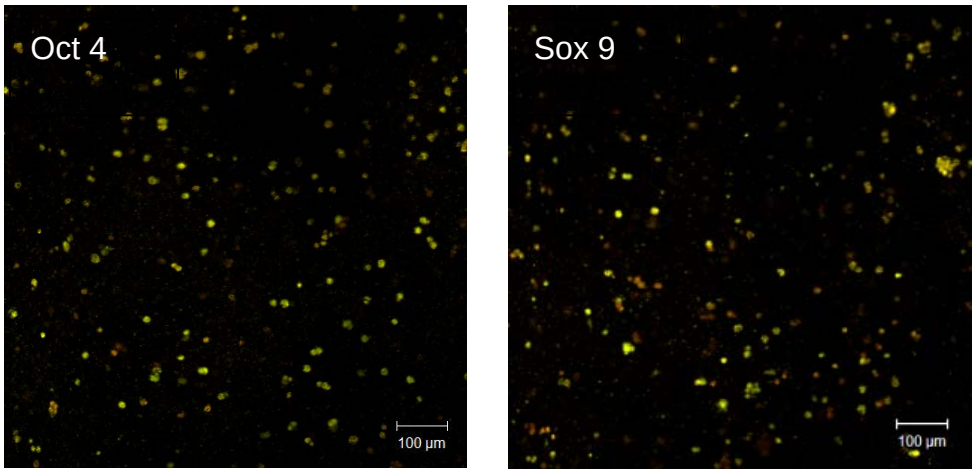

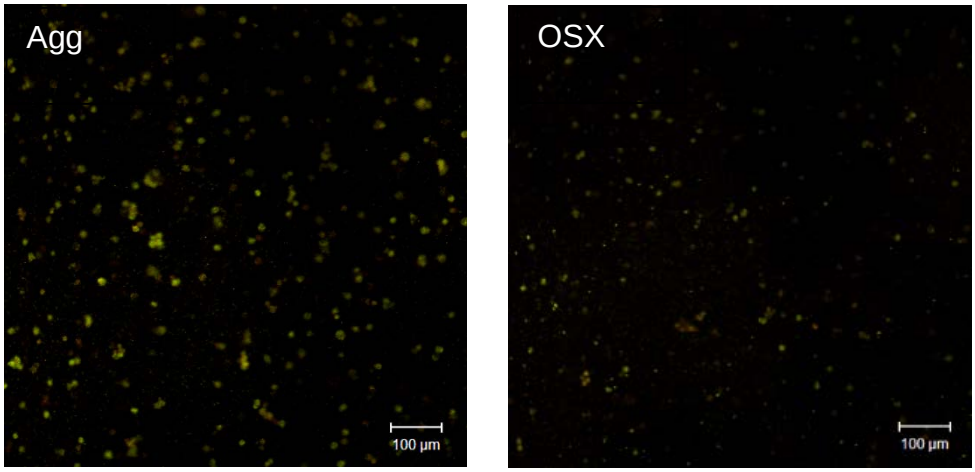

Figure 5.5: Immunofluorescence of selected proteins on day 15. Single slice images were obtained. Gels were counterstained with phallodin that binds to F-Actin and fluoresces red and positive stained cell fluoresce green.

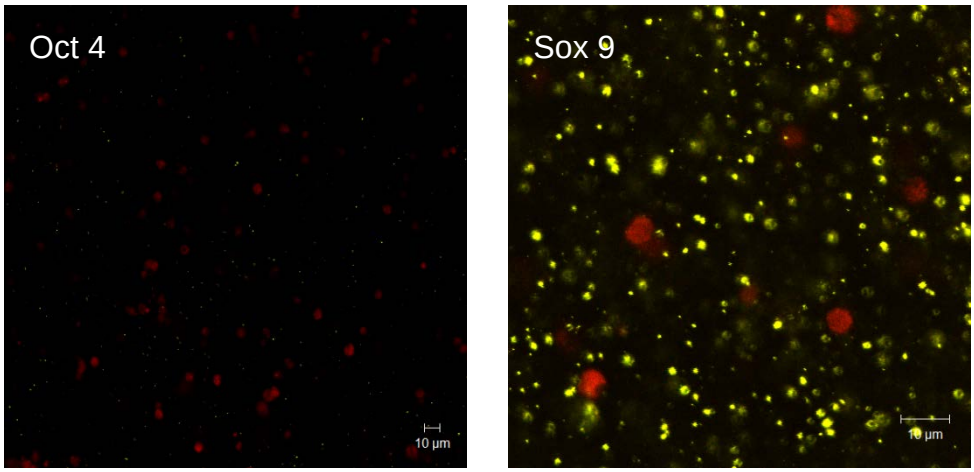

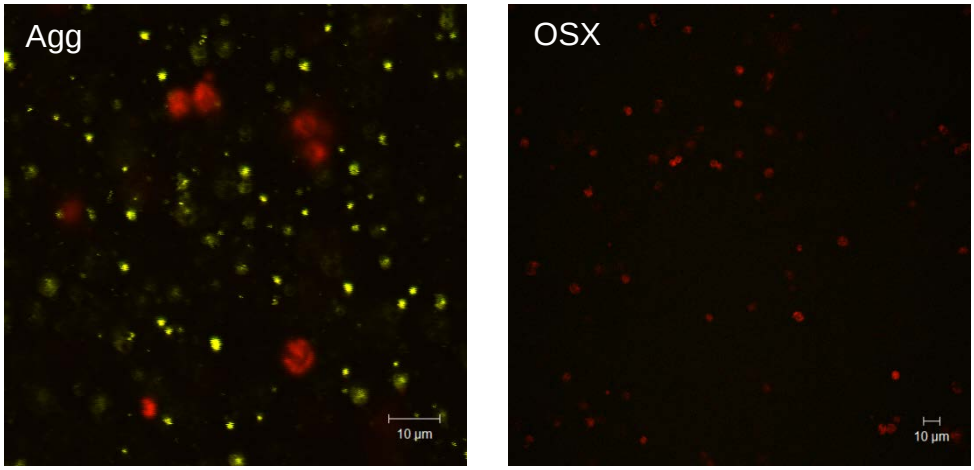

Figure 5.6: Immunofluorescence of selected proteins on day 30. Gels were counterstained with phallodin.

Immunofluorescence analysis revealed positive stained cells for pluripotent, osteogenic and chondrogenic proteins on day 15, confirming the above gene expression data. Specifically, cells were stained positive for Oct 4, Sox 9, Agg and Osx (shown in Figure 5.5) and for Col 2 and BSP (not shown in Figure 5.5) on day 15. However, on day 30 cells were positive for chondrogenic proteins but not for osteogenic.

For a better illustration of the difference between the proteins expressed on the specific time points, the percentage of positive stained cell is summarized in Table 5.1.

Table 5.1: Immunofluorescence analysis. Gels were stained for osteogenic and chondrogenic proteins on day 15 and day 30 and are expressed as a percentage of positive cells. Mean ± SD, n=2.

	Chondrogenic			**Osteogenic**		**Pluripotent**
Proteins	**Sox 9**	**Agg**	**Col 2**	**BSP**	**OSX**	**Oct 4**
Day 15, %Cell	2.73	0.84	0.16	0.15	0.19	2.17
Day 15, ±SD	1.58	0.12	0.02	0.01	0.07	0.03
Day 30 %Cell	8.14	1.84	0.27	0	0	0
Day 30, ±SD	2.19	0.50	0.18	0	0	0

In summary, pluripotent, osteogenic and chondrogenic cells are present on day 15, while only chondrogenic positive stained cells were observed on day 30. To further characterize this cell/gel system von Kossa staining to visualize mineralization was performed.

5.1.3.3 Matrix Mineralization

Von Kossa stain is a well established method to detect the deposition of calcium salt which is an indicator for mineralization (*113*). During the staining procedure, the samples are treated with silver nitrate and placed under UV light which leads to a reduction reaction of the calcium. Consequently, the calcium salts are visualized as dark dots. Because mineral deposition is a late stage process of osteogenic differentiation, only day 30 samples were evaluated as shown in Figure 5.7.

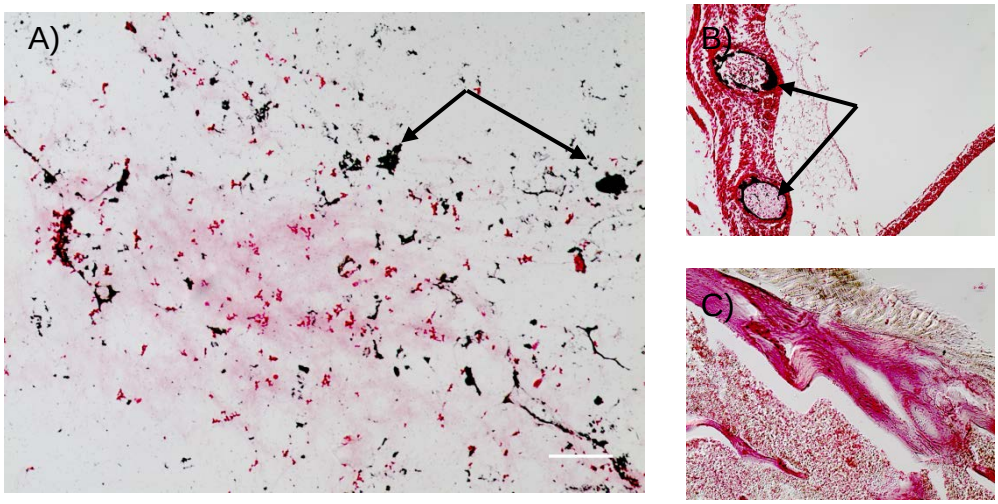

Figure 5.7: Von Kossa stain on sectioned collagen gels. A) mESCs seeded in the collagen gel at day 30 showed phosphate deposition which is indicated with black arrows, B) positive control: chicken embryo, C) negative control: demineralised bone. Phosphate salt is visualized as dark dots. Scale bar: 100 µm.

Von Kossa staining in the collagen gels showed a random distribution of mineralization nodules indicating that mESCs-derived osteoblasts started to develop a mineralized collagen matrix (Figure 5.7, A). To confirm that the resulting black deposits were calcium, chicken embryo and decalcified bone was used as positive and negative controls, respectively. Chicken embryo shows deposition of calcium during vertebral column formation (Figure 5.7, B) whereas no positive staining was observed in decalcified bone (Figure 5.7, C). These results verify that the black deposition found in the matrix is calcium salt.

5.1.4 Integrin-Mediated Differentiation of mESCs Seeded in Col I

The above findings indicate mESCs seeded on collagen gels support a heterogeneous cell population of osteoblasts and chondrocytes. In addition to our study, others have reported that collagen can support the differentiation of heterogeneous cell populations. However, the involvement of integrins in cell-mediated differentiation was not examined. Therefore, we examined the gene expression of collagen-dependent and RGD-dependent integrins when mESCs were seeded in collagen gels and allowed to differentiate over time. The expression of these subunits was analyzed on day 1 and day 15 of mESCs differentiation and normalized to mESCs cultured on planar surface in the presence of LIF as shown in Figure 5.8.

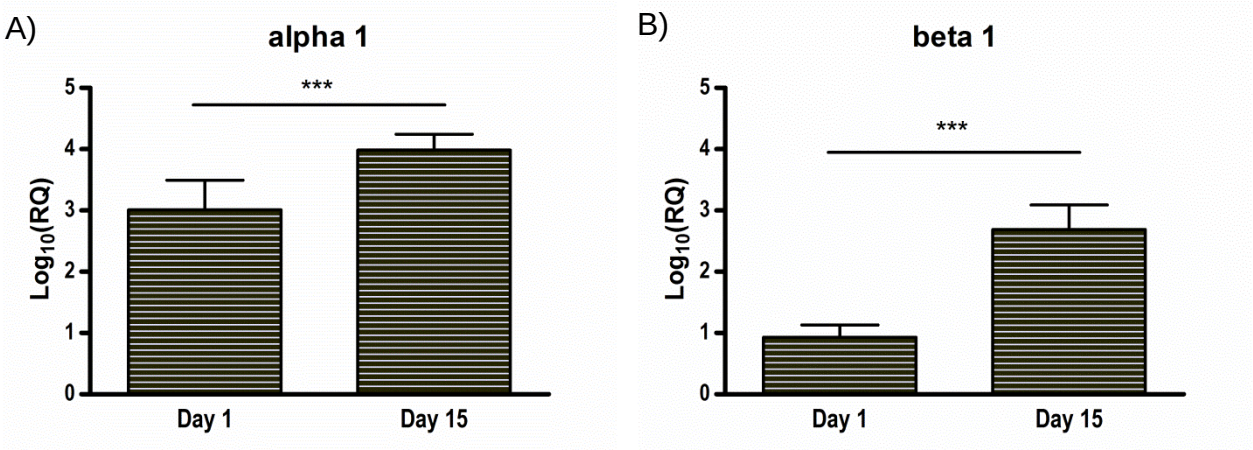

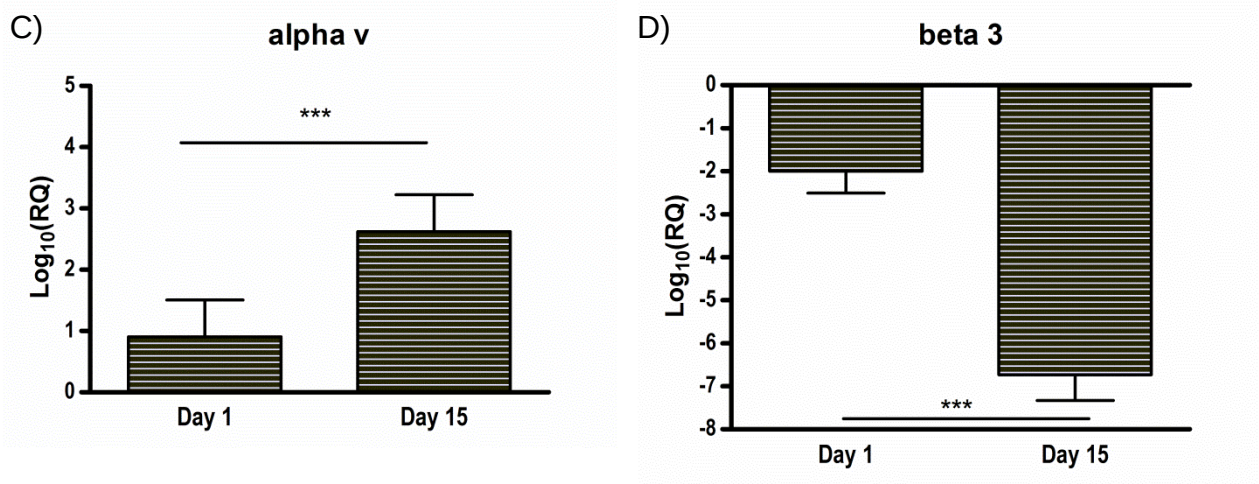

Figure 5.8: Integrin gene expression of mESCs seeded in collagen gels over 15 days. A) α1, B) β1, C) αV, and D) β3 subunit expression. Mean + SE, n=3. Abbreviation: RQ=Relative Quantification.

These results indicated that mESCs seeded in collagen gels express α1, β1, αV and β3 subunits and the expression of α1, β1 and αV was up-regulated while β3 subunit was down regulated when mESCs differentiated into osteogenic and chondrogenic lineages. Specifically, the gene expression of the α1 subunit was up regulated 30 fold on day 1 and 40 fold on day 15, $p<0.001$. The gene expression of the β1 subunit was up regulated 9 fold on day 1 and 26 fold on day 15, $p<0.0002$.

The αV subunit was up regulated 10 fold at day 1 and 26 fold on day 15, $p<0.0001$. Only the expression of β3 subunit was down regulated at all time points. It was down regulated by 20 fold and 67 fold on day 1 and day 15, respectively, $p<0.0001$.

5.2 Discussion and Conclusion

Living tissue is a complex 3-D network made of cells that are surrounded by ECM. In order to gain deeper insights into the processes of musculoskeletal and orthopedic disorders occurring in the human body, and subsequently to develop transplantation material for diseased tissue, TE focuses on the challenge of combining cells and scaffolds as potential therapeutics. Collagen type I is a commonly used biomaterial which can be readily combined with cells because it is both highly bio– and osteo-compatible. ESCs are a promising cell source because an unlimited cell number can theoretically be achieved for transplantations. In combination, collagen matrix polymerized with βGP or βGP and chondrotin sulfate, have shown to direct mESCs differentiation into osteoblasts and chondrocytes, respectively (*18*) which could be attributed to cell matrix interaction via integrins. Integrins have a structural and a regulatory role during the early stage of development and throughout life. These heterodimers connect cells with the extracellular environment and allow cell attachment, migration, proliferation, and differentiation (*114*). In the present study this cell/gel construct was further characterized and the gene expression of integrins during mESCs differentiation evaluated.

Firstly, the morphological appearance of the cell/gel construct was examined. Over the investigated time period, collagen gels exhibit highly hydrated properties with no visible size contraction. In the next step, the ability of the collagen scaffold to sustain cell viability was evaluated over 30 days. It was shown that cells maintain their viability up to day 15 with a slight, but not significant increase from 83% to 85% from day 1 to day 15

following a rapid decrease to 43% on day 30. The significant reduction in cell viability by day 30 could be explained by cell metabolic activity over time. During cellular activities such as proliferation and differentiation, cells consume nutrients and consequently secrete metabolic waste. This 3-D collagen system is a self-sustaining system, and after preparation no additional nutrients are supplied. This means, cells have only media that was provided at the beginning within the gels for their nutrient intake. Another important parameter in maintaining cell viability is oxygen exchange. We found that when maintaining constant volume and increasing surface area of the gels, cell viability can be increased (data not shown). Therefore, collagen gels were prepared in 12 wells plates and not in 24 wells as reported by Krawetz et al. (*18*). However, their study did not examine mESCs viability in the 3-D collagen scaffolds but reported a 40% decrease in cell viability at day 15 when mESCs were cultured on a 2-D collagen film.

Assessment of cell differentiation was examined over 30 days. It was found that both on the gene and protein level, mESCs seeded on collagen I scaffold express chondrogenic and osteogenic markers on day 15. However, immunofluorescence showed consistent up-regulation of chondrogenic proteins and no expression of osteogenic and pluripotent proteins on day 30. Similar results were obtained by Krawetz et al. (*18*) in terms of osteogenic differentiation with the gene expression of osteocalcin up regulated and immunofluorescence showed positive stained cells for osterix protein on day 15. However, their study did not evaluate collagen/ βGP gels for chondrogenic markers but focused alone on whether collagen gels can support osteogenic and chondrogenic differentiation. The ability of a collagen matrix to support ASCs differentiation or to

regulate cell function of fully differentiated cells has been reported by others (*64-66, 82, 115*). Recently, showed collagen scaffolds prepared by fibrillogenesis do not specifically direct one lineage commitment but activate a variety of genes regulating osteogenic, chondrogenic, myogenic, and adipogenic differentiation in human MSCs (*66*). They stated that when human MSCs start to differentiate, they retain multiple possible lineages by maintaining their multipotency and additional signals are necessary for final lineage commitment. The observed expression of Oct 4 on the gene and protein level by day 15 supports the above postulation that some of the mESCs maintain pluripotency, possible similar to a transient amplifying pool of stem cells and thus remain uncommitted when seeded in collagen scaffold.

The expression of pluripotent markers is often associated with tumor formation. However, the interaction of cells with collagen matrix via integrins might also be involved in suppressing mESCs tumorgenic potential because no tumors were observed when mESCs were seeded in collagen matrix and directly transplanted subcutaneously into a SCID mouse (*18, 19, 116*).

Collagen-dependent integrins are required to physically attach mESCs to collagen matrix. Much insight of integrin functions have been learned in the past decades, yet the role of integrins in ESCs lineage commitment is not fully understood and only recently the potential of manipulating Integrins to promote differentiation or self-renewal came into focus (*117-119*). We evaluated the role of integrins in mediating mESCs differentiation within the cell/gel construct at early and intermediate stages of differentiation. Specifically, we looked at gene expression of α1, β1, αV and β3 subunits.

Initiation of mESCs seeded in 3-D collagen matrices was supported by the expression of α1, β1, and αV subunits while the β3 subunit was not required and therefore was down regulated.

In summary, to better understand the observed differentiation process it is necessary to look more closely at the process of ESCs differentiation into osteogenic and chondrogenic lineages *in vivo*.

Both cell types have the same origin, being derived from mesodermal germ layer, and further derived from mesenchymal progenitor cells. Furthermore, bone development involves two distinct processes; intramembranous and endochondral ossification. When bone develops by intramembranous ossification, osteoblasts derive directly from mesenchymal progenitor cells while during the process of endochondral ossification, chondrocytes are derived from mesenchymal progenitor cells forming cartilage and then osteoblasts (*35*). Thus, the following mechanism of collagen mediated mESCs differentiation into osteogenic and chondrogenic lineage is proposed in Figure 5.9.

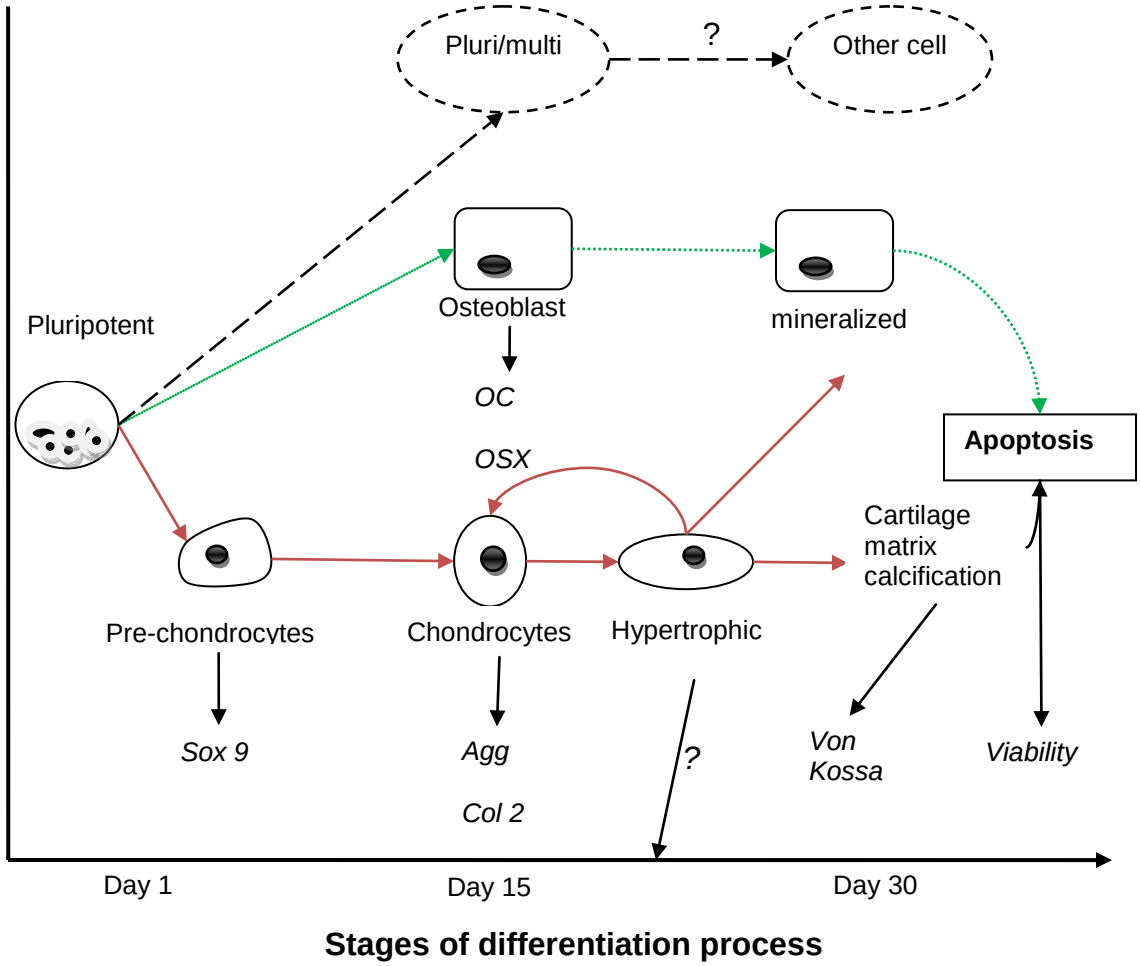

Figure 5.9: Proposed mechanism of mESCs when they are cultured on 3-D collagen matrix. Dashed lines represent the presence of progenitor cells, green solid line represent the differentiation pathway of mESCs into osteoblasts, and red solid lines represent the differentiation pathway of mESCs into chondrogenic lineage.

When mESCs are seeded within collagen scaffolds they may follow three different pathways, two of which are closely interconnected. As mentioned above, it is believed that some cells remain transient amplifying progenitors, and thus are able to differentiate into osteogenic or chondrogenic lineages over a time course of 15

days (black dashed lines). It is also possibly that other cell types of mesenchymal origin are present.

Another differentiation pathway involves mESCs differentiation into pre-chondrocytes as identified by the gene and protein expression level of Sox 9 which is the main regulator for chondrogenic differentiation (*120*). At day 15, mature chondrocytes form as identified on the protein level by Agg and Col 2. Mature chondrocytes can differentiate into hypertrophic chondrocytes which exclusively express Col X (*121*). In the present study, Col X expression was screened on day 30 but was not detected (data not shown). Therefore, it is believed that hypertrophic chondrocytes develop somewhere at the stage between day 15 and day 30. Hypertrophic chondrocytes have multiple functions. Firstly, they can re-differentiate back to chondrocytes, expressing a mature form of Col 2 as identified by its protein level at day 30. Secondly, they have the ability to trans-differentiate into osteoblasts or contribute to matrix mineralization which consequently leads to apoptosis (red solid lines) (*121, 122*).

The gene expression level of osteocalcin and the presence of osterix protein on day 15 (before hypertrophic chondrocyte stage) indicate that some cells directly differentiate into osteoblasts without going through the chondrocytic pathway (green dashed lines).

In future studies a wider range of genes specific for the proposed mechanism should be evaluated in a compact time frame. This could be conducted using micro array analysis.

Overall, the findings of the current study indicate that a collagen matrix supports both chondrogenic and osteogenic differentiation pathways and that derived chondrocytes have differentiation plasticity similar to findings reported by others (*122*).

mESCs differentiation by EBs formation result in heterogeneous cell population but the effect of ECM to support heterogeneous differentiation has not been largely explored (*123*). The first study reporting that ECM may trigger heterogeneous population was conducted by Santiago et al. (*123*) showing that collagen type I supported MSCs differentiation into a heterogeneous population of cardiomyocytes, adipocytes, and osteoblasts. Another study reported that collagen type I directs MSCs differentiation into chondrogenic and osteogenic lineages in the presence of Dexamethasone and TGFβ-1 (*124*). Our findings suggest initiation of mESCs seeded in 3-D collagen matrices into a heterogeneous population was supported by the expression of α1, β1, and αV subunits but not β3 subunit. The role of the integrins is further explored and described in Chapter 7.

The reported observations are also an indication that cells require additional cues for their final lineage commitment. These cues may be chemical (additional supplementation of osteogenic/chondrogenic factors), biological (BMP-2 or TGFβ) or mechanical (tensile/compressive load). As the supplementation of chemicals and biological cues to collagen matrix still resulted in a heterogeneous cell population (*124*) we first aimed to explore whether mechanical stimuli could trigger mESCs lineage commitment toward osteogenic or chondrogenic lineage and might be a better cue to drive mESCs differentiation.

CHAPTER 6: EFFECT OF CONFINED COMPRESSIVE LOAD ON MURINE EMBRYONIC STEM CELL DIFFERENTIATION

Mechanical forces play an important role in osteochondral tissue development, haemostasis, and repair. Throughout life, healthy bone is exposed to compressive and bending loads which cause strain of approximately 0.2% strain (*78*). Bending can cause fluid flow along a gradient from the location under compression to that under tension, flushing fluid through the canalicular network, and exposing osteocytes to shear stress, which can then transmit signals to osteoblasts and osteoclasts to maintain bone haemostasis (*73, 125*). Cartilage on the other hand is exposed to compressive strains as large as 10%, among other mechanical factors such as fluid flow and hydrostatic pressure that provide mechanical cues to the chondrocytes to maintain cartilage in a healthy state (*78, 79*).

During bone development, in addition to biochemical factors physical cues such as tension, compression and fluid shear stress can influence the rate of bone formation (*27*) while compressive loading and hydrostatic pressure pre-dominantly influences cartilage formation and calcification (*83, 126, 127*). Considering the importance of mechanical stimuli in bone tissue, it is of high interest to find the mechanical conditions that can induce SC differentiation into a specific lineage. Much research has been directed to understand and establish how physical factors (applying a variety of loading regimes) direct SC differentiation *in vitro* but the reported findings are controversial and difficult to adapt for one specific cell type or one specific loading regime for different cell types. For example, fluid flow shear stress has shown to induce

MSCs differentiation into multiple lineages by expressing genes of chondrogenic (Sox 9), osteogenic (Runx 2) and adipogenic (PPARγ) lineages (*128*). Others reported that fluid flow specifically induces endothelial (*129*) and, osteogenic differentiation (*130*) and induces glycosaminoglycan production in chondrocytes (*131*). Dynamic compressive and tensile strain have been shown to have a positive regulatory effect on both chondrogenic (*132, 133*) and osteogenic gene expression (*134, 135*). The reported studies have shown how mechanical factors can induce a variety of cellular responses but the biosynthetic cellular response to external mechanical stimuli is not an individual process, but is closely interconnected to ECM properties and to the stage of cell differentiation *in vivo* and *in vitro* (*121, 136*).

The importance of the interplay between ECM and mechanical stimuli on the differentiation and healing of ESCs has been shown by Taiani et al., (*19*) and Nakajama et al. (*7*), respectively. When Taiani et al. (*19*) transplanted osteoblasts derived from mESCs seeded in a collagen scaffold into a mouse burr-hole fracture model, the bone returned to the pre-injured state and there was no teratoma formation. In comparison, when mESCs were differentiated into osteoblasts and chondrocytes and transplanted into this fracture model without the support of an ECM, abnormal tissue formation was observed. The study of Nakajama et al. (*7*) highlights the importance of mechanical stimuli on the above results. They also seeded mESCs on collagen gels and evaluated the influence of mechanical factors on cartilage tissue formation *in vivo*. The results showed that when mESCs resided within a collagen matrix construct and experienced mechanical stimuli, then no teratoma formation was observed. Conversely,

the *in vivo* transplantation of such a scaffold without applying any load was associated with teratoma formation.

Based on the reported findings, the next objective of this project was to evaluate the effect of compressive load on mESCs differentiation *ex vivo*. Compressive force was chosen because it better replicates the burr-hole fracture model in which the collagen gel is placed in a confined space. Furthermore, it was evaluated whether mechanical stimuli under these conditions would trigger mESCs lineage commitment to osteoblasts over chondrocytes.

We evaluated whether a confined compressive load, which was applied using the custom made loading system (described in Chapter 3), affected mESCs viability. In the next step, we evaluated the effect of two different loading regimes on mESCs gene expression patterns at different time points. Prior to loading, the cell/gel system was tested using a Bose Electroforce machine to estimate their mechanical properties. These results are shown in Appendix E and a summary is provided in this Chapter.

6.1 Results

6.1.1 Cell Viability

Cell viability was evaluated at day 1 and day 15 of differentiation in duplicates. The viability is expressed as the percentage of cells remained alive in comparison to the total cell number when cultured in collagen gels. Three groups were evaluated: 1) mESCs seeded in collagen gels, 2) mESCs seeded in collagen gels placed in the loading system with a porous platen on top but no applied load, 3) mESCs seeded in

collagen gel subjected to compressive load at 1 Hz, 5% strain for 2 cycles. One cycle is equivalent to 4 hours load followed by 16 hours of rest.

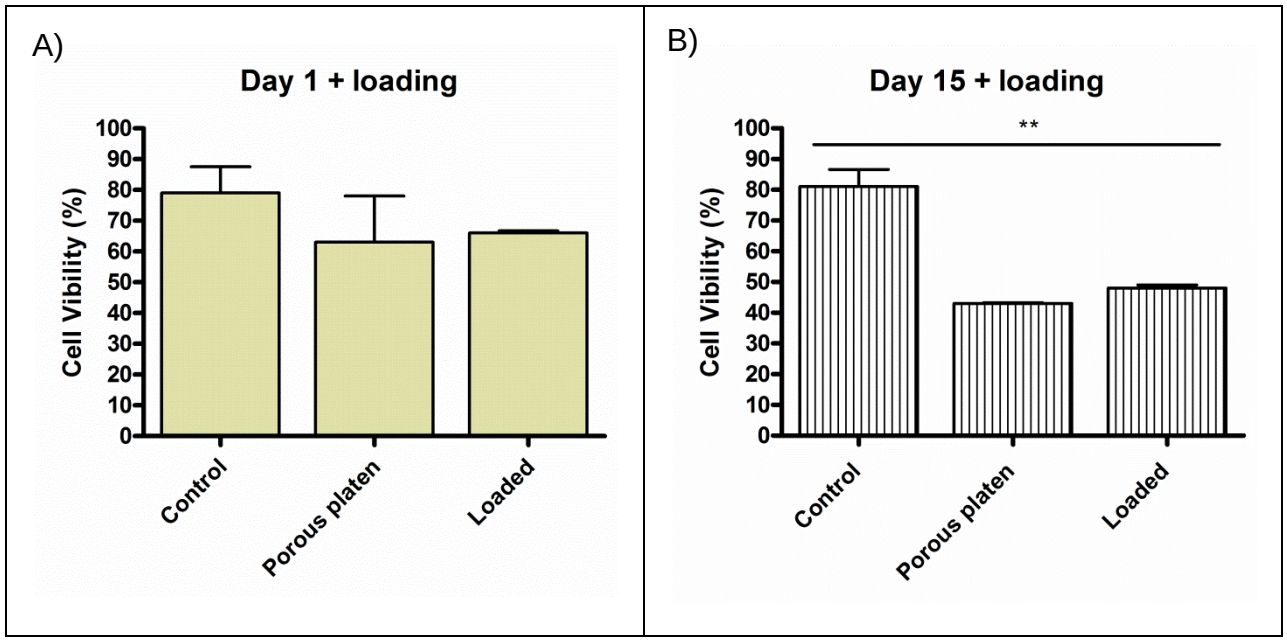

Figure 6.1: Cell viability of mESCs seeded in the collagen gels and subjected to loading after one day (A) and fifteen days post polymerization. Three conditions were tested, control (mESCs/Col I), porous platen on top of the gels but not loaded and loaded collagen gels at 1 Hz, 5% strain over 40 hours after one or fifteen days post-polymerization. Mean ± SD, n=2, **= $p<0.01$

Overall, mESCs sustained viability upon mechanical stimuli using the modified loading system. Compressive load did not significantly influenced mESCs viability at day 1, $p>0.05$ (Figure 6.1 A) but did at day 15, $p<0.05$ (Figure 6.1 B).

The control samples had a viability of 79%±8.5 on day 1 and 81%±5.6 on day 15. The placement of a porous platen on top resulted in a reduction of cell viability to 63%±15 at day 1 and 43%±0.3 for day 15 gels. In the loaded samples, viability increased to 66%±0.7 for day 1 gels and 48%±1 at day 15 gels. Statistical analysis was performed

on four images obtained from two gels. The viability was calculated for each picture and the results were used for one-way ANOVA analysis.

6.1.2 The Effect of Compressive Load Frequency on mESCs Gene Expression at an Early Stage of Differentiation

The cell/gel constructs were subjected to confined compressive loads at two different frequencies of 1 Hz or 0.1 Hz while maintaining the strain constant. This strain range corresponded to an amplitude range of 0.1 N to 2.85 N with the Flexcell system (see Figure 3.10).The effect of the load amplitude and variation in load frequency was evaluated by studying the gene expression levels for mESCs seeded in collagen gels at day 1 which was considered as an early stage of differentiation.

Three groups were tested:) mESCs seeded in the collagen gels, 2) mESCs seeded in the collagen gels with a porous platen on top, and 3) mESCs seeded in the collagen gels with applied compressive load of 1 Hz and 0.1 Hz, respectively.

The gene expression changes for Oct 4 and Sox 2, which are markers for pluripotency, are shown in Figure 6.2.

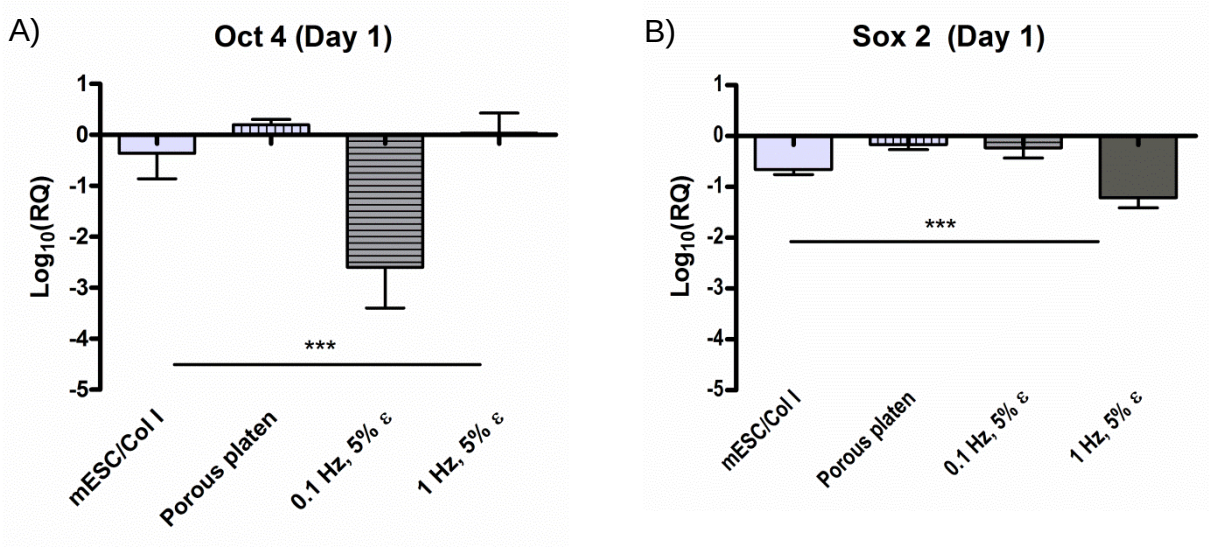

Figure 6.2: Effect of applying same amplitude of load while changing frequency on mESCs gene expression. mESCs were allowed to differentiate for one day in collagen gels and the different loading regimes were applied for 40 hours. A) Changes in Oct 4 gene expression and B) Sox 2 gene expression. Mean + SE, n = 3. ***=$p<0.05$.

The presence of a porous platen had a non-significant effect on the gene expression of pluripotent markers while the effect of loading frequencies was significantly different for Oct 4 and Sox 2 gene expression. The expression of osteocalcin and Col 2 was undetermined at day 1.

When mESCs were seeded in collagen gels, Oct 4 gene expression was not significantly different from Oct 4 expression in mESCs cultured in the dish ($p>0.05$) and placement of the porous platen on top of the cell/gel constructs did not significantly changed Oct 4 expression in comparison to mESCs cultured in the dish, $p>0.05$. Changing frequency significantly influenced Oct 4 expression. When the collagen gels were subjected to 5% strain at 0.1 Hz, the Oct 4 gene expression was down regulated

26 fold in comparison to mESCs seeded in Col I, $p<0.001$ while the same strain but a higher frequency of 1 Hz showed no significant changes, $p>0.05$.

The Sox 2 gene expression changes for mESCs/Col I samples and mESCs/Col I with porous platen control samples were not significantly different in comparison to mESCs, $p>0.05$. The effect of low frequency showed no changes, $p>0.05$ while high frequency resulted in a 12.3 fold down regulation, $p<0.001$ in comparison to the mESCs control sample.

In conclusion, placement of the porous platen had no effect on both Oct 4 and Sox 2 gene expression. Low frequency loading influenced Oct 4 gene expression but not Sox 2 and high frequency loading had no significant effect on both Oct 4 and Sox 2 gene expression indicating that these two genes are differently regulated by loading frequency.

6.1.3 The Effect of Compressive Load Frequency on mESCs Gene Expression at a Moderate Stage of Differentiation

When mESCs were seeded in collagen gels and allowed to differentiate for 15 days, a heterogeneous cell population of osteoblasts and chondrocytes was observed as described in Chapter 5. To evaluate whether mechanical stimuli could trigger specific lineage commitment of osteoblasts over chondrocytes, the cell/gel construct was allowed to differentiate for 15 days after which the two loading regimes were applied. The effect of mechanical stimuli on mESCs differentiation was evaluated based on the gene expression for pluripotent, osteogenic and chondrogenic markers as shown in Figure 6.3.

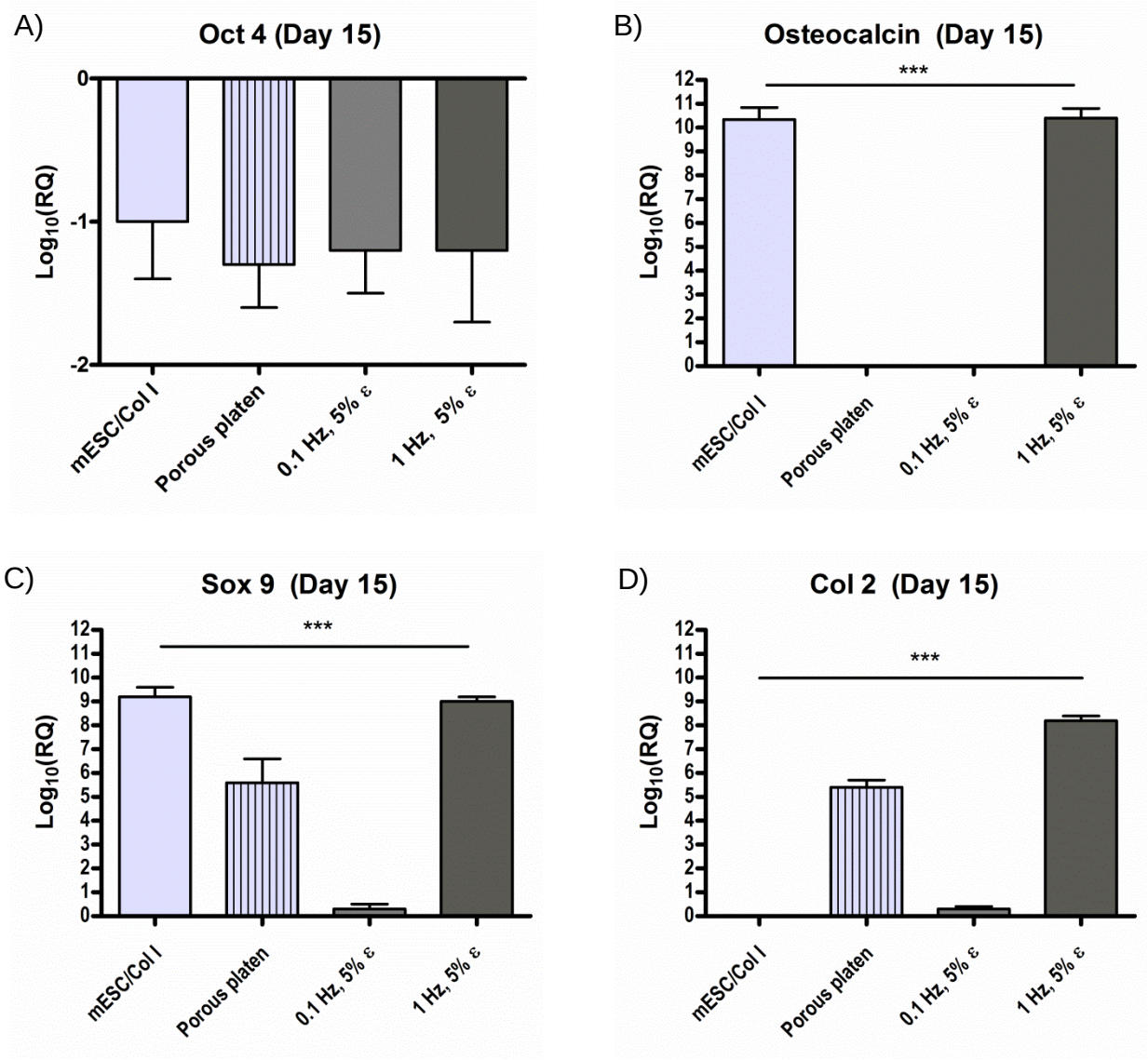

Figure 6.3: Effect of compressive load on mESCs gene expression when seeded in collagen gels after 15 days of differentiation compared to mESCs cultured in a dish. A) Oct 4, $p>0.05$, B) Osteocalcin, $p<0.0001$, C) Sox 9, $p<0.0001$ and D) Col 2 gene expression, $p<0.0002$. Mean + SE, n = 3.

The effect of low loading frequency significantly down regulated the expression of osteogenic and chondrogenic markers while 1 Hz promoted mESCs differentiation into chondrogenic lineage. Moreover, the placement of a porous platen up regulated Col 2 gene expression and down regulated the expression of the Sox 9 transcription factor.

The Oct 4 gene expression was not affected by either 0.1 Hz or 1 Hz loading frequency and its gene expression was maintained constant at day 15 of differentiation. Osteocalcin was not detected when the cell/gel construct was loaded at low frequency or when porous platen was placed on top and changes were not significant at higher frequency, $p>0.05$. However, the changes in gene expression between 1 Hz and 0.1 Hz were significantly different ($p<0.0001$) with a mean difference of 104.

The changes in Sox 9 gene expression between the two tested frequencies were significantly different with a mean difference of 86, $p<0.0001$. When the porous platen was placed on top of the cell/gel construct, Sox 9 gene expression was down regulated 3.6 fold and it was down regulated 87 fold when mechanical stimuli was applied at low frequency, $p<0.0001$. A higher frequency had no significant effect in comparison to mESCs/Col I control groups, $p>0.05$.

The placement of porous platen on top of the gels and a loading frequency of 1 Hz significantly influenced Col 2 gene expression. The expression of Col 2 was not detected in the mESCs/Col I control groups. However, the placement of a porous platen on top of the sample resulted in an up regulation of Col 2 gene expression of up to 54 fold, $p<0.0001$. When mechanical stimuli were applied using low frequency, Col 2 gene expression was up regulated 3 fold while high frequency up-regulated Col 2 gene

expression 82 fold. The changes in Col 2 gene expression between 1 Hz and 0.1 Hz were significantly different with a mean difference of 79, $p<0.0001$.

6.1.4 The Effect of Compressive Load Frequency on the Mechanical Properties of Cell/Gel Constructs

The influence of compressive load frequency on the mechanical properties of the collagen gels was studied for day 1, day 15, and day 30 collagen gels. The cell/gel construct was characterized using a Bose Electroforce material testing machine and a summary of the mechanical characterization results is provided in Table 6.1.

Table 6.1: Summary of maximum (Max) force and maximum displacement for each loading condition and different time points with the estimated Young's modulus.

Condition	**Max Force (N)**	**Max Displacement (mm)**	**Est. Young's modulus (kPa)**
Day 1, 1 Hz	0.90	0.037	205
Day 1, 0.1 Hz	1.00	0.039	308
Day 15, 1 Hz	0.75	0.038	207
Day 15, 0.1 Hz	0.60	0.045	251
Day 30, 1 Hz	0.65	0.039	236
Day 30, 0.1 Hz	0.60	0.044	274

Force changes were observed in a range of 0.6 N to 1 N with strain in a range of 3.7% to 4.5% for the two loading regimes used to study the effect of compressive load on

mESCs differentiation at the different time points, not 5% as previously estimated. The Young's modulus was slightly higher at low frequency in comparison to high frequency at all time points. The force displacement graphs for day 1 collagen gels can be found in Chapter 3 while the force displacement graphs for day 15 and day 30 gels are shown in Appendix E.

6.2 Discussion and Conclusion

The effect of mechanical stimulation on MSCs differentiation into osteogenic and chondrogenic lineages cultured on different scaffold systems has been extensively studied (*77, 83, 91, 137*). These studies, among others, have revealed that MSCs can respond to a variety of loading regimes by up regulating mRNA gene expression (*81, 83*), ECM production (*137*) or enhancing matrix mineralization (*138*). The recent findings in the field of mechanobiology and TE suggest that cellular responses to mechanical loading not only depend on the applied loading regime, but also on the stage of cell differentiation and on the biomaterial used with which cells interact (*136*). The selected cell/gel construct represents a promising scaffolding system because three studies have independently reported that collagen gels can inhibit mESCs tumorgenic potential (*19, 116, 139*) which is a critical concern in ESCs research.

In this chapter, we explored the effect of compressive load on mESCs seeded in collagen type I scaffolds at different stages of differentiation using a custom built loading system. Moreover, collagen scaffolds support mESCs differentiation into a heterogeneous cell population of osteoblasts and chondrocytes, thus two loading

regimes were tested to see if they can affect the lineage commitment. Specifically, we tested the effect of changing loading frequency on mESCs lineage commitment.

Bone haemostasis *in vivo* is regulated by the rate of strain and the frequency that causes fluid flow (*73, 140, 141*). Using the developed loading system, changing frequency would lead to an alteration of fluid flow within the scaffold system and it was expected that a frequency of 1 Hz would trigger osteogenic differentiation because 1 Hz has been established as an optimal stimulus for bone differentiation (*140, 142*). In addition to osteogenic differentiation, 1 Hz has been shown to be stimulatory for chondrocytes differentiation (*143*), however, it was expected that the strain value of 5% would be too low because most of the studies uses 10% or 15% to trigger chondrogenic differentiation (*77, 144, 145*). Overall, in order to isolate the effect of frequency, we kept the force amplitude and cycle duration the same.

When using a custom built *in vitro* loading system, it is important to evaluate cell viability. Thus, mESCs viability was examined after subjecting them to 5% strain at 1 Hz, for 40 hours and by placing the porous platen on top of the gels without loading as a control. It was found that at day 1 and day 15 of differentiation, loading caused 13% and 33% cell death, and the placement of a porous platen caused 16% and 38% cell death in comparison to cell/gel constructs that were not loaded. The observed increase in cell death in the porous platen control groups could be due to a decrease in oxygen tension because of no movement of the platen rather than its permeability. When the porous platen was placed on the cell/gel construct, it absorbed fluid from the gels and saturated the platen, which could inhibit oxygen penetration to the explants.

Furthermore, the absence of cyclic movement could inhibit the gas exchange and possibly explains the slightly higher cell death in porous platen control groups in comparison to the loaded cell/gel construct. However, the remaining cell viability of 66% at day 1 and 48% at day 15 of in samples under compressive loading was considered sufficient to evaluate mRNA gene expression changes in mESCs.

The effect of compressive loading on the early stages of differentiation showed that a higher loading frequency significantly decreased Oct 4 gene expression (a key regulator of the pluripotency transcription network) at day 1. However, Oct 4 gene expression was not affected by either 1 Hz or 0.1 Hz at day 15 of differentiation as compared to cells in gels. Therefore, it might be concluded that mESCs are still present in all tested samples (collagen gels, porous platen, loaded samples) and amplify progenitor cells at both frequencies. Only a few studies have focused on the effect of stress-induced mESCs differentiation. The study of Chowhury et al. (*56*) exposed mESCs to a local cyclic stress of 17.5 Pa at 0.3 Hz which lead to Oct 4 down regulation while control samples still continued to express Oct 4. Furthermore, they have shown that mESCs are more sensitive to mechanical load than their differentiated counterparts. These results could explain our finding why Oct 4 expression is affected by loading frequency at day 1 but not at day 15.

Overall, the effect of mechanical stimuli on pluripotent ESCs and the underlying molecular mechanism is hardly explored, other pluripotent markers such as Rex 1 and Nanog should be screened to fully understand the effect of compressive load on mESCs early differentiation.

The effect of compressive loading was also evaluated at day 15 of differentiation which was considered a moderate stage of differentiation. When mESCs were seeded in collagen scaffolds they continued to amplify progenitors and both chondrogenic and osteogenic differentiation was observed. The effect of changing frequency was significantly different for osteocalcin, Sox 9 and Col 2 gene expression. Specifically, a lower frequency of 0.1 Hz or/and the placement of the platen on top of the gels shuts down osteocalcin. A higher frequency of 1 Hz had no significant effect on osteocalcin and Sox 9 gene expression but significantly up regulated Col 2 in comparison to mESCs/Col I control samples.

Bone ECM mainly consists of collagen type I and one might expect that the interaction between mESCs and collagen would direct osteogenic differentiation or support chondrogenic dedifferentiation. However, when mature chondrocytes are seeded on collagen type I scaffolds, it has been shown that the chondrocytes started matrix remodeling and secreted their own ECM into the collagen matrix (*82*). These observations are consistent with our finding that mESCs derived chondrocytes expressed Sox 9 and started to secrete their own matrix as indicated by Col 2 expression when cell/gel construct was subjected to 1Hz.

As it can be concluded that the tested regime of 1 Hz and 5% strain accelerates chondrogenic differentiation and had no effect on osteogenic differentiation, future studies should evaluate more genes specific for chondrogenic differentiation and the presence of proteoglycans within mESCs/Col I constructs with this loading regime of 5% stain and 1 Hz. The negative effect on osteogenic differentiation at low frequency could

be attributed to a decrease in fluid flow because fluid flow has been shown to trigger osteogenic differentiation (*146*). In contrast, cartilage is about two orders of magnitude lower in permeability than cortical bone and cartilage is often under hydrostatic fluid pressure conditions (*78*). Furthermore, the use of 0.1 Hz frequency resulted in lower loading cycles in comparison to 1 Hz and the number of cycles might not be sufficient to trigger both chondrogenic and osteogenic differentiation as has been reported by others (*140*). However, as Oct 4 expression remains constant at both frequencies it can be concluded that a frequency of 0.1 Hz influences mESCs differentiation into a different lineage and screening of markers specific for other lineage commitment (i.e. myogenic, neurogenic and adopogenesis) could shed light onto the effect of low frequency on mESCs differentiation into osteogenic lineages. In addition to the loading regime, the loading type plays an important role in cell differentiation. Although, bone experiences bending and compressive forces *in vivo*, most studies have shown that osteogenic differentiation is influenced by tension rather than compression, while chondrogenic differentiation is accelerated by compressive force (*80, 81, 83, 96*).

The feasibility and applicability of the custom built loading system has also been summarized in this chapter. During Flexcell program execution, the pressure value was maintained at the same level, and thus the corresponding force values were kept the same for gel characterization over time. It was found that the strain range was not consistent across samples and was in the range of 3.7% to 4.5% for the two loading regimes over time. The differences could be attributed to the properties of the collagen gels. The properties of each scaffold system can vary in terms of fluid and solid phase

content, thus resulting in different force and displacement values on the gels. In order to maintain the strain values at a constant, future studies could first test the cell/gel system using the Bose Electroforce machine, generate a force displacement diagram and adjust the input parameters within the Flexcell system in order to keep the strain the same over time.

This chapter provides a base for further work. The loading regimes could be change to closely examine the lineage commitment of osteoblasts over chondrocytes. For example, although 1 Hz has been extensively studied to be conductive for osteogenic and chondrogenic differentiation it has also been shown that higher frequency of 20 Hz with low magnitude could enhance osteogenic differentiation (*147*). Another possibility is to increase the strain and keep the frequency at 1 Hz, this should trigger chondrogenic differentiation. Moreover, the effect of 0.1 Hz was not accelerating either osteogenic and chondrogenic, therefore it can be concluded that other cells types are presented. Cell from mesenchymal origin should be evaluated on their gene expression level.

In the next chapter the role of integrins in mediating differentiation and transducing mechanical signals is in more depth explores. Furthermore, the interplay of GF, mechanical stimuli and integrins is explored.

CHAPTER 7: ROLE OF INTEGRINS AND GROWTH FACTORS TO PROMOTE MURINE EMBRYONIC STEM CELL DIFFERENTIATIAN UNDER COMPRESSIVE LOAD

Stem cell functions such as their self-renewal, differentiation and proliferation are influenced by the surrounding micro-environment in which the SCs reside. This micro environment is also known as the SCs niche and is made of ECM proteins, neighboring cells and soluble factors. The interaction of these factors determines SCs fate (*88*). The understanding of SCs niche composition, their interaction with each other, and to external stimuli could help to develop robust strategies for TE. Moreover, it would lead to a better understanding of tissue development or, if something goes wrong, of tissue dysfunctions. Specifically, it is necessary to understand how cells interact with the extracellular environment, how the soluble factors influence their fate and what involvement physical factors such as mechanical stimuli have. *In vivo*, these cues are closely interconnected and work in synergy to control SCs functions (*89*).

Cells interact with ECM through transmembrane proteins such as integrins. Numerous combinations and permutations of α and β chains are observed in nature which, in some cases, can act as a mechanical linkage connecting the ECM with cell interior and/or act as mechanical sensors. Therefore, integrins are thought to play an important role in structural and regulatory cellular processes (*148*). For example, it is known that with various stages of differentiation, cells can change their surface receptors as part of adapting to a new environment. Furthermore, the intrinsic properties of a biomaterial such as structure, elasticity and porosity, can all influence cell differentiation via different

cell surface receptors (*54, 62*). Specifically, collagen-dependent integrins can mediate differentiation or maintain self-renewal (*62, 64, 65, 149*). In addition, another class of integrins, known as RGD-dependent integrins, have been identified to trigger osteogenic differentiation (*90, 112*). Moreover, both collagen and RGD-dependent integrins have been reported to be involved in sensing mechanical signals (*150-153*) and act in synergy with GFs to enhance osteogenic differentiation in progenitor cells (*154*).

Like integrins, GFs have regulatory functions and thus can influence cell fate decisions (*12*). Together, GFs and integrins can act in synergy triggering a stronger intracellular signal cascade. For example, both integrins and GFs can individually activate Erk-type mitogen-activated protein kinase (responsible for many cellular processes) which leads to a weak activation. However, in combination cells activation is enhanced (*155*). Furthermore, integrins can enhance GFs activation and vice versa. For example, the administration of TGF-β to a collagen scaffold seeded with MSCs enhanced integrin gene expression and thus MSCs attachment to collagen matrix; an important process for cell migration (*156*). Similarly, BMP-2 has been shown to enhance MSCs migration. Therefore, evidencing exists that cell migration, for example to the fracture site, is regulated by GFs (*157*). Due to GFs role in determining cellular functions, these molecules have been extensively studied for their potential use in regenerative medicine. In the past, different GFs types have been identified as relevant for a particular cellular response. For example, BMP-2 influences osteoblasts migration

and differentiation, TGF-β is involved in bone and cartilage tissue formation, and BMP-7 affects bone, cartilage and kidney regulation *(12, 93).*

A recent study systematically evaluated the interplay of integrins and BMP-2 on bone marrow stoma cells (BMSCs) differentiation into osteoblasts (*154*). BMSCs were seeded into hydrogel scaffolds covalently conjugated with BMP-2 alone, RGD peptide alone, and BMP-2 and RGD together. Both RGD and BMP-2 alone were able to induce BMSCs differentiation and increase mineralization. However, in the presence of both RGD and BMP-2 the calcium content significantly increased. These results indicate BMP-2 and integrins that bind to RGD act in synergy to enhance osteogenic differentiation. It is hypothesised RGD peptide allows cells to attach via integrins which in turn enhanced BMP-2 interaction. Another group independently tested the role of αVβ integrins on BMP-2 functions in osteogenic differentiation (*93*). It was observed that BMP-2 increased the expression of β1 and αV containing integrins and these two receptors are able to overlap with BMP-2 receptor. In order to test the role of αVβ integrins, a RGD peptide in soluble form was added to the cells, which then inhibited the interaction of RGD-dependent integrins with its surrounding and inhibited the action of BMP-2. Based on the above findings, a part of our hypothesis was established; BMP-2 in combination with cell adhesion molecules such as integrins αvβ3 and/or α1β1 will act synergistically and accelerate mESCs differentiation into osteoblasts. However, other studies have also reported that mechanical stimuli can enhance BMP-2 expression (*158, 159*). Therefore, we extended our hypothesis to include that BMP-2 in combination with cell adhesion molecules such as integrins αvβ3 and/or α1β1 will act

synergistically under compressive load to accelerate mESCs differentiation into osteoblasts. To the best of our knowledge, this is the first study that aims to test the effect of BMP-2, integrins (ECM) and mechanical stimuli to enhance mESCs differentiation into osteogenic lineage.

To test our hypothesis, we encapsulated BMP-2 into Nanoparticles (NPs) which were conjugated to RGD peptides. To specifically target RGD-dependent integrins, we used a cyclic RGD peptide (cyclo (Arg-Gly-Asp-d-Phe-Cys)). The advantage of cyclic peptides over linear ones is they enhance activity and selectivity to RGD dependent integrins. Moreover, the presence of Phe after Asp enhances the selectivity to αV containing integrins (*160*). NPs were fabricated using a simple coacervation procedure established by Dr. Uludag's laboratory at the University of Alberta. These NPs are made of bovine serum albumin (BSA) that are stabilized with poly-L-Lysine (PLL). PLL has been reported to stabilize BSA NPs containing BMP-2, resulting in a GFs encapsulation efficiency of ~90% (*37, 108*). Moreover, the concentration of stabilization agents can be manipulated to change the release rate of GFs. In order to conjugate RGD to the NPs we used polyethylene glycol (PEG), which has two functional groups on its terminal ends. Therefore, PEG was conjugated to PLL on one side and to RGD via the maleimide (MAL) group on the other side. The NPs delivery system used to test the hypothesis of this study is depicted in Figure 7.1 below.

BSA NPs with BMP-2 stabilized with PLL-PEG and conjugated to RGD

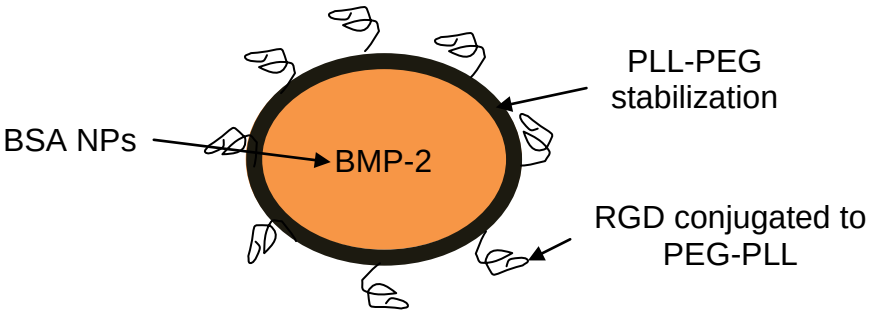

Figure 7.1: BMP-2 was encapsulated into BSA NPs which were stabilized by PLL. In order to conjugate RGD to the NPs, PEG was used as a link between PLL and RGD.

The effect of RGD on mESCs has not been studied so far. Therefore, we first supplemented RGD peptide in a soluble form to mESCs cultured on a planar surface and evaluated their morphology. In the next step, we were interested to understand the effect on RGD blocking peptide on the cell/gel system. The incorporation of RGD in our cell/gel system would allow the study of integrin involvement in mediating differentiation as well as the role of integrins in mechanotransduction because RGD in soluble form is expected to inhibit specifically RGD dependent integrins which have been proposed to act as mechanosensors. Using the above methods we tested the fourth objective of this thesis, and characterized two variables (the role of integrins under compressive load) of the hypothesis.

In order to examine the synergistic effect between ECM mediated differentiation, mechanical stimulation and BMP-2, specifically designed NPs (see Figure above) were incorporated into the cell/gel system. To predict the behaviour of BMP-2 within the NPs we used Dextran as a model drug and evaluated NPs size, zeta potential, encapsulation

efficiency and predicted BMP-2 release rate. The use of Dextran as a model drug to predict BMP-2 behaviour is utilized due to the high price of GFs (*160*). Finally, NPs containing BMP-2 with conjugated RGD were characterized for size and zeta potential then incorporated into the cell/gel system and subjected to compressive load.

7.1 Results

7.1.1 Role of Integrins in Mediating Differentiation and Mechanotransduction

This part of the chapter evaluated the role of RGD-dependent integrins in mediating mESCs differentiation and transducing mechanical signals by blocking RGD dependent integrins.

7.1.1.1 Effect of RGD Peptide on mESCs Morphology

As mentioned above, the effect of RGD on mESCs has not been studied. Therefore, we first supplemented RGD peptide in a soluble form to mESCs cultured in a dish. This experiment was performed to evaluate whether this peptide would influence cell morphology and viability and/or have an effect on mESCs attachment. mESCs were seeded in a 12 well plate at a cell density of 30,000 cells/well in the presence of DMEM medium. Cells were allowed to attach for 24 hours after which 0.5 mM RGD was added to the wells. 0.5 mM RAD (which doesn’t bind to integrins) was added as a control for RGD. Pictures were taken every day for the following conditions: 1) mESCs, 2) mESCs in the presence of RGD, and 3) mESCs in the presence of RAD. Figure 7.2 shows mESCs morphology on the second day as an example.

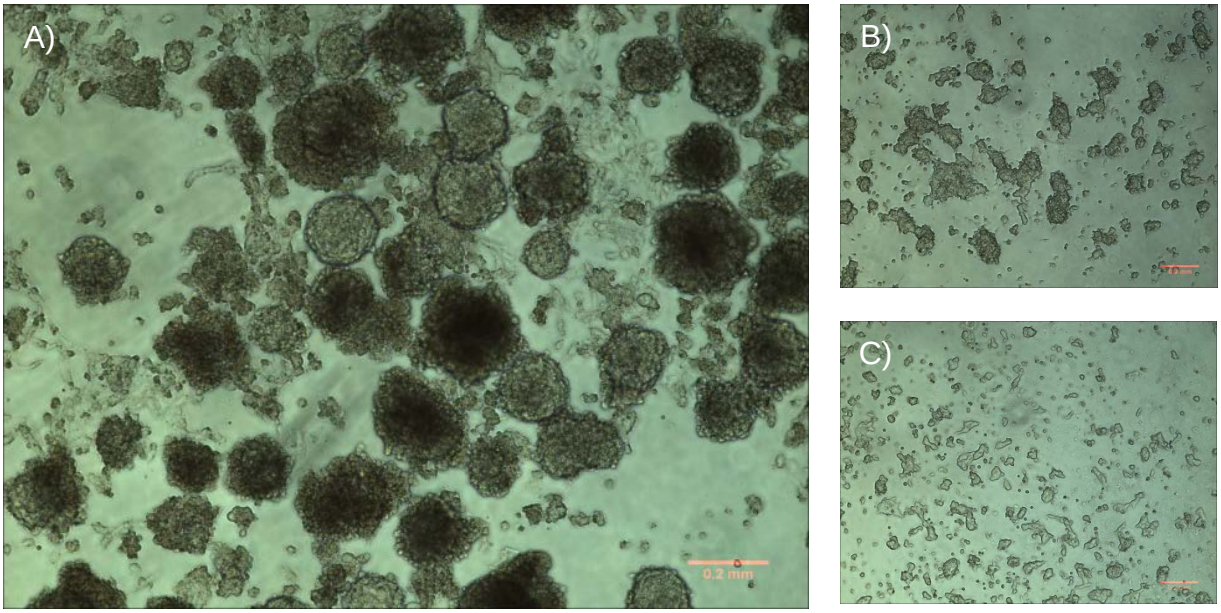

Figure 7.2: A) mESCs cultured in the presence of 0.5 mM RGD blocking peptide which influenced mESCs attachment, B) mESCs control samples maintained attached to the dish, C) mESCs cultured in the presence of RAD had no effect on mESCs attachment. Presented pictures were taken two days post seeding. Scale bar 0.2 mm.

The presence of soluble RGD peptide significantly influenced mESCs morphology as shown in Figure 7.2, A. RGD blocked mESCs integrins and inhibited cell attachment to the dish. As a result of integrin blocking, mESCs formed round shaped cell aggregates that were found in suspension. The presence of RAD which is shown in Figure 7.2, C had no effect on cell morphology and thus was not used as a control for subsequent experiment. The mESCs control sample represented similar morphology to the RAD control groups as shown in Figure 7.2, B. These results confirmed that RGD blocking

peptide successfully inhibited integrins in mESCs. However, RGD blocking peptide had no effect on mESCs viability (data not shown).

7.1.1.2 Effect of RGD Peptide on mESCs Differentiation in 3-D Culture System

After determination that RGD blocking peptide had no significant effect on mESCs viability but influenced mESCs integrins in 2-D culture, RGD-blocking peptide was incorporated into the cell/gel system. As cells behave differently in 3-D in comparison to planar culture, the cell/gel construct in the presence of 0.5 mM RGD was examined for viability using a Live/Dead viability kit as shown in Figure 7.3.

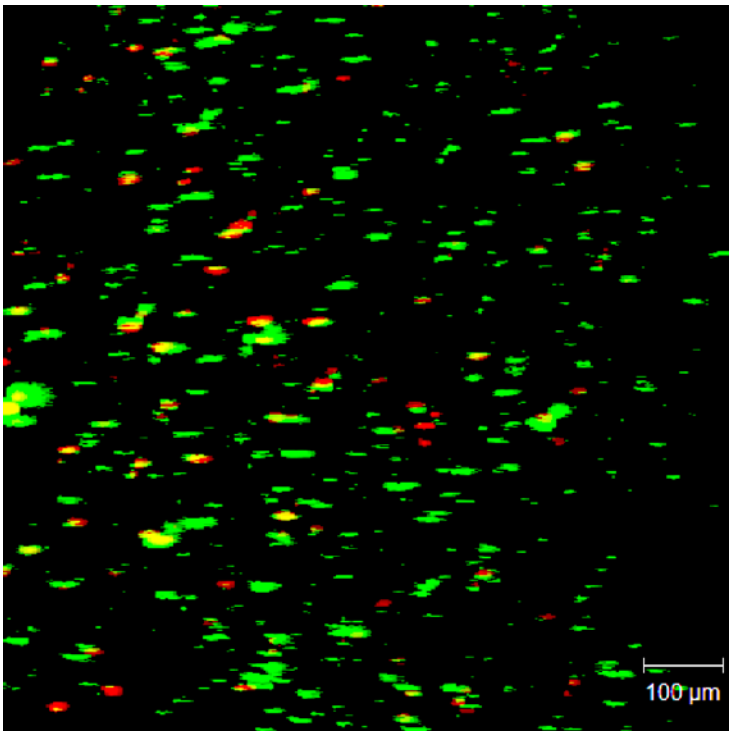

Figure 7.3: mESCs viability when seeded in collagen gel with 0.5 mM RGD at day 15 of differentiation. Image shows 3-D projection of one from the two analyzed gels.

It was determined that cells maintained a viability of 75.3%±2.5 on day 15 post polymerization in the presence of RGD. In comparison, mESCs seeded in collagen sustained a viability of 85%±5.6 on day 15 as reported in chapter 5. The viability values were not significantly different as determined using unpaired t-test, p=0.3206.

Next, the expression of pluripotent and differentiation markers was evaluated at day 1 and day 15 of mESCs differentiation. Two groups were tested: mESCs seeded in collagen gels and mESCs seeded in collagen gels in the presence of 0.5 mM RGD. The gene expression of Oct 4, Sox 2, Sox 9 and OC is shown in Figure 7.4.

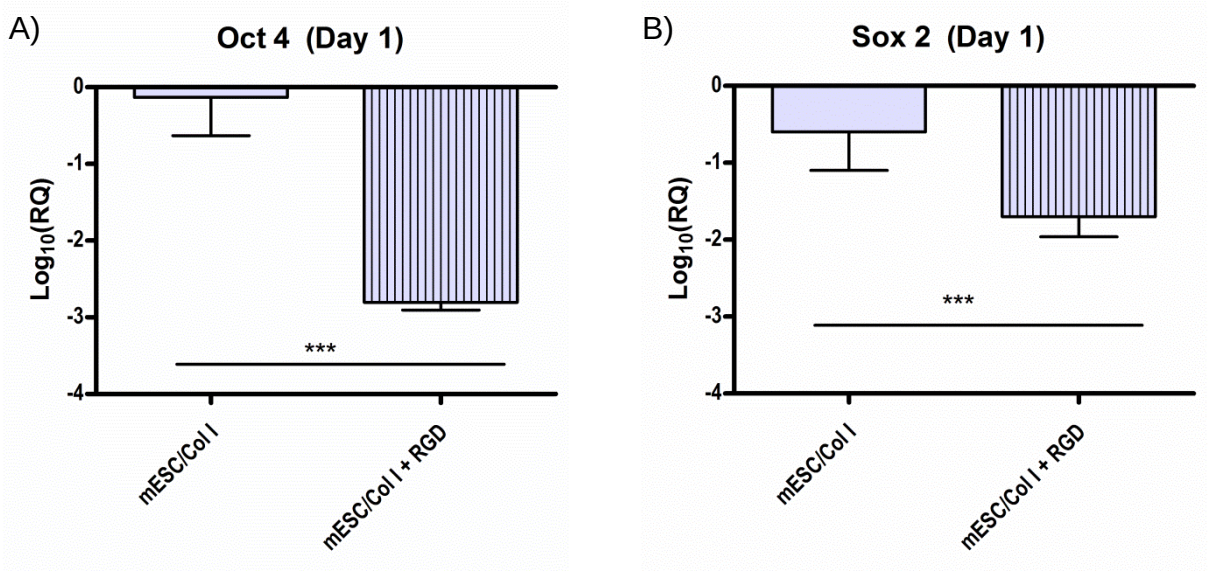

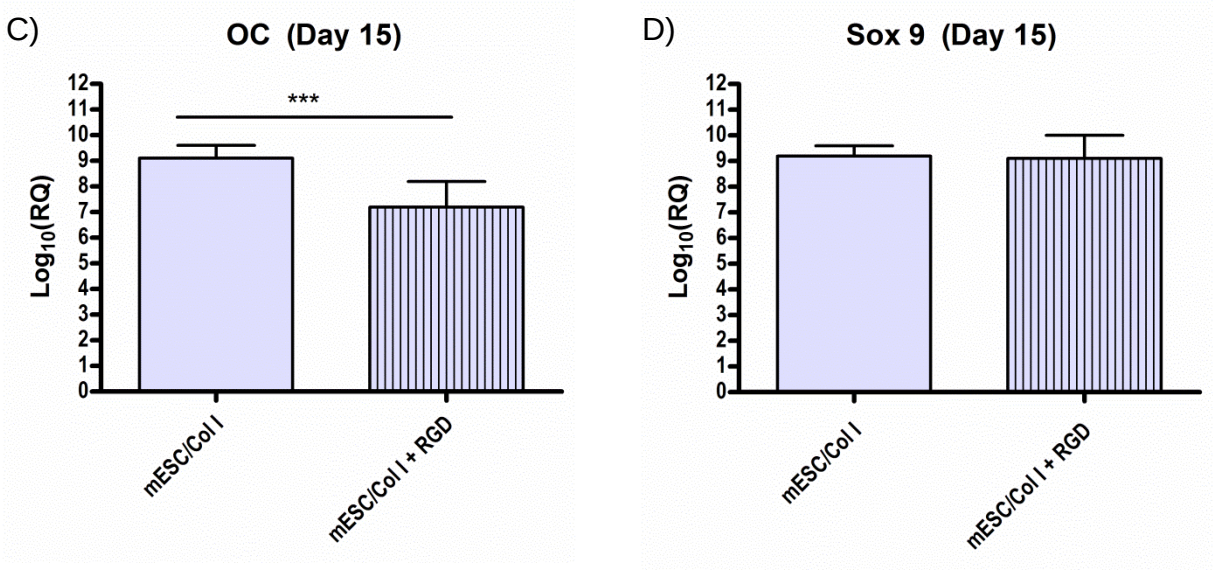

Figure 7.4: Gene expression of mESCs seeded on Col I matrix with and without the presence of RGD were compared to mESCs cultured in the dish. A) Oct 4 on day 1, B) Sox 2 on day 1, C) Osteocalcin (OC) on day 15, D) Sox 9 on day 15. Mean + SE, n=3.

The presence of RGD blocking peptide significantly down regulated pluripotent, ($p<0.001$) and osteogenic ($p<0.01$) markers but had no effect on chondrogenic ($p>0.05$) differentiation. These results indicate that RGD-dependent integrins are necessary to stimulate osteogenic differentiation.

7.1.1.3 Effect of Compressive Load on mESCs Differentiation in 3-D Culture System with RGD Peptide

To evaluate objective four of this thesis, and thus to determine the role of integrins in mediating mESCs differentiation and in transducing a compressive load into a biosynthetic response, we incorporated RGD blocking peptide to the cell/gel system. As before the following groups were evaluated for their gene expression level: 1) mESCs/Col I control, 2) mESCs/Col I with RGD, 3) mESCs/Col I loaded at 1 Hz, 5%

strain, and 4) mESCs/Col I with RGD, loaded at 1 Hz, 5% strain on day 1 and day 15 of differentiation.

The gene expression of specific genes on early stage of differentiation is summarized in Figure 8 and the gene expression at moderate stage of differentiation is depicted in Figure 7.5.

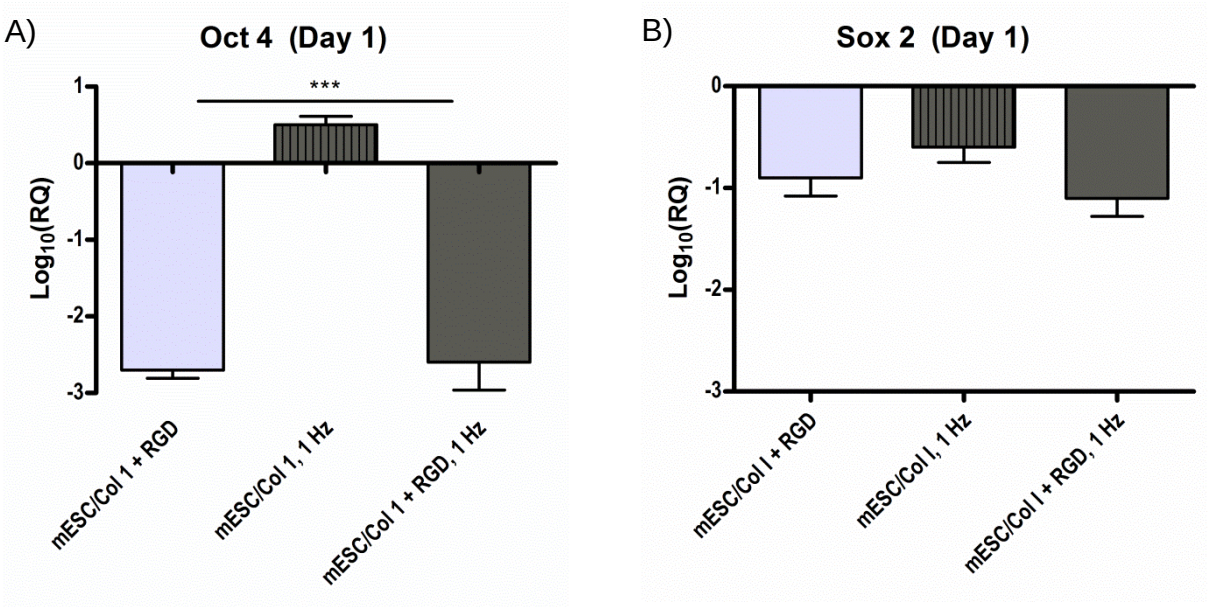

Figure 7.5: Gene expression of mESCs seeded in Col I matrix with the presence of RGD blocking peptide, with free integrin receptors and mechanical load, and with blocked integrin receptors and mechanical load. A) Oct 4 on day 1, B) Sox 2 on day 1. Mean + SE, n=3.

When the cell/gel constructs were subjected to mechanical stimuli in the presence of RGD, no load was transduced and thus, the gene expression was not changed which is an indication that RGD dependent integrins act as mechanoreceptors.

Similarly, integrins which recognize RGD sequence play an important role in mechanotransduction at a moderate stage of mESCs differentiation when seeded in a collagen matrix as shown in Figure 7.6.

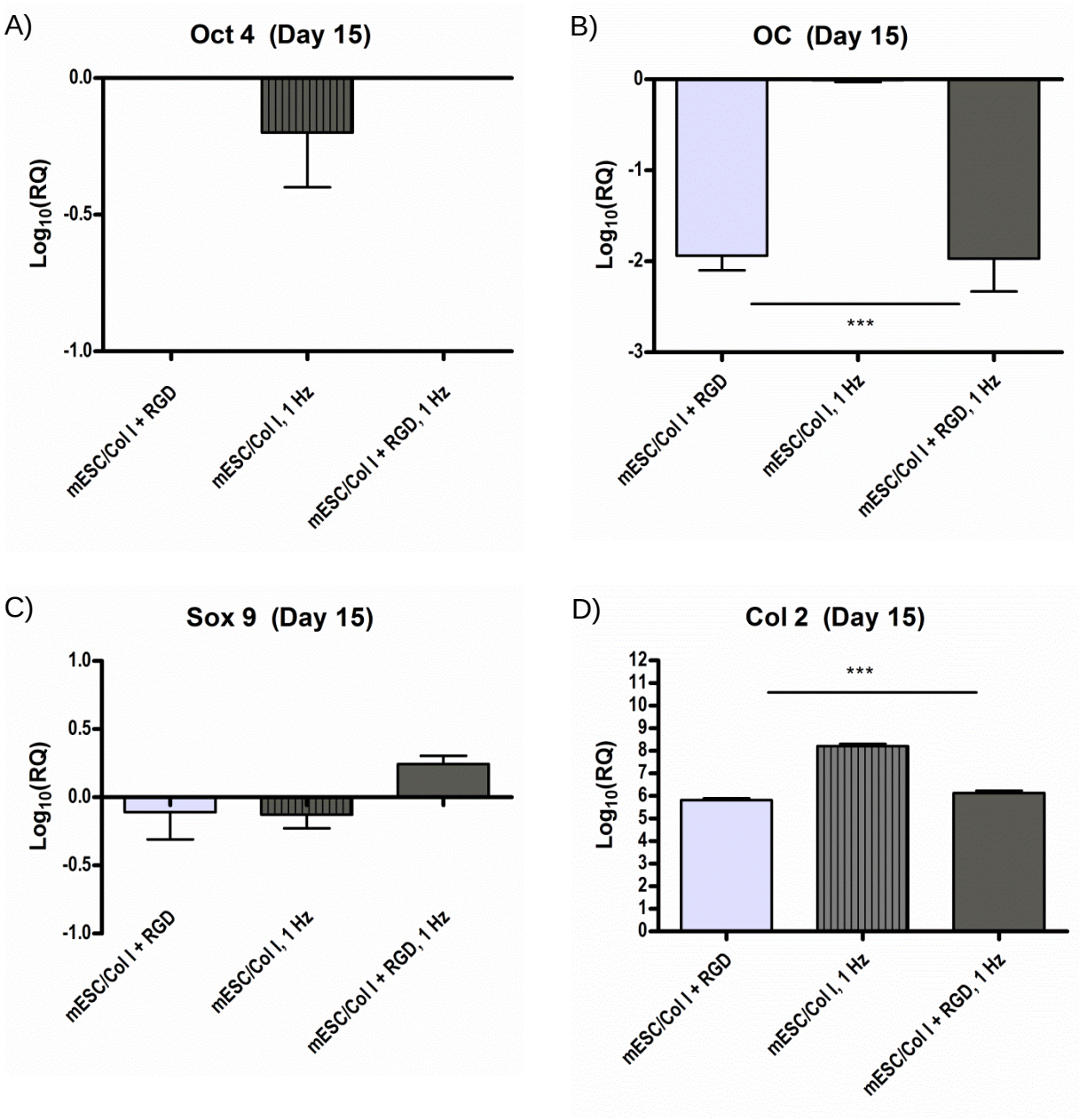

Figure 7.6: Gene expression of mESCs seeded on Col I matrix with the presence of RGD blocking peptide, with free integrin receptors and mechanical load and with

blocked integrin receptors and mechanical load. A) Oct 4 on day 15, $p=0.8045$, B) Osteocalcin on day 15, $p<0.0001$, C) Sox 9 on day 15, $p=0.68$ and D) Col 2 on day 15, $p<0.0001$. Mean + SE, n=3.

Blocking RGD dependent integrins down regulated the expression of all tested genes and the transduction of mechanical stimuli into biochemical responses was inhibited.

In summary, this data confirms that integrins which recognize RGD sequence play an important role in mechanotransduction at early stage and moderate stages of differentiation.

7.1.2 Synergy between Growth Factor, Integrins and Mechanical Stimuli

This part of the chapter characterized the BSA NPs stabilized using PLL and PEG (BSA-NPs-PLL-PEG) using Dextran as a model drug to predict BMP-2 behaviour. First, the conjugation efficiency between PLL-PEG was determined. Then, four different Dextran concentrations were used to evaluate the encapsulation efficiency of the NPs and to predict the release rate of BMP-2. Next, the size and zeta potential was determined for BSA-NPs. Finally, BSA NPs containing BMP-2 and conjugated to RGD (BSA-NPs-BMP-2-PLL-PEG-RGD) were characterized and encapsulated into the cell/gel system.

7.1.2.1 Poly-L-Lysin-Polyethylene Glycol Conjugation Efficiency

Poly-L-Lysine (PLL) was conjugated to PEG and the conjugation efficiency was determined using TNBS assay. PLL is a homo polymer which means it consists only of lysine repetition. Thus, one amine group per lysine within a PLL molecule is accessible

for reaction with PEG. To determine the free amine groups of PLL before conjugating to PEG and after conjugation a TNBS assay was performed as described and the encapsulation efficiency determined using (Equation 4.2) based on a standard curve generated with known L-Lysine as shown in Figure 7.7.

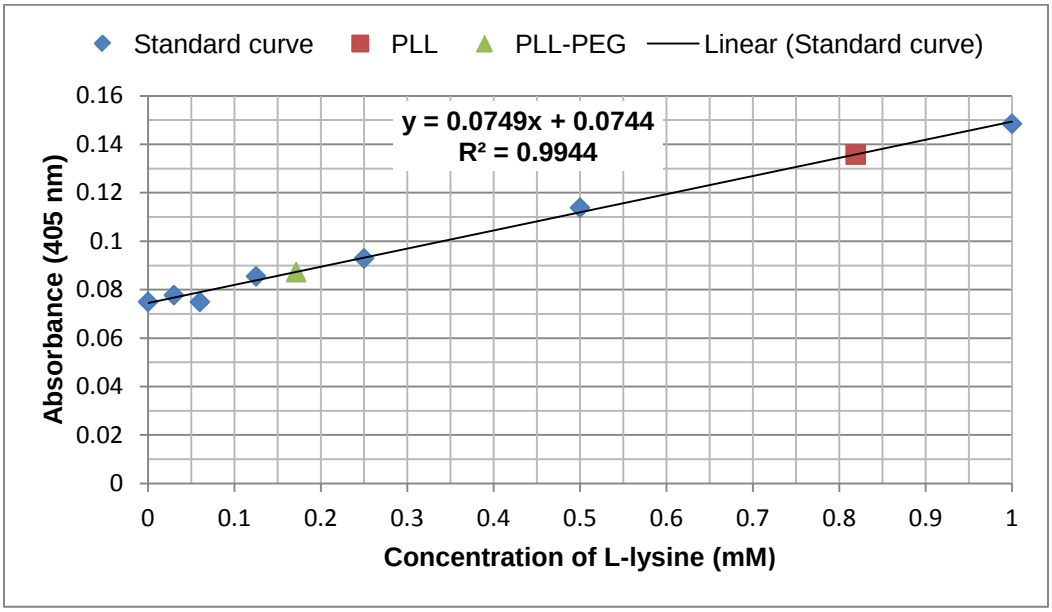

Figure 7.7: Amount of PLL-PEG concentration determined using a standard curve with known L-Lysine concentrations. PLL was collected before conjugating to PEG and after conjugation.

The absorbance of PLL before conjugating to PEG, PLL conjugated to PEG and of known L-Lysine concentration ranging from 0 mM to 1 mM was evaluated. Based on the absorbance reading of two batches, it was determined that 76.99%±2.95 (Mean ± SD) amino acids presented in PLL were conjugated to PEG.

7.1.2.2 Encapsulation Efficiency of Dextran-FITC

In order to determine an optimal concentration of BMP-2 for subsequent experiments, Dextran-FITC concentrations ranging from 0 mg/mL 1.25 mg/mL, 2.5 mg/mL and 5 mg/mL were tested for their impact on encapsulation. For this, the FITC fluorescence of coated and uncoated NPs was determined based on a standard curve with known Dextran-FITC concentrations as shown in Figure 7.8.

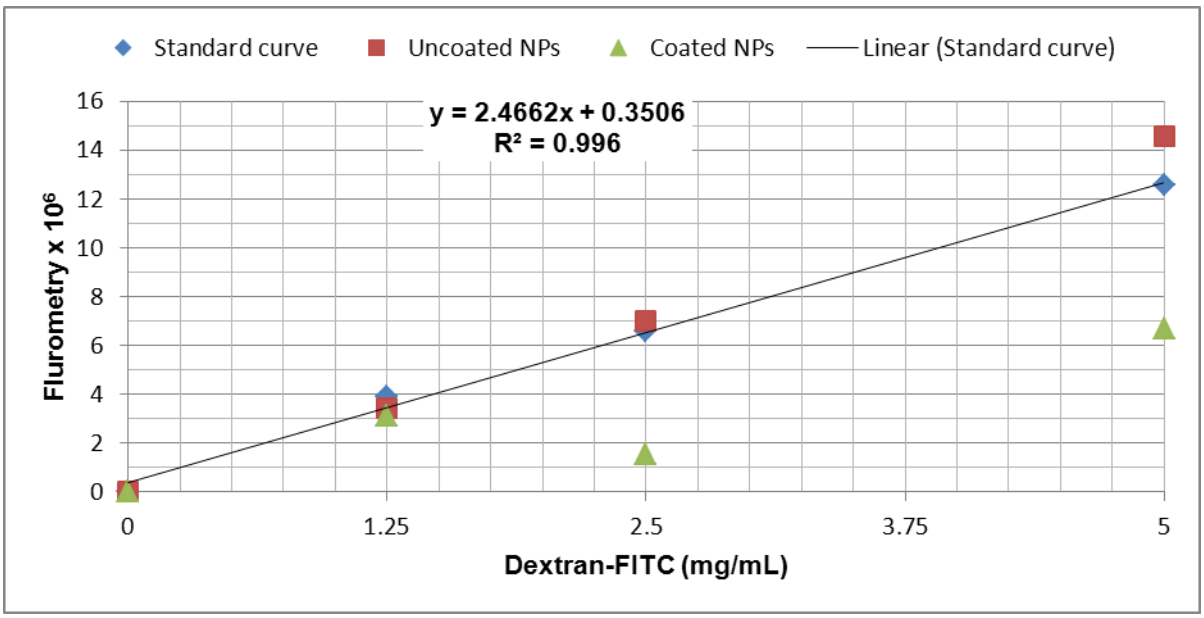

Figure 7.8: Encapsulation efficiency of uncoated and coated BSA-NPs containing different Dextran-FITC concentrations as determined using a standard curve with known Dextran-FITC concentrations. The Mean of two batches is plotted.

The encapsulation efficiency was calculated using (Equation 4.3) and the mean encapsulation efficiency is summarized in Table 2.1 for uncoated and coated BSA NPs.

Table 7.1: Calculated encapsulation efficiency for uncoated (UC) and coated (C) NPs containing different Dextran-FITC concentrations. Mean ± SD

$C_{initial}$ (mg/mL)	$C_{encapsulated}$ (mg/mL)	% Encapsulation Efficiency
UC 1.25	1.26±0.01	100.8±1.50
UC 2.5	2.72±0.04	108.7±1.62
UC 5	5.79±0.04	115.8±0.86
C 1.25	1.130±0.01	90.36±0.84
C 2.5	0.489±0.01	19.56±0.38
C 5	2.588±0.02	51.77±0.46

These results indicated that the concentration of the initial GFs influences the encapsulation efficiency. The encapsulation of uncoated NPs was 100% and above. These values are higher than the theoretical value and are an indication that the initial concentration of Dextran-FITC added to the NPs was slightly higher. The encapsulation efficiency of coated NPs was significantly different for Dextran-FITC concentration, $p<0.0001$. The encapsulation of 1.25 mg/mL resulted in a 90.36% efficiency, 2.5 mg/mL resulted in 19.56% efficiency and 5 mg/mL resulted in 51.77% encapsulation efficiency. Overall, the initial concentration of 1.25 mg/mL showed the highest encapsulation efficiency.

7.1.2.3 Nanoparticles Size and Zeta Potential Containing Dextran-FITC

In the next step, it was evaluated whether different initial GFs concentration would influence NPs size and zeta potential. The zeta potential can be used as an indication of colloid stability and the successful absorbance of PLL-PEG by BSA. BSA NPs containing 0 mg/mL, 1.25 mg/mL, 2.5 mg/mL and 5 mg/mL Dextran-FITC were evaluated. The mean size for all tested concentration is shown in Figure 7.9 and the mean zeta potential is shown in Figure 7.10.

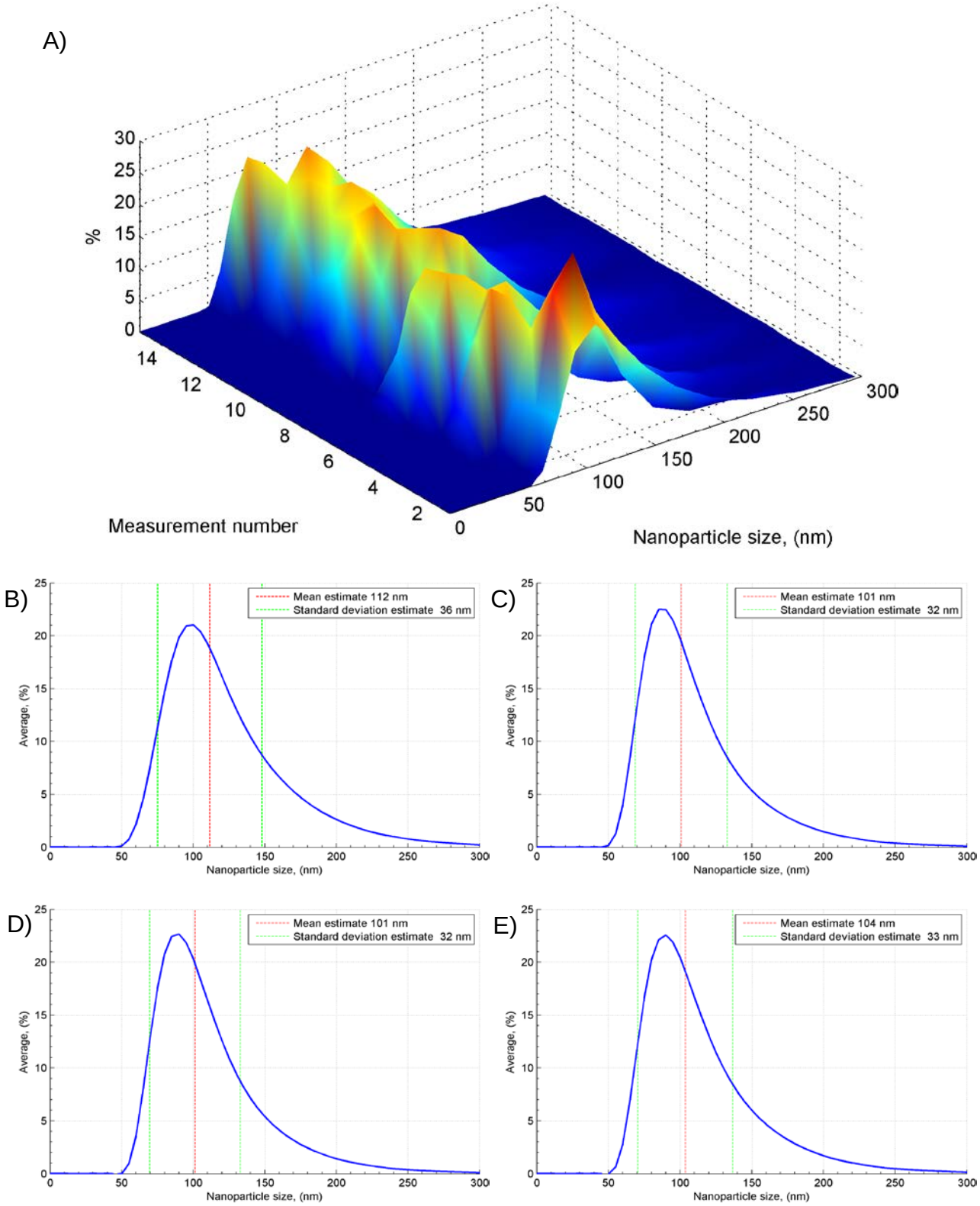
A)
%
Measurement number
Nanoparticle size, (nm)
B)
Mean estimate 112 nm
Standard deviation estimate 36 nm
C)
Mean estimate 101 nm
Standard deviation estimate 32 nm
D)
Mean estimate 101 nm
Standard deviation estimate 32 nm
E)
Mean estimate 104 nm
Standard deviation estimate 33 nm
Average, (%)
Nanoparticle size, (nm)

Figure 7.9: Size distribution of BSA Nanoparticles with different Dextran-FITC concentration. A) Surface plot of 0 mg/mL Dextran-FITC, B) Mean of NPs size with 0 mg/mL Dextran, C) 1.25 mg/mL, D) 2.5 mg/mL, and E) 5 mg/mL. The NPs size was similar for all tested concentrations, Mean ± SD.

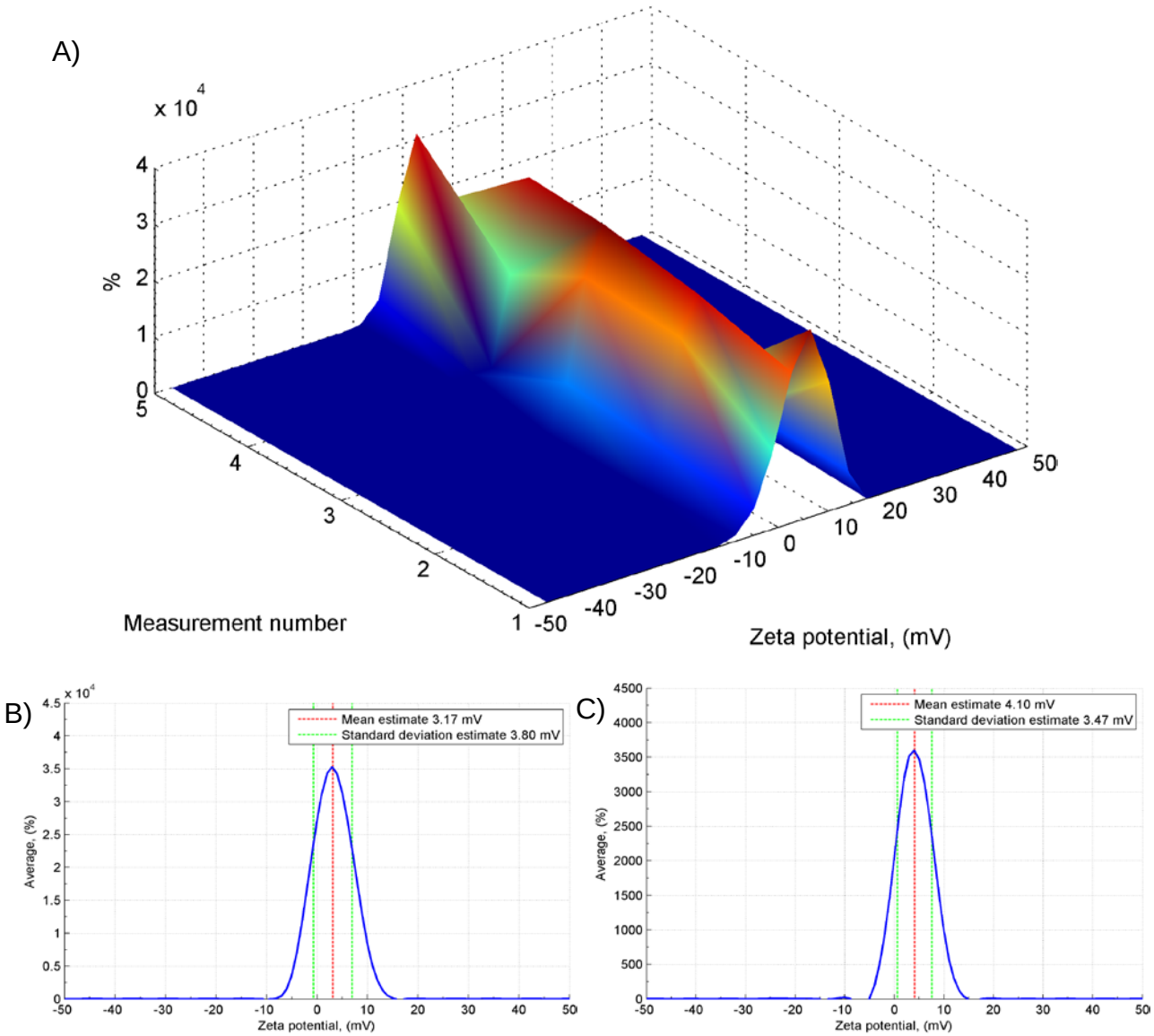

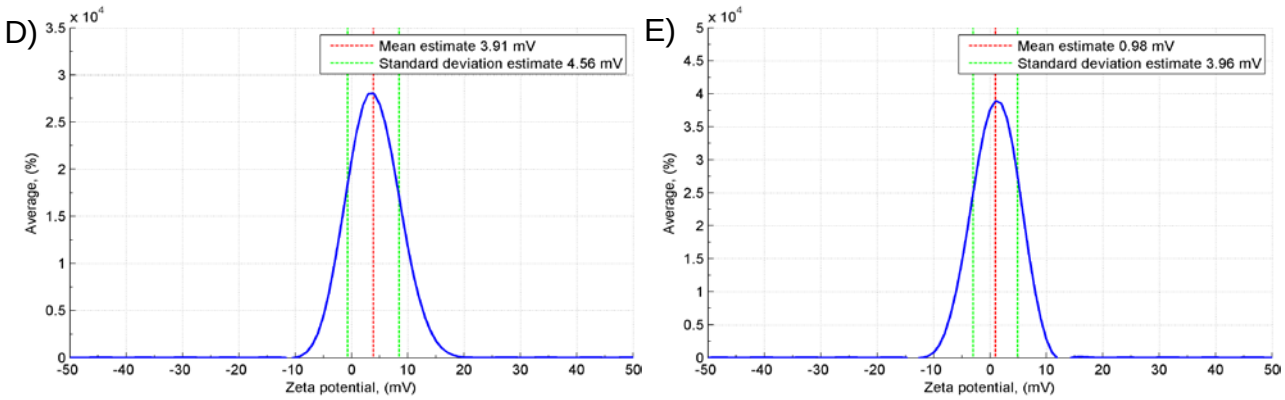

Figure 7.10: Zeta potential of BSA NPs with different Dextran-FITC concentration. A) Surface plot of 0 mg/mL Dextran-FITC, B) Zeat potential of NPs containing 0 mg/mL, C) 1.25 mg/mL, D) 2.5 mg/mL, and E) 5 mg/mL Dextran-FITC. Mean ± SD.

The mean NPs size for all tested Dextran-FITC concentrations were not significantly different from each other, $p<0.05$. The smallest NPs size was obtained using initial Dextran-FITC concentrations of 1.25 mg/mL and 2.5 mg/mL resulting in a mean of 101 nm ± 32. Similarly, the zeta potential for all tested concentrations was similar, 0 mg/mL (3.17 mV±3.80), 1.25 mg/mL (4.10 mV±3.47) and 2.5 mg/mL (3.91 mV±4.56) while 5 mg/mL resulted in the lowest zeta potential of 0.98 mV±3.96. These results were not statistically significant. In conclusion, we generated NPs with an average size of 105 nm±5.20 and an average zeta potential of 3.04 mV±1.43.

7.1.2.4 BMP-2 Release Rate using Dextran as a Model Drug

In order to study BSA-NPs release rate, NPs containing 1.25 mg/mL, 2.5 mg/mL, 5 mg/mL Dextran-FITC were prepared and transferred into 100 kDA dialysis tubing. The release of Dextran-FITC into the surrounding solution was evaluated over a time period of 6 days. For this, daily samples were taken in duplicates and the fluorescence

measured. The cumulative release rate of the tested Dextran-FITC concentrations over time is shown in Figure 7.11.

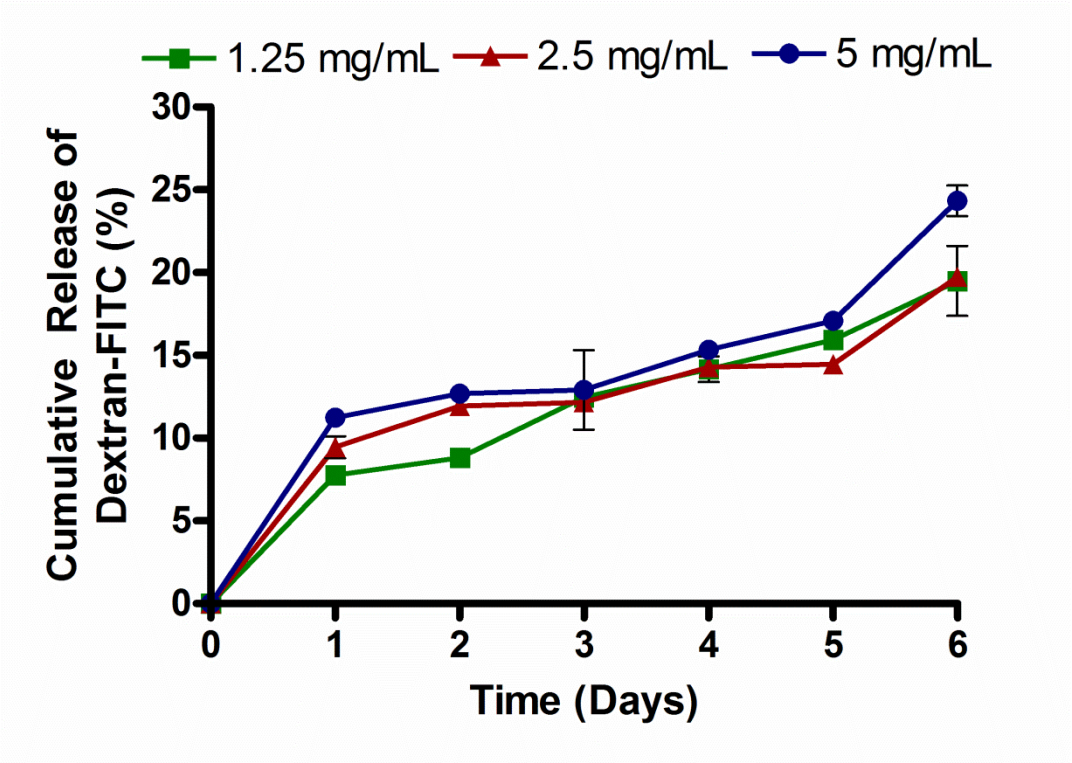

Figure 7.11: Cumulative release rate of Dextran-FITC incorporated into BSA NPs coated with PLL-PEG. FITC fluorescence was measured over 6 days every day. Mean ± SD, n=2

The release rate for all tested GFs concentration were similar. Two way ANOVA was performed to evaluate the contributions of both Dextran-FITC and time on the release rate. It was found that Dextran concentration accounts for 2.17% of the total variance ($p<0.0001$) and time accounts for 94.97% of the total variance ($p<0.0001$). Furthermore, the interaction between the two independent variables were considered as

significant, p=0.0021 which means that Dextran concentration had a similar effect on release rate at all time values.

Based on this result and the results obtained for the encapsulation efficiency where 1.25 mg/mL resulted in the highest encapsulation efficiency of 90.36±0.84%, and the smallest NPs size of 101 nm ±32, the lowest concentration of 1.25 mg/mL was chosen for the preparation on NPs containing BMP-2.

7.1.2.5 Characterization of BSA NPs Containing BMP-2 and Conjugated to PLL-PEG and PLL-PEG-RGD

Using Dextran-FITC as a model drug, we were able to predict the behaviour of BMP-2. The further conjugation of RGD to PEG could lead to some variations in encapsulation efficiency, release rate, NPs size and especially NPs zeta potential. Therefore, BSA NPs containing BMP-2 and conjugated to PLL-PEG (BSA-NPs-BMP-2-PLL-PEG), and BSA NPs containing BMP-2 and conjugated to PLL-PEG-RGD (BSA-NPs-BMP-2-PLL-PEG-RGD) were characterized for their encapsulation efficiency, release rate, size and zeta potential prior incorporating them into the cell/gel system.

To determine the initial BMP-2 concentration used for NPs preparation, an aliquot of dissolved BMP-2 was collected and stored at -80º C. The encapsulation efficiency and release rate of BMP-2 with PLL-PEG and PLL-PEG-RGD coatings were evaluated using ELISA based on a standard curve with known BMP-2 concentration as shown in Figure 7.12 and the encapsulation efficiency of BMP-2 was calculated using (Equation 4.3).

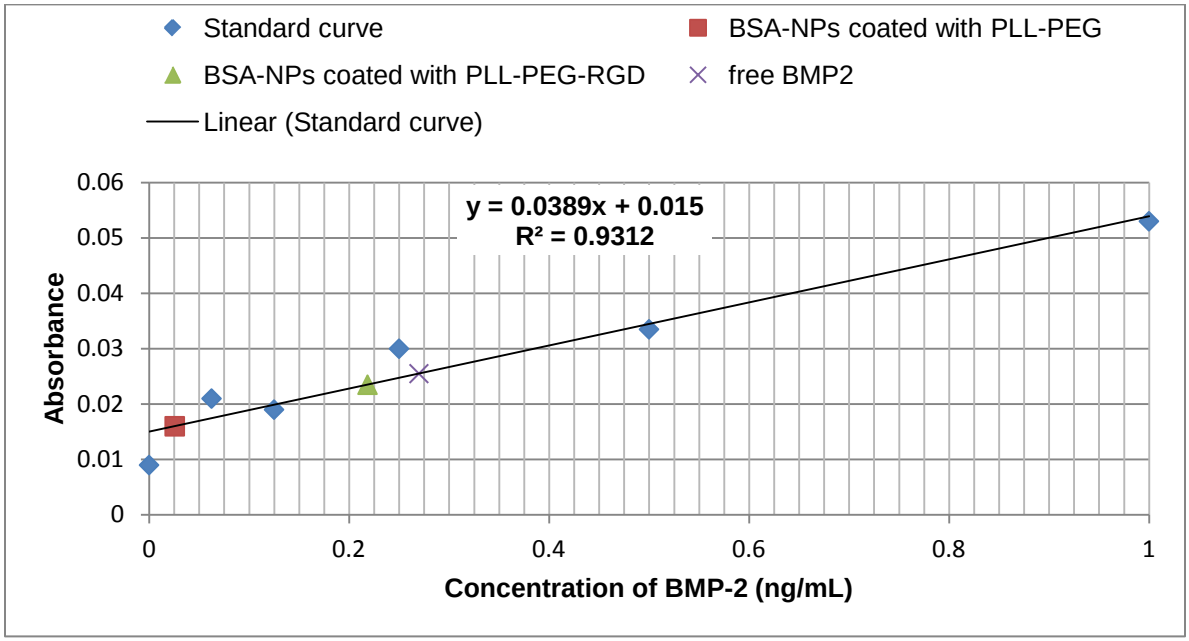

Figure 7.12: Encapsulation efficiency of BMP-2 with different coatings. BMP-2 was collected prior adding to the NPs (free BMP-2) and after conjugating with PLL-PEG (BSA-NPs coated with PLL-PEG) and PLL-PEG-RGD (BSA-NPs coated with PLL-PEG-RGD). N=2.

It was found that although the theoretical value of Cinital was 1.25 ng/µL, the actual value of BMP-2 concentration added to the NPs was 0.3 ng/µl (determined using free BMP-2). Taking the real concentration into account, the encapsulation efficiency for BSA-NPs coated with PLL-PEG was 9.52%±3.2 (0.0257 ng/µL) and with PLL-PEG-RGD coating 80.95%±27.35 (0.219 ng/µL).

Examining the release rate, it was found that the BSA-NPs containing BMP-2 and coated with PLL-PEG resulted in a 100% release at the first day. The cumulative release rate of BMP-2 coated with PLL-PEG-RGD was 69% ±15.56 on the first day and increased to 90%±6.36 at the fifth day.

The low encapsulation efficiency and rapid release of BMP-2 indicated that the BSA-NPs coated with PLL-PEG were not stable. Indeed, measurement of the BSA-NPs with PLL-PEG coating resulted in a mean size of 50 nm (data not shown). Therefore, these particles were not incorporated into the cell/gel system. Instead, BMP-2 in solution was added as a control for BMP-2. The BSA-NPs size containing BMP-2 and coated with PLL-PEG-RGD resulted in a mean size of 121 nm±41 and a zeta potential of 21.28 mV±5.08 as shown in Figure 7.13.

A)

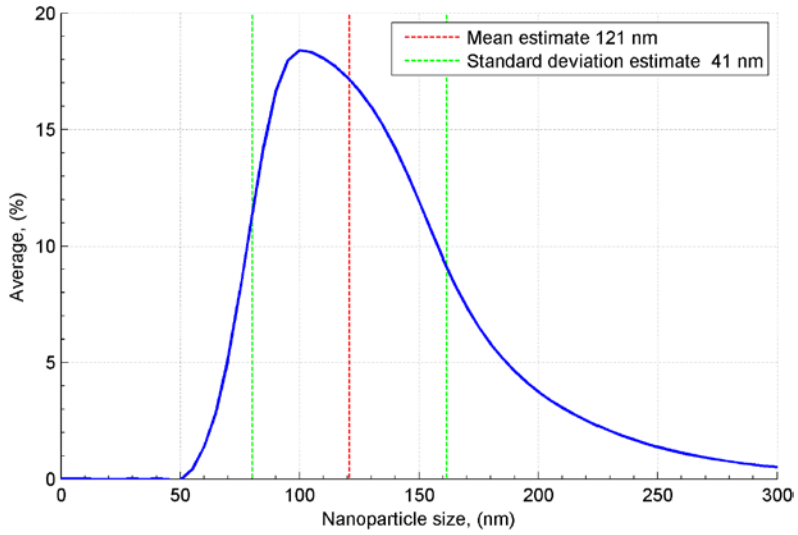

B)

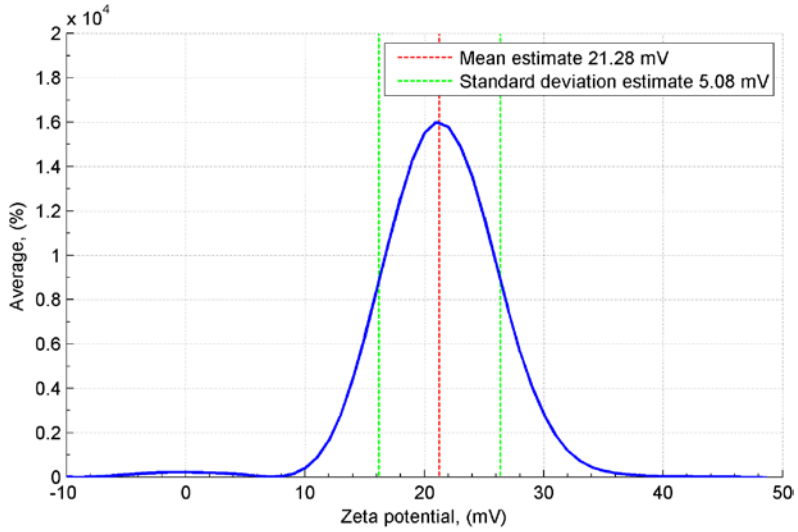

Figure 7.13: Size and zeta potential of BSA-NPs with BMP-2 coated with PLL-PEG-RGD. A) NPs had a mean size of 121±41 and B) zeta potential of 21.28 mV±5.08. Mean size ± SD.

7.1.2.6 Gene Expression

To test the hypothesis of this thesis, BSA NPs encapsulated BMP-2 stabilized with PLL-PEG and conjugated to RGD were incorporated into the cell/gel system. The supplementation of free BMP-2 into the cell/gel and a cell/gel construct with no treatment were used as a control. During the gel preparation, 800 µL collagen type I solution was mixed with 200 µL βGP medium and additionally 100 µL NPs solution was supplemented to the cell/gel construct. The mESCs seeded in the gels were allowed to differentiate for 1 and 15 days but only day 15 samples were subjected to compressive load at 1 Hz, 5% strain for 40 hours as described in Chapter 6. The gene expression of pluripotent, osteogenic and chondrogenic markers was screened for all time points.

However, the gene expression at day 15 was not detected in any of the groups and only the gene expression of Oct 4 and Sox 2 was detected in mESCs/Col I and mESCs/Col I supplemented with BMP-2 control groups as shown in Figure 7.14.

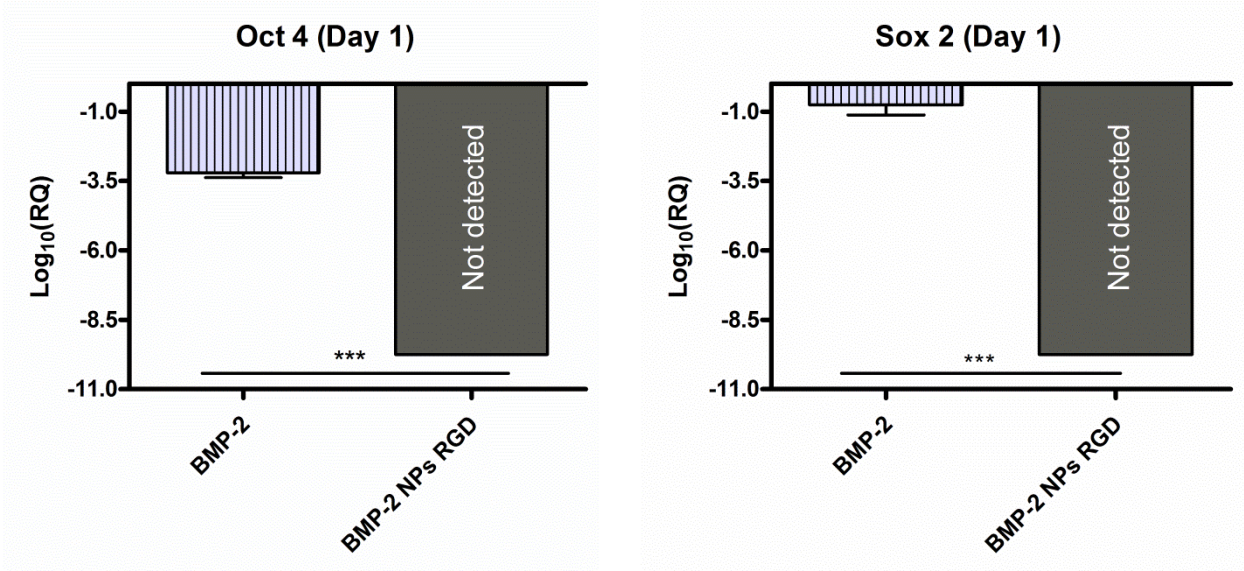

Figure 7.14: Gene expression of mESCs seeded in Col I matrix with the presence of BMP-2 and BSA-NPs containing BMP-2 and conjugated to PLL-PEG-RGD (BMP-2 NPs RGD). A) Oct 4 on day 1, and B) Sox 2 on day 1. Mean + SE, n=2.

No gene expression was detected in the presence of NPs containing BMP-2 conjugated to RGD for any of the tested markers at day 1 and day 15. Therefore, further work is required to evaluate the cause of it.

7.2 Discussion and Conclusion

In the past two decades substantial progress in the field of TE has occurred. Establishing basic cell culture techniques, identifying new cell types and biomaterials, and increasing the access to smart technologies has contributed to a deeper understanding of cellular functions *in vitro* and *in vivo*. However, with the progress made, it also becomes evident that cells residing in the tissue are exposed to complex

micro environmental cues which determine their fate. Understanding of these cues can significantly contribute to the field of TE and regenerative medicine.

Cells as the basic unit of the living system have regulatory functions and can alter their fate in response to intrinsic or extrinsic signals. The interaction of integrins with ECM, the presence of biological factors and the exposure to physical stimuli can influence cellular functions (*87*). Therefore, we aimed to understand the effect of integrins individually and then combined with GFs and mechanical stimuli on mESCs differentiation when seeded in a collagen gel using NPs.

The interaction of integrins with ECM starts as early as with the beginning of gastrulation (*161*) and continues throughout life. The deletion or dysfunction of this connection can influence the early development of the three germ layers (ectoderm, mesoderm and endoderm) and maintenance of cellular functions (*161, 162*). Therefore, the role of integrins in mediating mESCs differentiation was studied. In particular, a cyclic RGD blocking peptide was incorporated into the cell gel system to specifically target the RGD dependent integrins and evaluate their role in mediating differentiation. It was found that RGD blocking peptide down regulated osteogenic gene expression but not that of chondrogenic. Mature bone cells, such as osteoclasts, express the αVβ3 integrin which is important for cell proliferation and deletion of this integrin leads to inhibition of bone mass resorption. Moreover, the α5 subunit, another important RGD-dependent integrin subunit, has been reported to be associated with skeleton abnormalities (*155*). Therefore, the current results indicated that RGD-dependent integrins are important in mESCs osteogenic differentiation but most likely not in

chondrogenic differentiation. These results are consistent with others, reporting that RGD immobilized into matrix supports chondrocyte attachment but cannot promote chondrogenic differentiation (*163*).

Due to the ability of integrins to physically bind to the ECM, they have also been identified to act as mechanosensors. A variety of integrins have been identified to play a role in mechanotransduction. For example, blocking αVβ3 and β1 inhibited endothelial cell responses to shear stress (*164*). Mouse embryonic fibroblasts required α5β1 to develop adhesion complex to fibronectin while αVβ3 transduced mechanical signals (*165*). Similarly, αVβ3 has been identified to play a role in bone mechanotransduction. This integrin complex is expressed in osteocytes which have been identified as mechanical sensitive cell types in bone tissue (*166*). Chondrocytes are another class of mechanosensitive cells and the α5β1 integrin complex has been proposed to act as a mechanoreceptor in this type of cells (*167*). All these integrin complexes are RGD-dependent. To evaluate the role of integrins in transducing mechanical signals, mESCs seeded in collagen gels were incubated with RGD blocking peptide and subjected to confined compressive load. Interestingly, when RGD blocking peptide was supplemented to the cell/gel construct, all tested genes were down regulated and mechanical stimuli could not trigger the same response as described in Chapter 6. However, the inhibition of mechanotransduction process may not specifically be attributed to RGD-dependent integrins and future work is needed to specifically block the individual subunits and evaluate their role in mESCs fate decision.

To verify the hypothesis of this thesis and to study the combined effect of integrins, BMP-2 and mechanical stimuli, we used BSA-NPs as a delivery system. The use of NPs for this approach was advantageous over chemical crosslinking because chemical crosslinking procedures are known to influence the properties of a collagen scaffolds, as the process is associated with water exclusion and tightening of the collagen strands in the treated matrix. Moreover, chemical crosslinking may result in cytotoxicity and would result in an additional variable of the study (*168, 169*). BSA is a natural polymer and has been shown to be biocompatible, biodegradable and non-toxic (*170*). Furthermore, the use of NPs have been shown to prolong the life span of GFs and control their release rate (*171*). GFs are labile molecules and reaching the targeting cells is dependent on their diffusion through ECM (*12*). ECM can bind and inhibit GFs delivery, but with the use of NPs these drawback was avoided.

Prior to incorporating GFs into the cells, it was required to characterize their encapsulation efficiency, release rate, size and zeta potential. Due to the high costs of GFs, model drugs with similar molecular weight are used to predict the behaviour of the actual particles (*172*). Dextran (MW=20,000) is commonly used to predict the behaviour of BMP-2 (MW~26,000). Using different Dextran-FITC concentrations we evaluated the encapsulation efficiency, release rate and NPs size and zeta potential to determine an optimal concentration of BMP-2 for subsequent experiments.

The use of different initial Dextran-FITC concentration significantly influenced the encapsulation efficiency of BSA-NPs stabilized with PLL-PEG. The lowest concentration of 1.25 mg/mL resulted in the highest encapsulation efficiency of 90.36%±0.84 while the

lowest encapsulation efficiency was found for 2.5 mg/mL resulting in 19.56±0.38. Theoretically, higher concentrations should result in better encapsulation efficiency because more GFs are present. Therefore, the differences are most likely due to the use of different stir plates utilized for preparing these NPs. It is recommended to generate NPs at a stir rate of 600 rpm. During this experiment, digital and manual controlled stir plates were used (manual stir plate labeled from 1 to 6) and the stirring rate could only be estimated because no specification was provided by the manufacture. However, the encapsulation efficiency had no significant effect on the release rate of different Dexran-FITC concentration and NPs size. The size of the NPs containing different Dextran-FITC concentrations was in the range of 101 nm±32 to 112 nm±36 and thus in the recommended size range. It is suggested to use NPs not exceeding 200 nm because larger NPs accumulate faster (*108*). Another critical parameter for NPs is their zeta potential. The zeta potential of all NPs was not significantly different resulting in an average zeta potential of 3.04 mV±1.43. Neutral zeta potential leads to a longer circulation time and does not interact with negatively charged nucleic acids (*108*). Overall, from all tested Dextran-FITC concentrations, an initial concentration of 1.25 mg/mL showed the best results in terms of encapsulation efficiency, release rate and NPs size and zeta potential and thus, this concentration was used for subsequent experiments using BMP-2.

To verify our hypothesis, we conjugated RGD to the NPs containing BMP-2 and stabilized them with PLL-PEG. As described above, RGD and BMP-2 alone have shown to trigger osteogenic differentiation and this process was enhanced in the presence of

both RGD and BMP-2. It was assumed, when NPs containing BMP-2 and RGD, the RGD peptide would attach to RGD-dependent integrins (such as αVβ), bring BMP-2 close to cell surface and the combined effect would trigger mESCs differentiation into osteogenic lineage. First, we characterized NPs based on their encapsulation efficiency, release rate, size and zeta potential. It was found that the initial BMP-2 concentration was lower than the theoretical values. This is most likely a result of not taking into account the additional dilution steps during NPs preparation. Moreover, it was found that NPs containing BMP-2 and stabilized with PLL-PEG resulted in an unstable colloid system. It can be only speculated at which step of the preparation procedure a mistake occurred because no such issues were observed with the use of Dextran-FITC and NPs conjugated to RGD. Especially as BSA-NPs by PLL-PEG and NPs stabilized by PLL-PEG-RGD were prepared together. The conjugation of RGD resulted in an encapsulation efficiency of 80.95%±27.35 and an increase in NPs means size and zeta potential was observed. This was expected due to the additional conjugation of RGD which is positively charged. However, as a result of no gene detection after incorporating NPs into the cell/gel system, the combined effect of integrins, BMP-2 and mechanical stimuli could not be evaluated in this study. It is most likely, that the incorporation of NPs to the cell/gel system resulted in cell death. Due to the low initial concentration of BMP-2, the final dialysis was reduced from 24 hours to 6 hours. The reduced time in dialysis was necessary to increase the concentration of BMP-2 in the cell/gel system considering its low concentration. However, the reduced time in dialysis also reduced the purity of NPs solution as the preparation of NPs is associated with the use of extensive amount of ETOH.

Overall, this chapter provided a base for future work. The role of integrins in mediating differentiation and transducing mechanical signals should be evaluated using specifically designed antibodies against an integrin complex. It is suggested to further examine the role of αVβ integrin complexes as the αV subunit is highly expressed when mESCs differentiate in a collagen matrix. Moreover, the effect of micro environmental cues should be further explored. Due to the complexity of the delivery system used in this study, the effect of the individual variables used to prepare the NPs should be systematically examined on mESCs when grown in static culture and incorporated into the cell/gel system.

CHAPTER 8: Conclusion and Recommendations

In this study, the mechanobiological behaviour of a BTE construct made from mESCs and a collagen type I gel was investigated. Our long term goal is to develop this cell/gel system as a delivery system to help stimulate bone formation in osteoporotic fractures and in the repair of diseased bone tissue. Moreover, considering that a majority of fractures result in broken fragments or large defects excluding non-union fractures, a construct like this could be used to fill the random cracks or could even be injected in soluble form prior to polymerization. The potential and applicability of the developed BTE has been successfully tested in a mouse animal model, resulting in bone regeneration. However, as the application of ESCs therapies still faces many challenges (including teratogenic potential), and the host-graft interaction is not completely understood, this thesis focused on understanding how biochemical and biophysical factors influenced mESCs differentiation and bone regeneration within this burr-hole fracture model. Ultimately, improved understanding of these micro environmental factors will accelerate the translation of this therapy to human applications. Therefore, this project aimed to systematically evaluate the effect of micro environmental cues on mESCs differentiation when seeded in a collagen gel.

The commercial Flexcell system loading plate was successfully modified to enable confined compressive loading to very soft, biphasic materials such as the cell/collagen construct. The system was calibrated and characterized based on spring theory and its consistency established experimentally using a Bose material testing machine. The cell/gel constructs were subjected to mechanical stimuli at day 1, day 15, and day 30

using a sinusoidal waveform with two frequencies of 1 Hz and 0.1 Hz, in a force range from 0.1 N to 2.85 N that roughly corresponded to 4-5% total strain. Additionally, the mechanical properties of the cell/gel system at the specified time points were obtained by testing samples on a Bose machine with the same compressive loading regimes. The force variation fell in a range of 0.6 N to 1 N and the corresponding strain was in a range of 3.7% to 4.5% for the two tested loading frequencies. Most of the existing systems, whether commercial or custom built by other researchers, are not capable of measuring force and displacement simultaneously. The Young's modulus was estimated based on the force-displacement diagrams for all time points. For future work, more samples should be tested to gain more representative properties of the collagen gels.

The further characterization of this cell/gel system showed that mESCs differentiate into a heterogeneous population of osteoblasts and chondrocytes, and some cells remain transient amplifying progenitors. Considering the burr-hole fracture again, upon transplantation of the cell/gel construct, the mESCs derived chondrocytes may initiate callus formation while simultaneously mature osteoblasts can initiate a calcification process. Moreover, the progenitor cells could differentiate into both osteoblasts and chondrocytes upon demand, in response to paracrine signaling exerted by the cells which could potentially contribute to fracture healing enhancement. Similarly, during bone regeneration *in vivo*, there are chondrocytes, osteoblasts and progenitor cells, and not only one specific cell type. Therefore, it can be concluded that the obtained results are similar to endochondral bone development and repair. In future work, this construct should be further analyzed in a shorter time frame to better identify the underlying

mechanisms of endochondral ossification and mESCs differentiation into a heterogeneous cell population. It is also possible that other cells from different lineages are present and, thus it is suggested to undertake a broader screening of different markers using micro array analysis. Furthermore, the presence of a heterogeneous cell population enables the examination of different cues directing one lineage commitment over the other and thus provides a base for future work. We studied the effect of loading frequency on mESCs lineage commitment and found that at higher frequencies, chondrogenic differentiation predominates over osteogenic. These observations are an example how mechanical conditions can alter cellular functions. Although, we have postulated that the applied loading regime would trigger osteogenic differentiation, it could be that the combination of such a soft material (whose properties closer match cartilaginous tissue) and the loading type better promoted chondrogenic differentiation. Therefore, it could be assumed that when the cell/gel construct is transplanted into the burr-hole fracture model *in vivo* the cells in this scaffold system stimulate cartilage formation. It would be interesting to see in future studies if the cell/gel constructs when mechanically pre-stimulated *in vitro* would have an impact on bone regeneration *in vivo*. As the loading frequency of 1 Hz had no effect on osteogenic differentiation, future work should consider other factors such as duration, strain and frequency to identify a preferable mechanical environment for osteoblast differentiation. This would enable us to better understand the mechanobiological switch to trigger one lineage commitment over the other and control ESCs fate decision. In terms of chondrogenic differentiation it is suggested to maintain the applied loading regime and further characterize the genes and proteins expressed in mESCs derived chondrocytes. In this study we evaluated the

role of collagen dependent and RGD-dependent integrin subunits in mediating differentiation and mechanotransduction. The integrin subunits α1, αV, and β1 were identified as important for mESCs differentiation when seeded in the collagen scaffold. The role of β1 subunit is well described in the literature; however, the role of RGD dependent integrins in directing ESCs differentiation and mechanotransduction, especially when seeded in a collagen matrix, has not been greatly explored. Due to the fundamental role of integrins in key cellular processes, their role in mediating differentiation and transducing mechanical signals should be further evaluated. We specifically recommend an examination of the role of αVβ integrins in this cell/gel system because they were highly expressed over the course of differentiation and blocking integrins using a specifically designed cyclic RGD peptide down regulated pluripotency and osteogenic differentiation. Moreover, the transduction of mechanical signals into biochemical responses was inhibited in pluripotent, osteogenic and chondrogenic cell types, indicating a ubiquitous role of RGD-dependent integrins in mechanotransduction.

Finally, this project aimed to examine the synergistic effect between several micro environmental factors that may influence mESCs differentiation. We specifically utilized the advances in nanotechnology to deliver encapsulated BMP-2 with conjugated RGD to stimulate osteogenic differentiation. In this study, the protocol of successfully preparing NPs in 100 nm size range with ~90% encapsulation efficiency and a slow release rate was established. However, the interplay of these factors could not be examined because of the reduced time in final dialysis step and thus incorporating impure NPs to the cell/gel system that may have caused cell apoptosis. Although this

hypothesis could not be fully verified in this project, preliminary results indicate that it was possible and further studies should be conducted to attempt to verify that BMP-2 in combination with cell adhesion molecules such as αVβ3 and/or α1β1 will act synergistically under compressive load to accelerate mESCs differentiation into osteoblasts.

References

1. M. Ellegaard, N. R. Jorgensen, P. Schwarz, Parathyroid hormone and bone healing. *Calcif Tissue Int* **87**, 1 (Jul).
2. T. Shisha, Parameters for defining efficacy in fracture healing. *Clin Cases Miner Bone Metab* **7**, 15 (Jan).
3. M. S. Gaston, A. H. Simpson, Inhibition of fracture healing. *J Bone Joint Surg Br* **89**, 1553 (Dec, 2007).
4. G. J. Meijer, J. D. de Bruijn, R. Koole, C. A. van Blitterswijk, Cell-based bone tissue engineering. *PLoS Med* **4**, e9 (Feb, 2007).
5. D. P. Pioletti, Biomechanics in bone tissue engineering. *Comput Methods Biomech Biomed Engin* **13**, 837 (Dec).
6. P. V. Giannoudis, Fracture healing and bone regeneration: autologous bone grafting or BMPs? *Injury* **40**, 1243 (Dec, 2009).
7. J. A. Goulet, L. E. Senunas, G. L. DeSilva, M. L. Greenfield, Autogenous iliac crest bone graft. Complications and functional assessment. *Clin Orthop Relat Res*, 76 (Jun, 1997).
8. S. Varghese, J. H. Elisseeff, Hydrogels for musculoskeletal tissue engineering. *Polymers for Regenerative Medicine*, 95 (2006).
9. R. Langer, J. P. Vacanti, Tissue engineering. *Science* **260**, 920 (May 14, 1993).
10. A. G. Mikos *et al.*, Engineering complex tissues. *Tissue Eng* **12**, 3307 (Dec, 2006).
11. S. Bose, M. Roy, A. Bandyopadhyay, Recent advances in bone tissue engineering scaffolds. *Trends Biotechnol* **30**, 546 (Oct).

12. K. Lee, E. A. Silva, D. J. Mooney, Growth factor delivery-based tissue engineering: general approaches and a review of recent developments. *J R Soc Interface* **8**, 153 (Feb 6).
13. T. Dvir, B. P. Timko, D. S. Kohane, R. Langer, Nanotechnological strategies for engineering complex tissues. *Nat Nanotechnol* **6**, 13 (Jan).
14. J. A. Thomson *et al.*, Embryonic stem cell lines derived from human blastocysts. *Science* **282**, 1145 (Nov 6, 1998).
15. F. Couet, D. Mantovani, Perspectives on the advanced control of bioreactors for functional vascular tissue engineering in vitro. *Expert Rev Med Devices* **9**, 233 (May).
16. N. Mabvuure, S. Hindocha, W. S. Khan, The role of bioreactors in cartilage tissue engineering. *Curr Stem Cell Res Ther* **7**, 287 (Jul).
17. E. Salter *et al.*, Bone tissue engineering bioreactors: a role in the clinic? *Tissue Eng Part B Rev* **18**, 62 (Feb).
18. R. J. Krawetz *et al.*, Collagen I scaffolds cross-linked with beta-glycerol phosphate induce osteogenic differentiation of embryonic stem cells in vitro and regulate their tumorigenic potential in vivo. *Tissue Eng Part A* **18**, 1014 (May).
19. R. J. K. Jaymi T. Taiani, Akihiro Yamashita, Yves Pauchard, Helen R. Buie, Dragana Ponjevic, Steven K. Boyd, Derrick E. Rancourt, John R. Matyas, Embryonic Stem Cells Incorporate into Newly Formed Bone and do not Form Tumors in an Immunocompetent Mouse Fracture Model. *Cell Transplant*, (2012, accepted).
20. B. Clarke, Normal bone anatomy and physiology. *Clin J Am Soc Nephrol* **3 Suppl 3**, S131 (Nov, 2008).

21. M. Doblare, J. M. Garcia, On the modelling bone tissue fracture and healing of the bone tissue. *Acta Cient Venez* **54**, 58 (2003).
22. J.-Y. Rho, L. Kuhn-Spearing, P. Zioupos, Mechanical properties and the hierarchical structure of bone. *Medical Engineering & Physics* **20**, 92 (1998).
23. A. J. Salgado, O. P. Coutinho, R. L. Reis, Bone tissue engineering: state of the art and future trends. *Macromol Biosci* **4**, 743 (Aug 9, 2004).
24. F. H. Martini, *Fundamentals of Anatomy and Physiology*. (Prentice Hall, Inc., New Jersey, ed. Fourth Edition, 1998), vol. 4, pp. 1123.
25. J. C. Thomson, *Netter's Concise Atlas of Orthopaedic Anatomy*. (Icon Learning Systems LLC, ed. 1, 2004), vol. 1, pp. 320.
26. D. J. Hadjidakis, I. I. Androulakis, Bone Remodeling. *Annals of the New York Academy of Sciences* **1092**, 385 (2006).
27. M. Braddock, P. Houston, C. Campbell, P. Ashcroft, Born again bone: tissue engineering for bone repair. *News Physiol Sci* **16**, 208 (Oct, 2001).
28. U. Kneser, D. J. Schaefer, E. Polykandriotis, R. E. Horch, Tissue engineering of bone: the reconstructive surgeon's point of view. *J Cell Mol Med* **10**, 7 (Jan-Mar, 2006).
29. P. V. Giannoudis, E. Jones, T. A. Einhorn, Fracture healing and bone repair. *Injury* **42**, 549 (Jun).
30. T. Tosounidis, G. Kontakis, V. Nikolaou, A. Papathanassopoulos, P. V. Giannoudis, Fracture healing and bone repair: an update. *Trauma* **11**, 145 (2009).
31. B. Ø. P. a. S. N. Bhatia, *Tissue Engineering*. (Pearson Education, Inc. , 2004), pp. 407.

32. R. Langer, Tissue engineering: a new field and its challenges. *Pharm Res* **14**, 840 (Jul, 1997).

33. C. A. Heath, Cells for tissue engineering. *Trends Biotechnol* **18**, 17 (Jan, 2000).

34. L. G. Griffith, G. Naughton, Tissue engineering--current challenges and expanding opportunities. *Science* **295**, 1009 (Feb 8, 2002).

35. Y.-S. Hwang, Y. Kang, A. Mantalaris, Directing embryonic stem cell differentiation into osteogenic chondrogenic lineage<i>in vitro</i&gt. *Biotechnology and Bioprocess Engineering* **12**, 15 (2007).

36. H. Hentze, R. Graichen, A. Colman, Cell therapy and the safety of embryonic stem cell-derived grafts. *Trends in Biotechnology* **25**, 24 (2007).

37. S. Zhang *et al.*, Polyethylenimine-coated albumin nanoparticles for BMP-2 delivery. *Biotechnol Prog* **24**, 945 (Jul-Aug, 2008).

38. P. W. Andrews *et al.*, Embryonic stem (ES) cells and embryonal carcinoma (EC) cells: opposite sides of the same coin. *Biochem Soc Trans* **33**, 1526 (Dec, 2005).

39. .

40. T. A. Prokhorova *et al.*, Teratoma Formation by Human Embryonic Stem Cells Is Site Dependent and Enhanced by the Presence of Matrigel. *Stem Cells and Development* **18**, 47 (Jan-Feb, 2009).

41. N. I. zur Nieden, G. Kempka, H. J. Ahr, In vitro differentiation of embryonic stem cells into mineralized osteoblasts. *Naunyn-Schmiedebergs Archives of Pharmacology* **365**, R154 (Mar, 2002).

42. N. L. Woll, S. K. Bronson, Analysis of embryonic stem cell-derived osteogenic cultures. *Methods Mol Biol* **330**, 149 (2006).

43. L. D. Buttery *et al.*, Differentiation of osteoblasts and in vitro bone formation from murine embryonic stem cells. *Tissue Eng* **7**, 89 (Feb, 2001).

44. T. Komori, Regulation of osteoblast differentiation by transcription factors. *J Cell Biochem* **99**, 1233 (Dec 1, 2006).

45. G. R. Beck, B. Zerler, E. Moran, Phosphate is a specific signal for induction of osteopontin gene expression. *Proceedings of the National Academy of Sciences of the United States of America* **97**, 8352 (Jul 18, 2000).

46. C. Farquharson, J. L. Berry, E. B. Mawer, E. Seawright, C. C. Whitehead, Ascorbic acid-induced chondrocyte terminal differentiation: the role of the extracellular matrix and 1,25-dihydroxyvitamin D. *Eur J Cell Biol* **76**, 110 (Jun, 1998).

47. B. Johnstone, T. M. Hering, A. I. Caplan, V. M. Goldberg, J. U. Yoo, In vitro chondrogenesis of bone marrow-derived mesenchymal progenitor cells. *Exp Cell Res* **238**, 265 (Jan 10, 1998).

48. B. C. Heng, T. Cao, E. H. Lee, Directing Stem Cell Differentiation into the Chondrogenic Lineage In Vitro. *Stem Cells* **22**, 1152 (2004).

49. R. T. Franceschi, G. Xiao, Regulation of the osteoblast-specific transcription factor, Runx2: responsiveness to multiple signal transduction pathways. *J Cell Biochem* **88**, 446 (Feb 15, 2003).

50. C. H. Streuli, Integrins and cell-fate determination. *J Cell Sci* **122**, 171 (Jan 15, 2009).

51. M. Barczyk, S. Carracedo, D. Gullberg, Integrins. *Cell Tissue Res* **339**, 269 (Jan).

52. A. P. Roy Zent, *Cell-Extracellular Matrix Interactions in Cancer*. (Springer, 2009), pp. 314.

53. J. L. Myles, B. T. Burgess, R. B. Dickinson, Modification of the adhesive properties of collagen by covalent grafting with RGD peptides. *J Biomater Sci Polym Ed* **11**, 69 (2000).

54. G. C. Reilly, A. J. Engler, Intrinsic extracellular matrix properties regulate stem cell differentiation. *Journal of Biomechanics* **43**, 55 (Jan 5, 2010).

55. N. Huebsch *et al.*, Harnessing traction-mediated manipulation of the cell/matrix interface to control stem-cell fate. *Nat Mater* **9**, 518 (Jun).

56. F. Chowdhury *et al.*, Material properties of the cell dictate stress-induced spreading and differentiation in embryonic stem cells. *Nat Mater* **9**, 82 (Jan).

57. N. D. Evans *et al.*, Substrate stiffness affects early differentiation events in embryonic stem cells. *Eur Cell Mater* **18**, 1 (2009).

58. B. Chevallay, D. Herbage, Collagen-based biomaterials as 3D scaffold for cell cultures: applications for tissue engineering and gene therapy. *Med Biol Eng Comput* **38**, 211 (Mar, 2000).

59. R. L. Ehrmann, G. O. Gey, The growth of cells on a transparent gel of reconstituted rat-tail collagen. *J Natl Cancer Inst* **16**, 1375 (Jun, 1956).

60. H. K. Kleinman, R. J. Klebe, G. R. Martin, Role of collagenous matrices in the adhesion and growth of cells. *J Cell Biol* **88**, 473 (Mar, 1981).

61. J. Glowacki, S. Mizuno, Collagen scaffolds for tissue engineering. *Biopolymers* **89**, 338 (May, 2008).

62. N. D. Evans *et al.*, Extracellular matrix-mediated osteogenic differentiation of murine embryonic stem cells. *Biomaterials* **31**, 3244 (Apr).

63. K. Warstat *et al.*, TGF-beta enhances the integrin alpha2beta1-mediated attachment of mesenchymal stem cells to type I collagen. *Stem Cells Dev* **19**, 645 (May).

64. J. Parreno, G. Buckley-Herd, I. de-Hemptinne, D. A. Hart, Osteoblastic MG-63 cell differentiation, contraction, and mRNA expression in stress-relaxed 3D collagen I gels. *Mol Cell Biochem* **317**, 21 (Oct, 2008).

65. M. Mizuno, R. Fujisawa, Y. Kuboki, Type I collagen-induced osteoblastic differentiation of bone-marrow cells mediated by collagen-alpha2beta1 integrin interaction. *J Cell Physiol* **184**, 207 (Aug, 2000).

66. A. W. Lund, J. P. Stegemann, G. E. Plopper, Inhibition of ERK promotes collagen gel compaction and fibrillogenesis to amplify the osteogenesis of human mesenchymal stem cells in three-dimensional collagen I culture. *Stem Cells Dev* **18**, 331 (Mar, 2009).

67. H. Fernandes *et al.*, The role of collagen crosslinking in differentiation of human mesenchymal stem cells and MC3T3-E1 cells. *Tissue Eng Part A* **15**, 3857 (Dec, 2009).

68. U. C. Ensanya A. Abou Neel, Jonathan C. Knowles, Robert A. Brown and Showan N. Nazhat, Use of multiple unconfined compression for control of collagen gel scaffold density and mechanical properties. *Soft Matter*, 986 (2006).

69. J. Cho, M. C. Heuzey, A. Begin, P. J. Carreau, Physical gelation of chitosan in the presence of beta-glycerophosphate: the effect of temperature. *Biomacromolecules* **6**, 3267 (Nov-Dec, 2005).

70. A. Faikrua, R. Jeenapongsa, M. Sila-asna, J. Viyoch, Properties of beta-glycerol phosphate/collagen/chitosan blend scaffolds for application in skin tissue engineering. *Scienceasia* **35**, 247 (Sep, 2009).

71. P. Aleljung *et al.*, Purification of Collagen-Binding Proteins of Lactobacillus-Reuteri Ncib-11951. *Current Microbiology* **28**, 231 (Apr, 1994).

72. C. C. Cohen DM. (Cambridge (MA): Harvard Stem Cell Institute;, 2008).

73. I. Owan *et al.*, Mechanotransduction in bone: osteoblasts are more responsive to fluid forces than mechanical strain. *Am J Physiol* **273**, C810 (Sep, 1997).

74. , (!!! INVALID CITATION !!!).

75. J. H. Wang, B. P. Thampatty, An introductory review of cell mechanobiology. *Biomech Model Mechanobiol* **5**, 1 (Mar, 2006).

76. E. Chung, M. N. Rylander, Response of a preosteoblastic cell line to cyclic tensile stress conditioning and growth factors for bone tissue engineering. *Tissue Eng Part A* **18**, 397 (Feb).

77. Z. Li, S. J. Yao, M. Alini, M. J. Stoddart, Chondrogenesis of human bone marrow mesenchymal stem cells in fibrin-polyurethane composites is modulated by frequency and amplitude of dynamic compression and shear stress. *Tissue Eng Part A* **16**, 575 (Feb).

78. L. A. McMahon, F. J. O'Brien, P. J. Prendergast, Biomechanics and mechanobiology in osteochondral tissues. *Regen Med* **3**, 743 (Sep, 2008).

79. M. Mullender *et al.*, Mechanotransduction of bone cells in vitro: mechanobiology of bone tissue. *Med Biol Eng Comput* **42**, 14 (Jan, 2004).

80. A. Ignatius *et al.*, Tissue engineering of bone: effects of mechanical strain on osteoblastic cells in type I collagen matrices. *Biomaterials* **26**, 311 (Jan, 2005).

81. V. Terraciano *et al.*, Differential response of adult and embryonic mesenchymal progenitor cells to mechanical compression in hydrogels. *Stem Cells* **25**, 2730 (Nov, 2007).

82. C. J. Hunter, S. M. Imler, P. Malaviya, R. M. Nerem, M. E. Levenston, Mechanical compression alters gene expression and extracellular matrix synthesis by chondrocytes cultured in collagen I gels. *Biomaterials* **23**, 1249 (Feb, 2002).

83. I. Takahashi *et al.*, Compressive force promotes sox9, type II collagen and aggrecan and inhibits IL-1beta expression resulting in chondrogenesis in mouse embryonic limb bud mesenchymal cells. *J Cell Sci* **111 (Pt 14)**, 2067 (Jul 30, 1998).

84. T. M. Maul, D. W. Chew, A. Nieponice, D. A. Vorp, Mechanical stimuli differentially control stem cell behavior: morphology, proliferation, and differentiation. *Biomech Model Mechanobiol* **10**, 939 (Dec).

85. K. L. Au-Yeung, K. Y. Sze, M. H. Sham, B. P. Chan, Development of a micromanipulator-based loading device for mechanoregulation study of human mesenchymal stem cells in three-dimensional collagen constructs. *Tissue Eng Part C Methods* **16**, 93 (Feb).

86. R. D. Sumanasinghe, J. A. Osborne, E. G. Loboa, Mesenchymal stem cell-seeded collagen matrices for bone repair: effects of cyclic tensile strain, cell density, and media conditions on matrix contraction in vitro. *J Biomed Mater Res A* **88**, 778 (Mar 1, 2009).

87. E. Alsberg, H. A. von Recum, M. J. Mahoney, Environmental cues to guide stem cell fate decision for tissue engineering applications. *Expert Opin Biol Ther* **6**, 847 (Sep, 2006).

88. D. E. Discher, D. J. Mooney, P. W. Zandstra, Growth factors, matrices, and forces combine and control stem cells. *Science* **324**, 1673 (Jun 26, 2009).

89. T. L. Deans, J. H. Elisseeff, The Life of a Cell: Probing the Complex Relationships with the World. *Cell Stem Cell* **6**, 499 (Jun 4, 2010).

90. S. X. Hsiong, N. Huebsch, C. Fischbach, H. J. Kong, D. J. Mooney, Integrin-adhesion ligand bond formation of preosteoblasts and stem cells in three-dimensional RGD presenting matrices. *Biomacromolecules* **9**, 1843 (Jul, 2008).

91. R. D. Sumanasinghe, S. H. Bernacki, E. G. Loboa, Osteogenic differentiation of human mesenchymal stem cells in collagen matrices: effect of uniaxial cyclic tensile strain on bone morphogenetic protein (BMP-2) mRNA expression. *Tissue Eng* **12**, 3459 (Dec, 2006).

92. E. A. Wang *et al.*, Recombinant human bone morphogenetic protein induces bone formation. *Proc Natl Acad Sci U S A* **87**, 2220 (Mar, 1990).

93. C. F. Lai, S. L. Cheng, Alphavbeta integrins play an essential role in BMP-2 induction of osteoblast differentiation. *J Bone Miner Res* **20**, 330 (Feb, 2005).

94. A. Jikko, S. E. Harris, D. Chen, D. L. Mendrick, C. H. Damsky, Collagen integrin receptors regulate early osteoblast differentiation induced by BMP-2. *J Bone Miner Res* **14**, 1075 (Jul, 1999).

95. L. M. Kock *et al.*, RGD-dependent integrins are mechanotransducers in dynamically compressed tissue-engineered cartilage constructs. *J Biomech* **42**, 2177 (Sep 18, 2009).

96. T. Masuda *et al.*, Development of a cell culture system loading cyclic mechanical strain to chondrogenic cells. *J Biotechnol* **133**, 231 (Jan 20, 2008).

97. N. Basso, J. N. Heersche, Characteristics of in vitro osteoblastic cell loading models. *Bone* **30**, 347 (Feb, 2002).

98. Y.-C. Poh, F. Chowdhury, T. S. Tanaka, N. Wang, Embryonic Stem Cells Do Not Stiffen on Rigid Substrates. *Biophysical journal* **99**, L19.

99. D. S. Perie, J. J. Maclean, J. P. Owen, J. C. Iatridis, Correlating material properties with tissue composition in enzymatically digested bovine annulus fibrosus and nucleus pulposus tissue. *Ann Biomed Eng* **34**, 769 (May, 2006).

100. K. A. Myers, N. G. Shrive, D. A. Hart, A novel apparatus applying long term intermittent cyclic hydrostatic pressure to in vitro cell cultures. *J Biosci Bioeng* **103**, 578 (Jun, 2007).

101. J. M. Cloyd *et al.*, Material properties in unconfined compression of human nucleus pulposus, injectable hyaluronic acid-based hydrogels and tissue engineering scaffolds. *Eur Spine J* **16**, 1892 (Nov, 2007).

102. J. T. Cormier, N. I. zur Nieden, D. E. Rancourt, M. S. Kallos, Expansion of undifferentiated murine embryonic stem cells as aggregates in suspension culture bioreactors. *Tissue Eng* **12**, 3233 (Nov, 2006).

103. K. J. Livak, T. D. Schmittgen, Analysis of relative gene expression data using real-time quantitative PCR and the 2(-Delta Delta C(T)) Method. *Methods* **25**, 402 (Dec, 2001).

104. . (2011).

105. J. Bullock *et al.*, Comparison of results of various methods used to determine the extent of modification of methoxy polyethylene glycol 5000-modified bovine cupri-zinc superoxide dismutase. *Anal Biochem* **254**, 254 (Dec 15, 1997).

106. S. Zhang, J. E. I. Wright, N. Özber, H. Uludağ, The Interaction of Cationic Polymers and Their Bisphosphonate Derivatives with Hydroxyapatite. *Macromolecular Bioscience* **7**, 656 (2007).

107. R. B. Sashidhar, A. K. Capoor, D. Ramana, Quantitation of Epsilon-Amino Group Using Amino-Acids as Reference-Standards by Trinitrobenzene Sulfonic-Acid - a Simple Spectrophotometric Method for the Estimation of Hapten to Carrier Protein Ratio. *Journal of Immunological Methods* **167**, 121 (Jan 3, 1994).

108. G. Wang *et al.*, Preparation of BMP-2 containing bovine serum albumin (BSA) nanoparticles stabilized by polymer coating. *Pharm Res* **25**, 2896 (Dec, 2008).

109. S. Ehnert *et al.*, The possible use of stem cells in regenerative medicine: dream or reality? *Langenbecks Arch Surg* **394**, 985 (Nov, 2009).

110. L. Duplomb, M. Dagouassat, P. Jourdon, D. Heymann, Differentiation of osteoblasts from mouse embryonic stem cells without generation of embryoid body. *In Vitro Cell Dev Biol Anim* **43**, 21 (Jan, 2007).

111. J. A. Pedersen, M. A. Swartz, Mechanobiology in the third dimension. *Ann Biomed Eng* **33**, 1469 (Nov, 2005).

112. U. Hersel, C. Dahmen, H. Kessler, RGD modified polymers: biomaterials for stimulated cell adhesion and beyond. *Biomaterials* **24**, 4385 (2003).

113. J. Rungby, M. Kassem, E. F. Eriksen, G. Danscher, The von Kossa reaction for calcium deposits: silver lactate staining increases sensitivity and reduces background. *Histochem J* **25**, 446 (Jun, 1993).

114. M. G. Coppolino, S. Dedhar, Bi-directional signal transduction by integrin receptors. *Int J Biochem Cell Biol* **32**, 171 (Feb, 2000).

115. M. B. Keogh, O. B. FJ, J. S. Daly, A novel collagen scaffold supports human osteogenesis--applications for bone tissue engineering. *Cell Tissue Res* **340**, 169 (Apr).

116. M. Nakajima, S. Wakitani, Y. Harada, A. Tanigami, N. Tomita, In vivo mechanical condition plays an important role for appearance of cartilage tissue in ES cell transplanted joint. *J Orthop Res* **26**, 10 (Jan, 2008).

117. Y. Hayashi *et al.*, Integrins regulate mouse embryonic stem cell self-renewal. *Stem Cells* **25**, 3005 (Dec, 2007).

118. S. Li *et al.*, Matrix assembly, regulation, and survival functions of laminin and its receptors in embryonic stem cell differentiation. *J Cell Biol* **157**, 1279 (Jun 24, 2002).

119. S. T. Lee *et al.*, Engineering integrin signaling for promoting embryonic stem cell self-renewal in a precisely defined niche. *Biomaterials* **31**, 1219 (Feb).

120. H. Akiyama, M.-C. Chaboissier, J. F. Martin, A. Schedl, B. de Crombrugghe, The transcription factor Sox9 has essential roles in successive steps of the chondrocyte differentiation pathway and is required for expression of Sox5 and Sox6. *Genes & Development* **16**, 2813 (November 1, 2002, 2002).

121. D. J. Kelly, C. R. Jacobs, The role of mechanical signals in regulating chondrogenesis and osteogenesis of mesenchymal stem cells. *Birth Defects Res C Embryo Today* **90**, 75 (Mar).

122. C. Hegert *et al.*, Differentiation plasticity of chondrocytes derived from mouse embryonic stem cells. *J Cell Sci* **115**, 4617 (Dec 1, 2002).

123. J. A. Santiago, R. Pogemiller, B. M. Ogle, Heterogeneous differentiation of human mesenchymal stem cells in response to extended culture in extracellular matrices. *Tissue Eng Part A* **15**, 3911 (Dec, 2009).

124. D. Bosnakovski *et al.*, Chondrogenic differentiation of bovine bone marrow mesenchymal stem cells (MSCs) in different hydrogels: influence of collagen type II extracellular matrix on MSC chondrogenesis. *Biotechnol Bioeng* **93**, 1152 (Apr 20, 2006).

125. E. H. Burger, J. Klein-Nulend, Mechanotransduction in bone--role of the lacuno-canalicular network. *FASEB J* **13 Suppl**, S101 (1999).

126. K. Takahashi *et al.*, Hydrostatic pressure influences mRNA expression of transforming growth factor-beta 1 and heat shock protein 70 in chondrocyte-like cell line. *J Orthop Res* **15**, 150 (Jan, 1997).

127. J. P. Urban, The chondrocyte: a cell under pressure. *Br J Rheumatol* **33**, 901 (Oct, 1994).

128. E. J. Arnsdorf, P. Tummala, R. Y. Kwon, C. R. Jacobs, Mechanically induced osteogenic differentiation--the role of RhoA, ROCKII and cytoskeletal dynamics. *J Cell Sci* **122**, 546 (Feb 15, 2009).

129. K. Yamamoto *et al.*, Fluid shear stress induces differentiation of Flk-1-positive embryonic stem cells into vascular endothelial cells in vitro. *Am J Physiol Heart Circ Physiol* **288**, H1915 (Apr, 2005).

130. S. Kapur, D. J. Baylink, K. H. Lau, Fluid flow shear stress stimulates human osteoblast proliferation and differentiation through multiple interacting and competing signal transduction pathways. *Bone* **32**, 241 (2003).

131. P. Das, D. J. Schurman, R. L. Smith, Nitric oxide and G proteins mediate the response of bovine articular chondrocytes to fluid-induced shear. *J Orthop Res* **15**, 87 (Jan, 1997).

132. J. J. Campbell, D. A. Lee, D. L. Bader, Dynamic compressive strain influences chondrogenic gene expression in human mesenchymal stem cells. *Biorheology* **43**, 455 (2006).

133. M. Wong, M. Siegrist, K. Goodwin, Cyclic tensile strain and cyclic hydrostatic pressure differentially regulate expression of hypertrophic markers in primary chondrocytes. *Bone* **33**, 685 (Oct, 2003).

134. B. Rath, J. Nam, T. J. Knobloch, J. J. Lannutti, S. Agarwal, Compressive forces induce osteogenic gene expression in calvarial osteoblasts. *J Biomech* **41**, 1095 (2008).

135. L. Tang, Z. Lin, Y. M. Li, Effects of different magnitudes of mechanical strain on Osteoblasts in vitro. *Biochem Biophys Res Commun* **344**, 122 (May 26, 2006).

136. D. A. Lee, M. M. Knight, J. J. Campbell, D. L. Bader, Stem cell mechanobiology. *J Cell Biochem* **112**, 1 (Jan).

137. A. Sittichockechaiwut, A. M. Scutt, A. J. Ryan, L. F. Bonewald, G. C. Reilly, Use of rapidly mineralising osteoblasts and short periods of mechanical loading to accelerate matrix maturation in 3D scaffolds. *Bone* **44**, 822 (May, 2009).

138. C. A. Simmons *et al.*, Cyclic strain enhances matrix mineralization by adult human mesenchymal stem cells via the extracellular signal-regulated kinase (ERK1/2) signaling pathway. *J Biomech* **36**, 1087 (Aug, 2003).

139. R. Krawetz *et al.*, Collagen I Scaffolds Cross-Linked with Beta-Glycerol Phosphate Induce Osteogenic Differentiation of Embryonic Stem Cells In Vitro and Regulates their Tumorigenic Potential In Vivo. *Tissue Eng Part A*, (Dec 14).

140. D. Kaspar *et al.*, Proliferation of human-derived osteoblast-like cells depends on the cycle number and frequency of uniaxial strain. *J Biomech* **35**, 873 (Jul, 2002).

141. C. H. Turner, I. Owan, Y. Takano, Mechanotransduction in bone: role of strain rate. *Am J Physiol* **269**, E438 (Sep, 1995).

142. C. Neidlinger-Wilke, H. J. Wilke, L. Claes, Cyclic stretching of human osteoblasts affects proliferation and metabolism: a new experimental method and its application. *J Orthop Res* **12**, 70 (Jan, 1994).

143. D. A. Lee, D. L. Bader, Compressive strains at physiological frequencies influence the metabolism of chondrocytes seeded in agarose. *Journal of Orthopaedic Research* **15**, 181 (1997).

144. J. K. Mouw, J. T. Connelly, C. G. Wilson, K. E. Michael, M. E. Levenston, Dynamic compression regulates the expression and synthesis of chondrocyte-specific matrix molecules in bone marrow stromal cells. *Stem Cells* **25**, 655 (Mar, 2007).

145. C. Y. Huang, K. L. Hagar, L. E. Frost, Y. Sun, H. S. Cheung, Effects of cyclic compressive loading on chondrogenesis of rabbit bone-marrow derived mesenchymal stem cells. *Stem Cells* **22**, 313 (2004).

146. C. R. Jacobs *et al.*, Differential effect of steady versus oscillating flow on bone cells. *J Biomech* **31**, 969 (Nov, 1998).

147. Y. F. Hsieh, C. H. Turner, Effects of loading frequency on mechanically induced bone formation. *J Bone Miner Res* **16**, 918 (May, 2001).

148. S. J. Ellis, G. Tanentzapf, Integrin-mediated adhesion and stem-cell-niche interactions. *Cell Tissue Res* **339**, 121 (Jan).

149. H. N. Suh, H. J. Han, Collagen I regulates the self-renewal of mouse embryonic stem cells through alpha2beta1 integrin- and DDR1-dependent Bmi-1. *J Cell Physiol* **226**, 3422 (Dec).

150. D. E. Ingber, Tensegrity: the architectural basis of cellular mechanotransduction. *Annu Rev Physiol* **59**, 575 (1997).

151. D. E. Ingber, Cellular basis of mechanotransduction. *Biol Bull* **194**, 323 (Jun, 1998).

152. D. E. Ingber, Cellular mechanotransduction: putting all the pieces together again. *FASEB J* **20**, 811 (May, 2006).

153. H. Shin *et al.*, Osteogenic differentiation of rat bone marrow stromal cells cultured on Arg-Gly-Asp modified hydrogels without dexamethasone and beta-glycerol phosphate. *Biomaterials* **26**, 3645 (Jun, 2005).

154. X. He, J. Ma, E. Jabbari, Effect of grafting RGD and BMP-2 protein-derived peptides to a hydrogel substrate on osteogenic differentiation of marrow stromal cells. *Langmuir* **24**, 12508 (Nov 4, 2008).

155. E. H. Danen, A. Sonnenberg, Integrins in regulation of tissue development and function. *J Pathol* **200**, 471 (Jul, 2003).

156. X. Zhang *et al.*, Poly(ethylene glycol)-block-polyethylenimine copolymers as carriers for gene delivery: effects of PEG molecular weight and PEGylation degree. *J Biomed Mater Res A* **84**, 795 (Mar 1, 2008).

157. B. Lu, X. D. Xu, X. Z. Zhang, S. X. Cheng, R. X. Zhuo, Low molecular weight polyethylenimine grafted N-maleated chitosan for gene delivery: properties and in vitro transfection studies. *Biomacromolecules* **9**, 2594 (Oct, 2008).

158. J. Huang, R. J. Wigent, J. B. Schwartz, Nifedipine molecular dispersion in microparticles of ammonio methacrylate copolymer and ethylcellulose binary blends for controlled drug delivery: effect of matrix composition. *Drug development and industrial pharmacy* **32**, 1185 (Nov-Dec, 2006).

159. R. L. Cleek, A. A. Rege, L. A. Denner, S. G. Eskin, A. G. Mikos, Inhibition of smooth muscle cell growth in vitro by an antisense oligodeoxynucleotide released from poly(DL-lactic-co-glycolic acid) microparticles. *J Biomed Mater Res* **35**, 525 (Jun 15, 1997).

160. J. Li *et al.*, Self-assembled supramolecular hydrogels formed by biodegradable PEO-PHB-PEO triblock copolymers and alpha-cyclodextrin for controlled drug delivery. *Biomaterials* **27**, 4132 (Aug, 2006).

161. A. R. Cooper, H. A. MacQueen, Subunits of laminin are differentially synthesized in mouse eggs and early embryos. *Dev Biol* **96**, 467 (Apr, 1983).

162. A. B. J. Prowse, F. Chong, P. P. Gray, T. P. Munro, Stem cell integrins: Implications for ex-vivo culture and cellular therapies. *Stem Cell Research* **6**, 1.

163. B. Jeschke *et al.*, RGD-peptides for tissue engineering of articular cartilage. *Biomaterials* **23**, 3455 (Aug, 2002).

164. A. Katsumi, A. W. Orr, E. Tzima, M. A. Schwartz, Integrins in mechanotransduction. *J Biol Chem* **279**, 12001 (Mar 26, 2004).

165. P. Roca-Cusachs, N. C. Gauthier, A. Del Rio, M. P. Sheetz, Clustering of alpha(5)beta(1) integrins determines adhesion strength whereas alpha(v)beta(3) and talin enable mechanotransduction. *Proc Natl Acad Sci U S A* **106**, 16245 (Sep 22, 2009).

166. Y. Wang, L. M. McNamara, M. B. Schaffler, S. Weinbaum, A model for the role of integrins in flow induced mechanotransduction in osteocytes. *Proc Natl Acad Sci U S A* **104**, 15941 (Oct 2, 2007).

167. S. J. Millward-Sadler, D. M. Salter, Integrin-dependent signal cascades in chondrocyte mechanotransduction. *Ann Biomed Eng* **32**, 435 (Mar, 2004).

168. H. J. Xiowei Chen, Kunyu Wang, Degiang Su. vol. 2010.

169. A. Sionkowska, J. Skopinska-Wisniewska, M. Gawron, J. Kozlowska, A. Planecka, Chemical and thermal cross-linking of collagen and elastin hydrolysates. *Int J Biol Macromol* **47**, 570 (Nov 1).

170. A. O. Elzoghby, W. M. Samy, N. A. Elgindy, Albumin-based nanoparticles as potential controlled release drug delivery systems. *J Control Release* **157**, 168 (Jan 30, 2012).

171. L. Yang, T. J. Webster, Nanotechnology controlled drug delivery for treating bone diseases. *Expert opinion on drug delivery* **6**, 851 (Aug, 2009).

172. O. C. Farokhzad *et al.*, Nanoparticle-aptamer bioconjugates: a new approach for targeting prostate cancer cells. *Cancer Res* **64**, 7668 (Nov 1, 2004).

Appendices

Appendix A: Technical Drawing of the Load Cell Plate

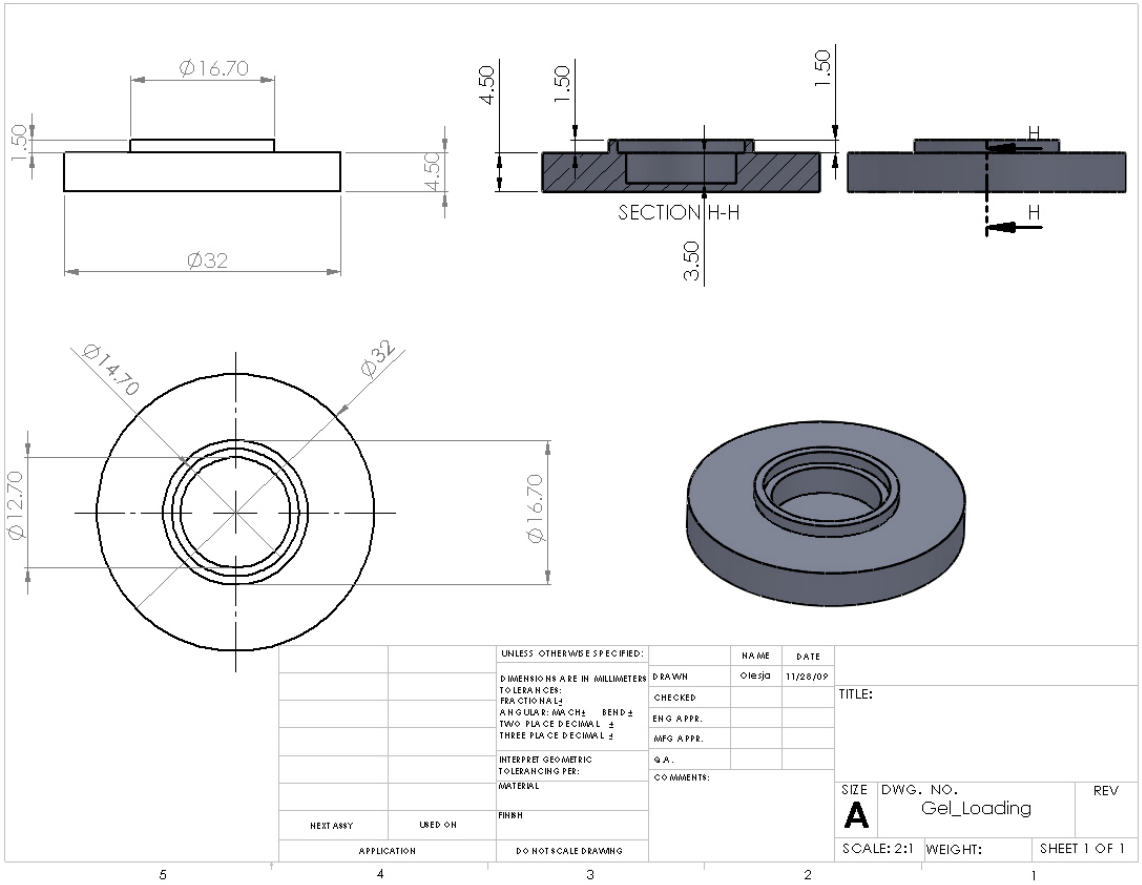

Appendix B: Adhesive Tape Specifications

Champion™ Tape

Technical Data Sheet

D5910 Differential Silicone/Acrylic Tape

Description

D5910 is a double-coated tape with a permanent silicone adhesive on one side and a high performance silicone adhesive on the other side. This tape is used for bonding differential substrates.

Features

The silicone adhesive creates good adhesion to silicone hard coats and release liners. The acrylic adhesive side permanently bonds to high and low energy surfaces.

Physical Characteristics	Standard Values
Carrier	1 mil PET
Adhesive Type	Silicone/Acrylic
Adhesive Thickness (each side)	1.5 mil – 0.038 mm
180° Peel Adhesion to Stainless Steel	52/72 oz/in – 14/20 N/25mm
Tape Color	Clear
Liner	2 mil PET / 4 mil PET
Total Tape Thickness	4.0 mil – 0.102 mm
Application Temperature Range	-40°F to 250°F – -40°C to 121°C
Available Lengths	36 and 72 yards

Tape Application

To achieve ultimate adhesion, the bonding surfaces should be dry, clean and free of dirt and oils. The strength of the adhesion bond is dependent on the amount of surface area directly contacting the adhesive. Firm pressure is recommended to obtain good adhesive to surface contact.

*Note: Values should be used for specification purposes and are averages taken from PSTC and ASTM test methods. The company does not warranty performance in specific applications. Since product performance may vary, each user should conduct their own test to determine the products fit for use in specific applications. The purchaser shall assume all risks and liabilities in connection therewith. Materials should be stored at 70°F (20°C) with 50% relative humidity. Champion Tape serves you better. Contact our team for qualified application support.

www.championtape.com
Phone 888-580-8588, 262-598-7400 Fax 262-598-7405
7900 Durand Ave. Bldg. 4, Sturtevant WI 53177

Appendix C: Silicone Rings Specification

(800) 775-6525 Fax: (800) 421-2923
engineering@marcorubber.com
www.marcorubber.com

Marco Compound # S1003
30 Durometer, Orange, General Use Silicone
Technical Datasheet

Common Names:
Silicone, VQM

General Description:
Silicones are excellent seal materials for extreme temperature in static applications. Silicones can be synthesized with a wide variety of properties and compositions. Please contact engineering@marcorubber.com for assistance in selecting a specialized compound when increased resistance to temperature, lubricants, or physical properties is required.

Features:
- Low durometer
- Excellent heat and compression resistance
- Excellent resistance to oxygen, ozone and sunlight
- Good chemical resistance
- Resistance to fungal and biological attack
- Flexible
- Good electrical insulation

Limitations:
- Not recommended for dynamic application
- Concentrated solvents, oils, concentrated acids, diluted sodium hydroxide.
- Poor abrasion resistance
- Low strength
- High gas permeability

Cure System:
Peroxide

Service Temperature:
-58 to 400 °F (-50 to 210 °C)

Specification:
ASTM D2000 M2GE303 A19 B37 EO16 EO36

PHYSICAL PROPERTY STANDARDS

ORIGINAL PROPERTIES	ASTM D2000 Requirements	Typical Test Results
Hardness, Shore A	30 +/- 5	26
Color	Orange	Orange
Tensile Strength, psi	432	630
Ultimate Elongation, %	300	600

HEAT RESISTANCE – A19, ASTM D 573 (70 hrs. @ 225°C)	**ASTM D2000 Requirements**	**Typical Test Results**
Hardness Change, points, Shore A	+10	+2
Tensile Strength Change, %, max.	-25	-23
Ultimate Elongation Change, %, max.	-30	+15

COMPRESSION SET – B37, ASTM D 325 Method B (22 hrs. @ 175°C)	**ASTM D2000 Requirements**	**Typical Test Results**
Permanent Set, %, max.	25	12

FLUID RESISTANCE –ASTM #1 Oil – EO16, ASTM D 471 (70 hrs. @ 150°C)	**ASTM D2000 Requirements**	**Typical Test Results**
Hardness Change, points, Shore A	0 to 10	-5
Tensile Strength Change, %, max.	-30	-27
Ultimate Elongation Change, %, max.	-30	-20
Volume Change, %	0 to15	+2

FLUID RESISTANCE – IRM 903 Oil, -EO36, ASTM D 471 (70 hrs. @ 150°C)	**ASTM D2000 Requirements**	**Typical Test Results**
Hardness Change, points, Shore A, max.	-30	-13
Volume Change, %, max.	+ 60	+27

Appendix D: Notes for Bose Electroforce Testing Machine

Preface:

- Try to keep load cells (known also as sensors, transducers) far away from machine mover (known also as LVDT - Linear Variable Differential Transformer, actuator, linear motor) until all preparation work is done (like program start, regime programming, limits setup, Local Energy turning on). The mover can change its position unexpectedly (fast moving like a jump) during the start/stop/tuning/ and, thus, damage the load cell and/or your sample
- It seems than the mover returns to zero position (displacement is 0) when you turn the system off (switch Local Energy to off). In other words, if the mover position is not 0 and you are going to switch off the system, the mover will jump suddenly to zero position (and can overshoot slightly that zero level).
- Virtually, every experiment requires setup/tuning of the machine and, strictly speaking, one's project file will not comply for your case (especially if system was tuned on solid sample for power and fast movement of loading mechanism but you intend to use it for soft sample and small strain values, or vise-versa).
- It is good practice to start using Bose machine/WinTest program without using of load cells (without installing them in machine frame; however load cells are connected and program registers some constant signals from them). You can learn the basics by programming the mover displacement and then setup all the parameters for your test (such as limits, rates, etc.).

! The new electronic version of manual can be found on computer desktop or under Help section in WinTest program (revision 4.0) while paper-based copy revision is 3.01.

! Please, try to avoid using of 45N load cell if you do not need high precision and/or do not need such small force (0-45N); use 450N instead.

! Do not forget to take into account the weight of fixture installed to load cell for the force limits (for example, if the mass of load plate is 100g, then load cell experiences 0.1kg*9.81N/kg=0.981N without sample loading start).

! Proper limits help to protect the system from overloading but do not guarantee that. From our experience: limits for 45N load sell were set to ±10N, however, system was not properly tuned up for experiment and load cell was damaged (load mover overshot the sample, the safety system lagged behind).

Program start

All control, power switch, and data acquisition is managed by WinTest program. Usually, there is no need to connect/turn on/start anything except to start this program and can be done as follows:

- Make sure there is no load cell installed in loading mechanism (usually we keep all our load cells in a plastic pocket (small cardboard sheet with transparent plastic on top) placed them edgewise to avoid force/pressure on sensor screw).
- Make sure that there is enough gap between mover (or, if applicable, fixture connected to the mover) and load table base ("bridge" between two smooth round support studs). Manufacturer limits for mover is -6.5mm to 6.5mm, thus the

maximum possible movement is 13mm. If you need to adjust the base height, just loose the big round nuts on each smooth leg (stud) of the machine, push the horizontal base, and then tighten nuts back.

- Usually computer is turned on, if not, turn it on, password: elf
- Find “WinTest 4.0” shortcut on desktop and run it. Wait for prompt to open project, select file

  “C:\Program Files\BOSE\project2start\prj_std.prg”

  wait until it is completely loaded and save a copy for yourself – go to

  “Files->Save As->|create/select your folder, type new name for project, and save it|”

  Good practice is to create your own folder using your name and keep all project files/data/everything there.
- Now you can modify this file for your needs. This file has been done using the last up-to-date calibration information, channel settings, etc. (as on February 15, 2013). This means that you do not need to do any calibration/channel setup/other common routines, but you still need to do things such define your test (waveform), define feedback channel(s) for your specific needs, tune the channel(s) for you sample type, setup data acquisition, etc.
- Below we try to list some critical parameters of the system and explain their meaning to the best of our understanding. These notes do not pretend to be comprehensive, we are not an ultimate authority, but we hope to share some of our experience (sometimes funny, sometimes very sad) and try to pay attention on some pitfalls.

Common definitions/settings and examples of system control

Here we try to list the system important/critical parameters. We do not explain basics, so, please refer to original manual for program interface details. Moreover, we try to provide the parameters in their importance sequence (as we think) rather than their complexity.

1. Channels definition/calibration settings/parameters

   These are very basic, common things, which usually require modification only if the system is changed and/or updated (such as load cell replacement, calibration update, any instructions from Bose company).

   Location: Tools (main window)->Advanced->Calibration

   Defined system physical channels (also known as meters):

   IN1_Displ – mover displacement, physical limits ±6.5mm (1/4 inch), calibration was done in 2005, blue color on screen (IN1 means it is connected to input 1 socket)

   IN2_450N – load cell of 100lbf (450N), physical limits ±450N, calibrated in November 2010, brown

   IN3_45N – load cell of 45N, physical limits ±45N, calibrated in March 2012, dark green

2. The WinTest program has many windows, sub windows, etc. In the very beginning it can be confusing to you, but do not worry, just try to pay attention on those which you are interested in. For example, focus now on IN1_Displ (blue), IN3_45N (green), IN2_450N (brown). These channels reflect current state of the system and must be updating their values on regular basis. You can slightly

touch mover to see the changes for IN1_Displ, slightly press sensor screws of the load cells to check the feedback.

Now you need to define channels limits for safety. This can be done through Setup (main window)->Limits. Usually you intend to use the mover (IN1_Disp) and one of the load cells, so you can change limits only for them. Also you can choose the action to be applied if limits are exceeded (it is explained later in text).

Current settings:

IN1_Disp: -5.1mm and 5.1mm, minimal possible time 0.0002, Controlled Stop.

IN2_450N: -101N and 101N, time 0.0002, Controlled Stop.

IN3_45N: -11N and 11N, time 0.0002, Controlled Stop.

You should made changes according to your needs. For instance, assume you need to perform load test for some sample and estimated load range 0-3mm (for loading it means from 0 to -3mm, as you need mover goes down) and 5N (-5N for loading, as the sensor crew is pressed downward), then you can set limits as: -4mm, +1mm for IN1_Disp and -7N, +1N.

Proper limits setup reduces the risk of sample/load cell overload (damage).

In case if any of those limits exceeding, the action will be applied in specified time. Currently, Controlled Stop will be applied. In simple words, this means the following: system switches in safe command mode, i.e. takes control from you and use direct command named DirCmd to drive the mover to some specific position. This “safe” position could be defined in

Setup (Group sub window)->Mover(s)->Controlled Stop->Controlled Stop Position. Value must be specified in Volts, current value is 0.1V that corresponds

approximately to level of 0.32mm (a little bit above the center position of the mover). More details on this can be found further in text and on page 5-5 of new manual only (revision 4.0).

3. You must to choose the feedback channel for the system based on your test requirements. While it is possible to record data from all channels (or any combination of them), the feedback channel is the one that controls the mover. In other words, the feedback completely defines the motion profile of actuator. For example, for simple tensile/compression test the displacement is usually changing uniformly (like 0.1mm/s) and the force is registered. So, in this case the system feedback channel should be set to displacement. Another example, a specific force level/profile (like sine-shape waveform in terms of force) is needed, so, the feedback channel should be set to one of the load cells. In this case system drives the mover base on the force signal (i.e. matches displacement).

   !!! However, do not switch feedback channel to displacement or load yet, leave (or set if it was not) feedback into DirCmd (which is most safe feedback). Change the feedback channel you can by clicking the Feedback button in group sub window. The current feedback channel is highlighted with white background.

   DirCmd directly manipulates the motor, the value is in Volts; 0V corresponds roughly to 0mm level, 1V – to 3.2mm, -1V – to -3.2mm. Note, for example, the rate of 0.1V is about 0.32mm. DirCmd feature is safe because it is direct command and does not use any tuning settings (which can amplify the mover reaction). It is recommended to use it as feedback in every experiment start.

4. Beside 3 physical channels/meters (displacement, 2 load cells) you can see also Axial Command (Axial Cmd) channel (black color). Axial Cmd reflects the current feedback channel (in V for DirCmd, in mm for IN1_Displ, in N for load cells) and shows the most resent command. This means you can see the “desired target condition” for the system. For example, if you set in DirCmd mode the desired value +1V, then mover will go to this state (1V or around 3.2mm), if mover is on (if not, the Axial Cmd will change to +1V, but actuator will not move and displacement will not be changed). Another example, you set -10N when feedback channel is set to one of load cells, then the context Axial Cmd will change to -10N and system will manipulate the mover (i.e. displacement) in order to match/level the load cell reading (IN2_450N or IN3_45N). In latter case the important thing is that the system must have a response from load cell (your sample must present) and system will use the load cell tuning settings/parameters. If these parameters is not properly tuned up (on sample similar to yours), the system can behave unpredictable and damage sample/load cell. Displacement channel also has tuning parameters (only DirCmd has not).
5. There are 2 pre-set buttons to control the system in direct mode and can be set in

   Setup (group sub-window)->Preset Properties

   In appeared window you can set the parameters for each button. Both buttons operate in DirCmd mode only and the Rate is set in Volts per second (remember, 0.1V/s corresponds to about 0.32mm/s). The system is supposed to more

actuator with this rate to some specific Level which depends on the chosen Channel. For example, you can choose IN1_Displ as a channel and +2mm for level, and rate of 0.1V/s, and then the system will move actuator with the constant rate of 0.1V/s (0.32mm/s) to the position +2mm (when you turn on the mover and press this pre-set button). Another example, you set IN2_450N as a channel and level of +20N, and then the mover will go up with the above constant rate (tensile test as we set +20N) until IN2_450N meter (brown) becomes +20N.

!!! Attention, in latter case you must have installed load set with sample to provide response for IN2_450N (otherwise mover goes to its limit and controlled stop will be applied).

!! It is good practise to configure one of those pre-set buttons as a displacement channel with level 0 and small rate like 0.1V/s and then use it to return the mover to zero position by the end of your experiment (note, when you press any of those buttons, the feedback channel will be changed automatically to DirCmd). Note, the mover will jump to zero position after system turning off, so drive mover to that zero position upon switching off.

6. There is another method to manipulate the mover manually – it is Position button in group sub window. There you can change the mover position by typing specific value and press Apply button or just use the arrows to make smooth changes. Please, note that position operates according to current feedback channel (i.e. in DirCmd you have Volts, in displacement – mm, and in load – N), the rate could be changed by right clicking in that window.

7. How to turn on the mover. The mover switch is associated with Local Energy term, i.e. you need to “bring” the Local Energy to High in order to turn on the mover. This can be done by clicking Local button in group sub window. However, there are some Local Energy settings which should be set before; go to Setup (group sub window)->Mover(s)->Local Energy. Remember, the Axial Cmd is the most recent command (desired state) and feedback channel is the real state of the system, In general case it could be difference between them, and thus mover can go to Axial Cmd upon turning on. To avoid that, you should check the setting Command=Feedback (this reset Axial Cmd to current real state of the mover, so there should be no motion on switching). Also, the I-term should be enabled that compensates the possible error between command and feedback.
8. Controlled Stop recall. Now, with the above background, you can understand and select appropriate value for the Controlled Stop mentioned in paragraph #2. Simply choose the “safe” mover level (its displacement which would be safe in your experiment if something goes wrong), then calculate approximately the Voltage for it (for example you chose +2mm, 1V means about 3.2mm, so this +2mm corresponds to +0.625V), define one of the pre-set buttons (paragraph #5), and test it. Or you can manipulate manually the mover instead of using the pre-set button (paragraph #6). Test means: make sure there is enough gap between mover and base table/load cell, choose DirCmd as a feedback (paragraph #3), turn on the mover (paragraph #7), press the pre-defined button (or use Position button from paragraph #6), and check/make sure

that you have correct values for Axial Cmd (your calculated V) and displacement level (“safe” position in mm).

After experiment you should move mover to zero position (displacement 0) and then you can turn the Local Energy off (Local button). You can drive the mover manually (paragraph #6) or use the pre-set button if you configured it as suggested in paragraph #5.

9. Peak/valley settings. Correct reading of peak/valley values is important especially in cyclic loading. Ideally, you should have no difference between peak/valley values and load program levels (like sine-loading from -2mm to +2mm), but in real experiment you can notice some difference. Based on this difference, it is possible to apply compensation (Compensation button on group sub window). To define Peak/valley settings, go to Setup (main window)->Peak/Valley. You can set Band % out of full scale for each channel. We tried to set some reasonable values for every channel. For more information please refer to original manual page 5-6.

Channel	Full scale	Band value	Band %
IN1_Displ	6.5	0.05	0.769231
IN2_450N	450	1.5	0.333333
IN3_45N	45	0.15	0.333333
DirCmd	10	0.015	0.15

10. Taring can be done by right click on specific channel reading or trough Setup (main window)->Channels->Tare. Click Auto button to set current channel

to zero level (i.e. you can set zero for load cell when you install fixture/load plate to it). The number is in a binary format (scale 32768). You do not need to use taring for displacement channel as the best value was chosen by Bose.

11. System tuning. For comprehensive information please return to original manual (Chapter #9).

    There are two methods of tuning system: 1) automatic TuneIQ, and 2) manual PID. TineIQ is a Bose featured method which uses proprietary technique; you do not need/cannot get the details. To use it, you should:

    - choose appropriate feedback channel (remember to have a gap between load cell and mover upon turning on),

    - click the Tune button in group window and choose type of tuning to TuneIQ mode (not manual PID) for above chosen feedback channel,

    - turn on the Local Energy, check channels, put and adjust your sample (or “draft” sample if you think your sample can change its properties during the tuning test),

    - adjust manually mover (accurately change the position with low rate through Position button in group sub window; rate can be changed by right click on position window, paragraph #6) if needed (especially in case of load feedback, you must pre-load sample to provide sensitivity),

    - define the waveform for your test (if you need a non-cyclic form, then choose the sine-form for tuning with amplitude similar to required test),

    - press TuneIQ Run button (green button in waveform window bottom-right) and wait couple minutes while system is tuned.

Note, auto-tuning starts with ramp to mean level of amplitude limits and then run dynamic test (frequency will be changing, you might hear some noise). "… the intention is that the TuneIQ process will not expose the sample to test conditions outside of the defined waveform…"

The manual mode based on adjusting PIDO parameters (proportional, integral, differential, and offset). It is required advanced knowledge and accurate approach; we recommend avoiding this method in the beginning or, at least, try to do manual tuning for mover (displacement) at first (without installing load cell).

Current tuning settings:

- displacement (IN1_Displ) was tuned automatically (TuneIQ) for sine-wave with amplitude from -3 to 3mm,
- load cell IN2_450N was tuned on some soft material with sine-wave (0-5N, very small displacement like 0.2mm),
- load cell IN3_45N) was tuned on some soft material with sine-wave (0-5N, very small displacement like 0.2mm).

We suggest you to keep and use current displacement tuning and make auto-tuning for load cells if you need load as feedback in your experiments.

12. Wave form generation (ramp, dwell, sine, triangle, block, etc.) is well explained in manual in Chapter #7. From our experience, the block waveform is useful if you need to repeat experiment a lot. For example, you can define in block to start in DirCmd mode (the most safe), drive mover very slowly (like 0.1V) while force meets some specific value (like -0.2N), then switch to load feedback (it is safe as load cell "feels" the specimen, you have some pre-loading force level), start you

loading (like sine-shape loading from -0.2N to -5N, for example), then drive the mover to zero position (ramp in DirCmd to zero displacement).

! However, you cannot use the standard data acquisition method in this case and need to define it in block waveform. Please, refer to original manual for more information on block waveform (page 7-8) and block data acquisition (page 8-11).

13. The data acquisition is explained in Chapter #8 of original manual. We advise you to pay attention to Data Export section on page 8-16. The point is that data is collecting in a binary file (to provide high data reading rate), so later you have to export data manually (or check the option Export on close in data acquisition setting window). And the format of exporting file is explained exactly in that section. Also, please, re-define the name/path for collecting data files (make your folder as a destination).

    Here is an example how to organize acquisition of timed data (click on first/left Data Acquisition button, choose appropriate parameters):

    Channels: IN1_Displ and current load cell (IN2_450N or IN345N)

    Scan Time: 1 (one scan will take one second)

    Scan Points: 1000 (read 1000 points during that one scan)

    Number of scans: 100 (this means 100 scans of one second, so the total time is 100 second in this case, but should depend on your experiment)

    File info: choose your folder and define name for time data file (tdf), name should be new if you do not intend to overwrite previous files

    Type: standard

    First Scan: Axial at count 0 (i.e. start reading data when you start waveform)

Subsequent scan: 1 Sec between (to provide continuous data reading)

File Close Info: check all three parameters (generally speaking, it means the binary data file will be exported automatically on the end of experiment)

Reverse Data Retention: check all two options (better to have that file just in case; it has data on last 64 second, while sometimes time data has no such detailed tail)

Click Start, the Data Acquisition button should turn in yellow color, i.e. becomes active.

Appendix E: Characterization of Cell/Gel Constructs at Day 15 and Day 30

1 Hz, day 15 **0.1 Hz, day 15**

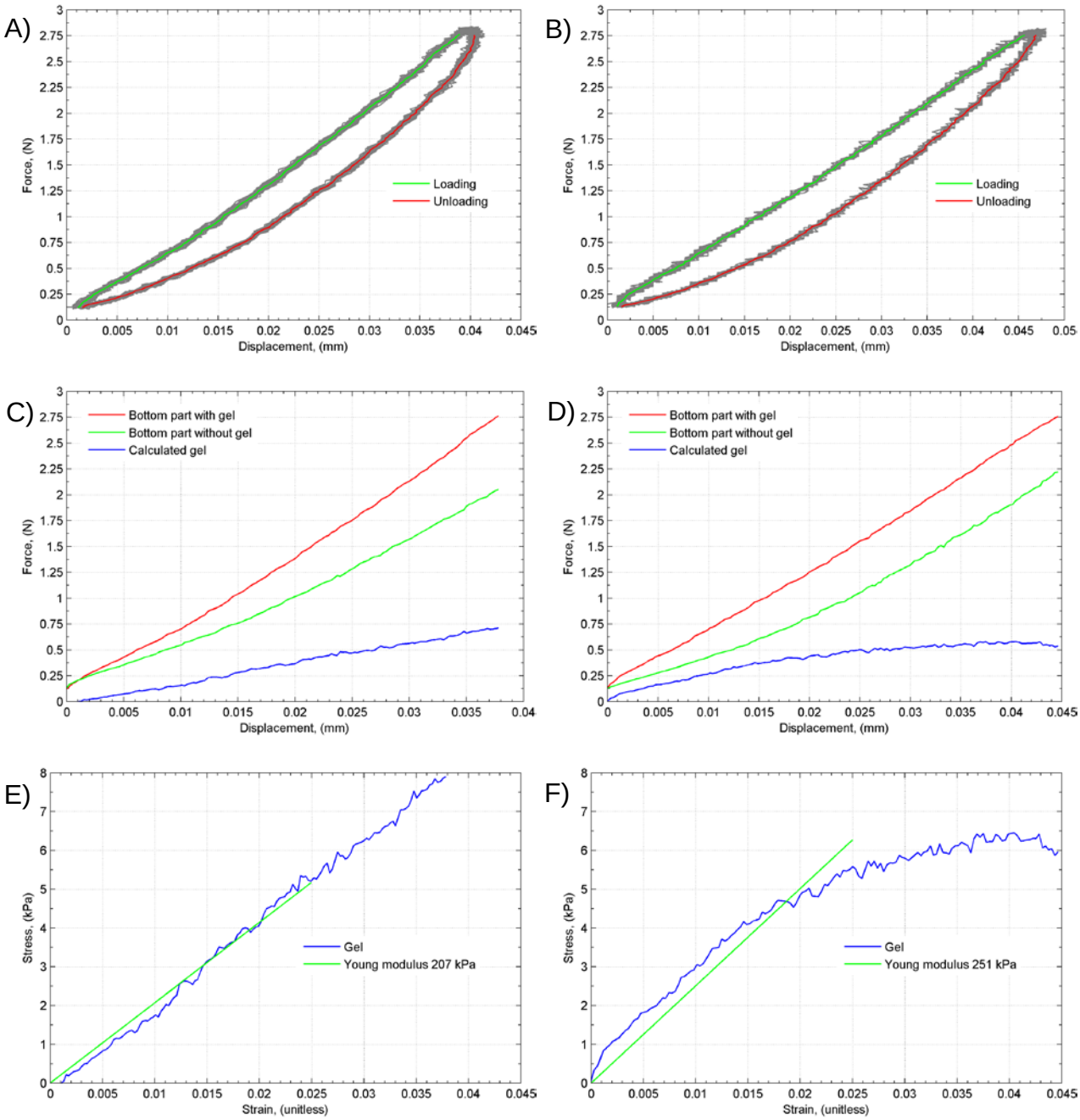

Force-displacement diagram for collagen gels at day 15 showing loading and unloading data of 40 cycles at A) 1 Hz and B) 0.1 Hz. Force-displacement diagram for bottom ring

(green), bottom part with gel (red), and a gel itself (blue) at C) 1 Hz and D) 0.1 Hz and the estimated Young's modulus for the collagen gels at day 15 at E) 1 Hz and F) 0.1 Hz.

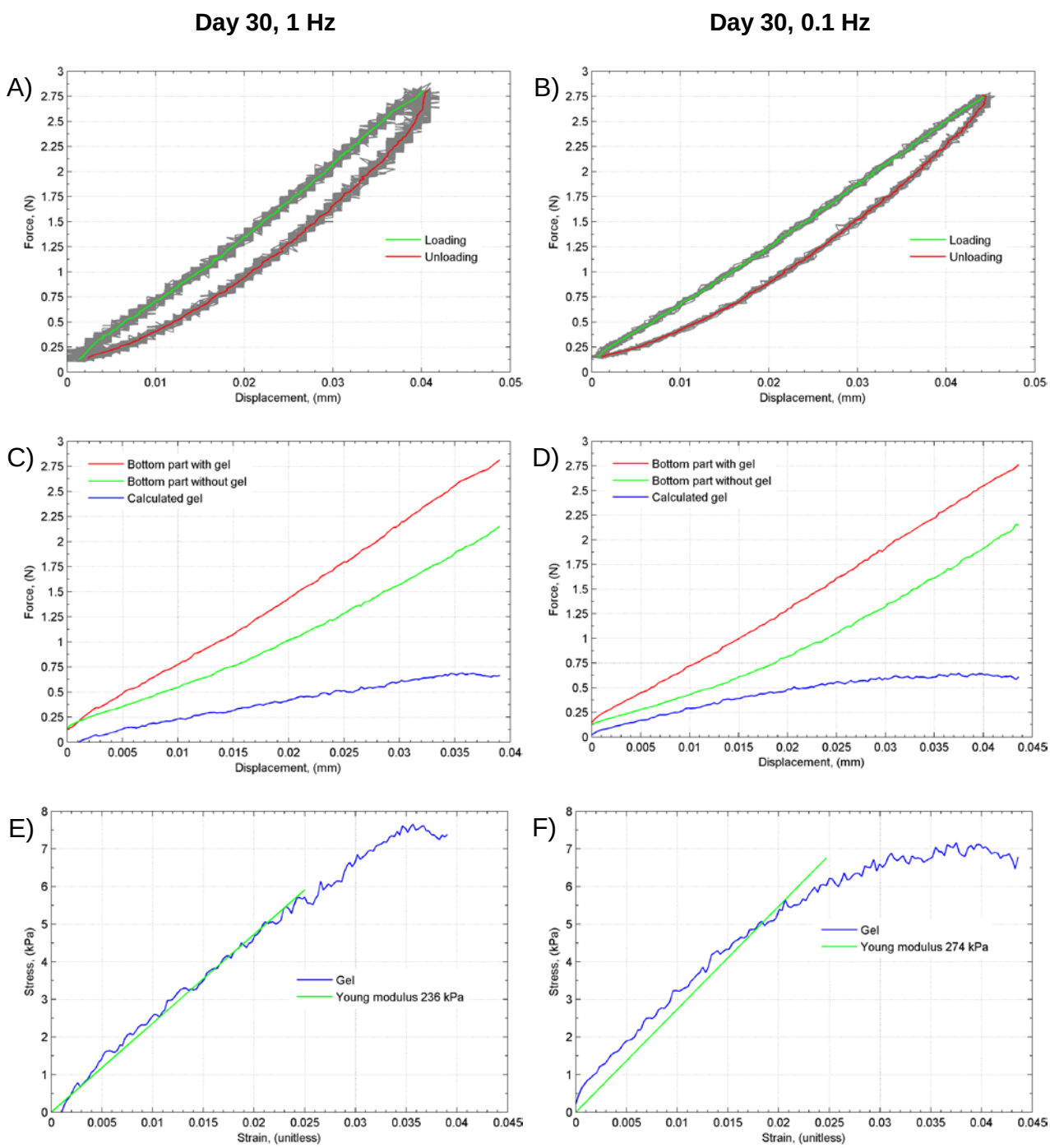

Force-displacement diagram for collagen gels at day 30 showing loading and unloading data of 40 cycles at A) 1 Hz and B) 0.1 Hz. Force-displacement diagram for bottom ring (green), bottom part with gel (red), and a gel itself (blue) at C) 1 Hz and D) 0.1 Hz and the estimated Young's modulus for collagen gel at day 30 at E) 1 Hz and F) 0.1 Hz.